Pharmacologic intervention in macrophage metabolism:
Mitochondrial pyruvate carrier inhibition by Mitoglitazone modulates inflammation

Doctoral thesis

to obtain a doctorate (PhD)

from the Faculty of Medicine

of the University of Bonn

Eike Christoph Geißmar
from Detmold, Germany
2023

Written with authorization of

the Faculty of Medicine of the University of Bonn

First reviewer: Prof. Dr. Eicke Latz

Second reviewer: Prof. Dr. Mihai Netea

Day of oral examination: 3rd July 2023

From the Institute of Innate Immunity

Director: Prof. Dr. Dagmar Wachten

Table of contents

List of Abbreviations

AA	Antimycin A; Complex III inhibitor
ACLY	ATP-citrate lyase
ADP	Adenosine diphosphate
ATP	Adenosine triphosphate
BMDMs	Murine bone-marrow derived macrophages
BSA	Bovine serum albumin
cDNA	complementary DNA
Cmpd.	Compound
Cxcl10	C-X-C motif chemokine 10
Cxcl5	C-X-C motif chemokine 5
DAMP	Danger associated molecular pattern
DMEM	Dulbecco's modified eagle medium
DMSO	Dimethyl sulfoxide
DPBS	Dulbecco’s Phosphate-Buffered Saline
ECAR	Extracellular acidification rate
ETC	Electron transport chain
FAD	Flavin adenine dinucleotide
FCCP	Mitochondrial inner membrane uncoupler; 2-[2-[4-(trifluoromethoxy)phenyl]hydrazinylidene]-propanedinitrile
FCS	Fetal calf serum
Glc.	Glucose
GW9662	PPARɣ inhibitor
HATs	Histone acetyltransferases
HRP	Horseradish peroxidase
HTRF	Homogenous time-resolved fluorescence
IL-10	Interleukin 10
IL-12p40	Interleukin-12p40 subunit

IL-1β	Interleukin 1 beta
IL-6	Interleukin 6
IMM	Inner mitochondrial membrane
LPS	Lipopolysaccharide
Mito	Mitoglitazone; MSDC-0160
MPC	Mitochondrial pyruvate carrier
NAD^+	Nicotinamide adenine dinucleotide
NADP	Nicotinamide adenine dinucleotide phosphate
Nos2	Inducible nitric oxide synthase
OCR	Oxygen consumption rate
Olig.	Oligomycin; Complex V inhibitor
PAMP	Pathogen associated molecular pattern
PPARɣ	Peroxisome proliferator-activating gamma
PRR	Pattern recognition receptor
PVDF	Polyvinylidenfluorid
qPCR	quantitative Polymerase Chain Reaction
R848	Resiquimod
Rot.	Rotenone; Complex I inhibitor
RT	Room temperature
SDS	Sodium dodecyl sulfate
TBS	Tris-buffered saline
TCA-cycle	Tricarboxylic acid cycle
TLR	Toll-like receptor
TNFα	Tumor necrosis factor α
UK5099	Covalent MPC inhibitor; 2-cyano-3-(1-phenyl-1H-indol-3-yl)-2-propenoic acid

1 Introduction

1.1 Metabolism

Metabolism is the sum of all chemical reactions within a living cell or organism. It underlies the orchestration of all processes attributed to life. Metabolic reactions convert food to provide energy equivalents and essential building blocks to synthesize proteins, lipids, nucleic acids and carbohydrates (Berg et al., 2013). Additionally, they also eliminate waste products that otherwise may represent a threat to the host. Metabolism confines a complex network of catabolic and anabolic reactions. Nevertheless, these reactions are commonly enabled through the utilization of energy equivalents – represented mainly by ATP – and reducing equivalents such as NADH, NADPH or FADH. As such, providing and balancing the available energy and reducing potential lies at the core of cellular metabolism.

The carbohydrate glucose displays a major source of energy for eukaryotic cells. Taken up from the extracellular environment into the cytosol of cells, it is used in glycolysis: A ten-step metabolic pathway that ultimately yields a net gain of two ATP molecules, two NADH molecules and two molecules of pyruvate per glucose molecule (Fig. I1 A).

Pyruvate displays a central metabolite in cellular energy metabolism. Under anaerobic conditions, it can be converted into lactate via Lactate Dehydrogenase to replenish the glycolytic NAD^+ pool and assert ATP production. In the Cahill cycle, pyruvate to alanine conversion is used to eliminate cell toxic nitrogen accumulation from amino acid breakdown mainly in mitochondria-scarce muscle cells. Importantly, the primary route of pyruvate metabolism connects glycolysis with the main metabolic pathway of cellular ATP production: The mitochondrial Tricarboxylic Acid Cycle (TCA-cycle) and the mitochondrial respiratory chain (Fig. I1 C & D). As such, pyruvate and its import into the mitochondrion exhibit a nexus of cellular energy metabolism (Fig. I1 B).

Tight control of metabolic reactions is essential to maintain the balance under cellular steady-state conditions. Yet, the flexible increase or decrease of distinct metabolic pathways exhibits the basis for the differential cellular responses to an intrinsic or extrinsic cue. As will be described later, the dysregulation of metabolism, throughout the organism and within cells, presents a key feature of many diseases that are on the rise in modern societies.

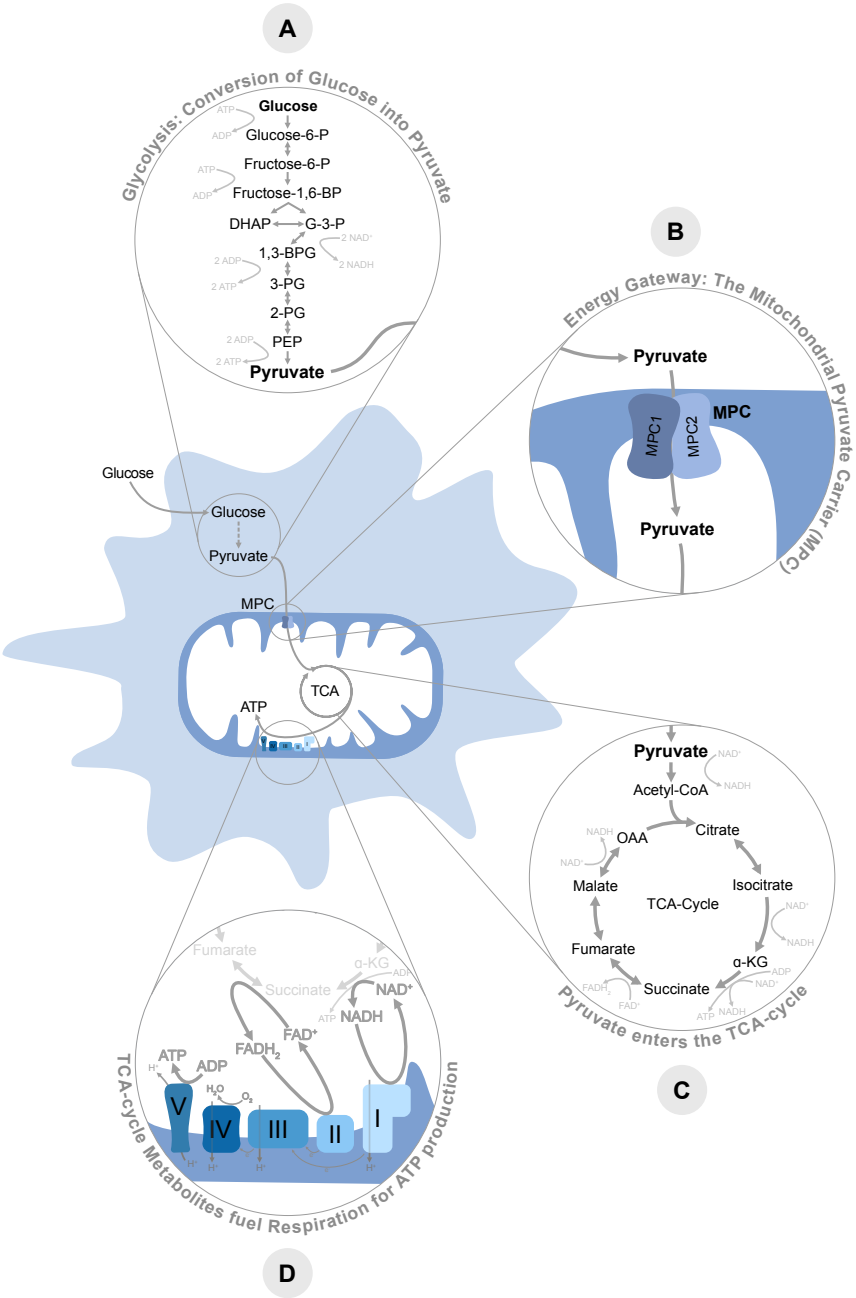

Fig. I1: Mitochondrial pyruvate import via the mitochondrial pyruvate carrier (MPC) connects glycolysis and mitochondrial metabolism. Glucose is taken up from the cellular environment and used in glycolysis, yielding two pyruvate molecules (A). The only entry point of pyruvate into the mitochondria is the mitochondrial pyruvate carrier (MPC) (B). It transports pyruvate over the inner mitochondrial membrane (IMM) into the mitochondrial matrix. Pyruvate is converted into acetyl-CoA and enters the TCA-cycle (C). The TCA-cycle yields biosynthetic precursor molecules, ATP and the reducing equivalents NADH and $FADH_2$. The latter are used by the electron transport chain (ETC) to produce a proton gradient over the IMM (D). This proton gradient is necessary for producing high amounts of ATP by oxidative phosphorylation at complex V of the mitochondrial respiratory chain.

1.2 The mitochondrial pyruvate carrier (MPC)

Metabolic reactions are catalyzed through enzymes and tightly controlled by transcriptional regulations, post-translational modifications, feedback inhibition, sequestration and provision of co-factors and the enzymatical substrates themselves. The latter strategy is aided by the principle of cellular compartmentalization. Mitochondria are the most well-known organelles of metabolic specialization among the different cellular compartments and organelles. They are often described as the “power-houses” of the cell as they host the most efficient metabolic pathway for ATP production.

While metabolites can pass the outer mitochondrial membrane relatively indiscriminate, the passage of the inner mitochondrial membrane is tightly controlled (Vanderperre et al., 2015). Early studies strongly indicated that mitochondrial pyruvate import had to be facilitated by a carrier, yet efforts failed to unravel its molecular identity (Halestrap, 1975; Halestrap & Denton, 1974; Papa et al., 1971). Only in 2012, the genes encoding the proteins forming the mitochondrial pyruvate carrier (MPC) were identified (Bricker et al., 2012; Herzig et al., 2012). The MPC is constituted by the individually encoded MPC1 (12 kDa) and MPC2 (14 kDa) subunits that are situated in the inner mitochondrial membrane as a heteromeric complex (Bricker et al., 2012; Vanderperre et al., 2015) (Fig. I1 B). As the mitochondrial pyruvate import is of central importance to cellular energy metabolism, the Mpc1 and Mpc2 genes are constitutively and ubiquitously expressed. Furthermore, phylogenetic comparison shows high conservation of the MPC1 and MPC2 amino acid sequence among eukaryotes and an approximately 94% identity between *Mus musculus* and *Homo sapiens* MPC1 and also MPC2. The knockout of either Mpc1 or Mpc2 in mice resulted in embryonic lethality, further highlighting the functional importance of the carrier (Vanderperre et al., 2016; Vigueira et al., 2014). In vitro assays showed that both human MPC1 and MPC2 can homodimerize, but the MPC1/MPC2 heterodimer was shown to represent the more stable and active form of the MPC capable of pyruvate transport (J. Lee et al., 2020; L. Xu et al., 2021). The function of the MPC as a heteromer is further supported by the interdependent regulation of the subunits’ expression. Knock-down of either MPC1 or MPC2 mRNA resulted in the loss of the respective mRNA transcription and protein expression of its counterpart (Vacanti et al., 2014). The exact mechanism of

how this interdependent regulation is facilitated remains to be unraveled. Pharmacologic inhibition or knock-down experiments demonstrated that loss of MPC-facilitated mitochondrial pyruvate import entails metabolic adaptions (Divakaruni et al., 2013; Lauterbach et al., 2019; Vacanti et al., 2014; Wenes et al., 2022) Concomitantly, the MPC is now considered to be a promising target for pharmacologic intervention originating from and exacerbated through metabolic dysregulation.

1.3 The innate immune system facilitates inflammation

The immune system is a network comprising of physical barriers, cells and soluble factors such as proteins. It evolved to defend against chemicals (e.g. microbial toxins) and invading pathogens such as bacteria, viruses or fungi. Our bodies are constantly challenged to defend against these detrimental cues; Their recognition is of utmost importance to react accordingly and prevent or limit harmful consequences (Murphy, 2012).

Our immune system comprises two parts: the adaptive- and the innate immune system. They each harbor their respective strengths and weaknesses. The adaptive immune system is slow in mediating a response to a perceived danger; Its reaction takes days until it raises an effective defense mechanism. Nevertheless, adaptive immune cells raise highly specific recognition molecules, expand and potently ward off threats. The plasticity and maintenance of these recognition molecules throughout life compose an effective immune memory system. This allows to fend off newly encountered threats and recurring challenges even many years after the initial encounter.

By contrast, the innate immune system initiates the first defensive reaction against danger to our body. Its activation by and appropriate response to a danger signal happen swiftly; Within the first minutes to hours, innate immune cells initiate their fight against the danger and recruit other immune cells to the site of invasion. However, the distinct patterns recognized by innate immune cells are genetically predefined. This limits their repertoire to recognize distinct danger signals and their adaptation towards co-evolving pathogens as well as ever-changing environmental cues shaped by socioecological transformation. Interestingly, more recent research also points towards an innate immune memory mainly based on the epigenetic remodeling of previously activated innate immune cells (Charles-Messance & Sheedy, 2021; Netea et al., 2020; Quintin et al., 2012). Trained innate immune cells might still be on patrol even after an infection has been cleared. They may

harbor the potential to react to a recurring threat more effectively, following a similar concept historically attributed to the adaptive immune system.

The innate immune response is facilitated by the complement system and innate immune cells: natural killer cells, innate lymphoid cells, mast cells, eosinophils and basophils as well as the phagocytic macrophages, dendritic cells and neutrophils. Innate immune cell responses to danger recognition manifest as inflammation. The inflammatory response of innate immune cells aims to fight an imminent threat, clear the site of invasion and ultimately re-establish tissue homeostasis (Medzhitov, 2008).

Macrophages patrol the tissues and are among the first cells to encounter a danger signal. They are capable of sensing pathogens via specific pattern recognition receptors (PRRs); Proteins that are capable of recognizing molecules either derived from pathogens, so-called pathogen-associated molecular patterns (PAMPs), or self-molecules, termed danger-associated molecular patterns (DAMPs) (Newton & Dixit, 2012). While PAMPs indicate an infection, DAMPs are molecular cues of tissue damage. Upon binding of a PAMP or DAMP to its respective PRR, macrophages get activated and initiate an inflammatory response. They phagocytose pathogens and release eliminating nitric oxide as well as cytokines to activate bystander cells and chemokines to recruit other immune cells from the bloodstream into the tissue. The recognition of the cell wall component of gram-negative bacteria Lipopolysaccharide (LPS) by its PRR Toll-like receptor 4 (TLR4) is the best-studied example of how a PAMP leads to the activation of macrophages. It is expressed on the cell surface of macrophages. TLR4 is unique among all other TLRs as it is the only receptor signaling through both, TIR-domain-containing adaptor-inducing interferon-β (TRIF) and Myeloid differentiation primary response 88 (MyD88). Other TLRs signal either through TRIF or MyD88. For example, recognition of single-stranded RNA (ssRNA) by endosomal TLR7 and 8 leads to recruitment of MyD88. TLR activation and adaptor recruitment further evoke a signaling cascade involving a series of kinases and transcription factors. In macrophages, this culminates in the transcription of inflammatory genes such as the cytokines Tnf, Il1b, Il12b or Il6. The secretion of these cytokines initiates further immune responses aiming to contain, fight and eliminate an infection. However, dysregulation of the innate immune response can result in inflammatory pathologies. It is now accepted that many diseases on the rise in modern societies have an underlying

inflammatory component (Christ et al., 2019; Hotamisligil, 2017). Thus, pharmacologic regulation of aberrant inflammation is of high interest to current research.

1.4 Metabolic dysregulation and inflammation

As indicated above, dysregulation of our metabolism has aggravating consequences for our health. Modern societies favor a more sedentary lifestyle with ample supply and intake of calorie-dense, highly processed food. Together, these lifestyle changes are considered key etiological drivers of non-communicable diseases (NCDs). Nowadays, NCDs are responsible for 71% of deaths worldwide (Word Health Organization, 13. April 2021). 80% of NCD-caused deaths are accountable to cardiovascular diseases (17.9 million people), cancer (9.3 million people), respiratory diseases (4.1 million people) and diabetes (1.5 million people). Prominent examples include obesity-associated metabolic syndrome, cardiovascular diseases (CVDs), non-alcoholic fatty liver disease (NAFLD), non-alcoholic steatohepatitis (NASH), neurodegenerative diseases like Alzheimer's disease (AD) as well as type 2 diabetes mellitus (T2DM) (Canevari & Clark, 2007; Christ et al., 2019; Hosseini et al., 2016; Kerr et al., 2017; Mozaffarian, 2016). It is therefore of little surprise, that more than one of these diseases frequently coincide in the same patient. For example, 55% and 37% of T2DM patients are estimated to also have NAFLD or NASH, respectively (Younossi et al., 2019). Moreover, the detrimental clinical outcomes of both T2DM and NASH are primarily due to cardiovascular events (J. Colca, 2020). This highlights the complexity of these multi-organ diseases.

It is now accepted that metabolic regulation and tissue-specific as well as systemic inflammation are tightly interlinked. Dysregulation of either of these systems affects the other and, if prolonged, can disturb our health. Notably, research has linked the development and progression of NCDs to a chronic-inflammation (Christ et al., 2019; Christ & Latz, 2019; Y. S. Lee & Olefsky, 2021). Moreover, the consumption of a western type diet was shown to elevate inflammatory serum markers both in rodents and humans (Christ et al., 2018; Hosseini et al., 2016; Lopez-Garcia et al., 2004). As primary facilitators of inflammation, macrophages were shown to be key contributors to the systemic- and tissue-specific inflammation present in the aforementioned diseases. This includes metabolic tissues such as the adipose- and hepatic tissue as well as pancreatic islands, but also non-metabolic tissue like the brain. For example, the characteristic chronic-inflammation of obese

adipose tissue is majorly determined by inflammatory macrophages (Michailidou et al., 2022; Weisberg et al., 2003; H. Xu et al., 2003). This is reflected by their increase from 5 – 10% of the cells in lean to approximately 40% in obese visceral adipose tissue (Lumeng, Bodzin, et al., 2007). Moreover, these macrophages express higher levels of TNFα, IL-6, IL-1β and nitric oxide synthase (NOS2) (Gao et al., 2014; Lumeng, Deyoung, et al., 2007; Lumeng et al., 2008; Wentworth et al., 2010). Prolonged adipose tissue inflammation can result in insulin resistance and glucose intolerance, both hallmarks of diabetes. Moreover, similar processes described for adipose tissue macrophages were found in hepatic tissue and the brain (Christ et al., 2019).

While research has unraveled some of the mechanisms of chronic-inflammation in specific tissues, it should be noted that none of these processes happen in isolation. Understanding the complex interplay between inflamed tissues originating from metabolic challenges throughout our body will be of great importance in developing strategies for pharmacologic intervention. Importantly, targeting the inflammatory response of macrophages promises to be an effective strategy to ameliorate chronic-inflammation in multiple organs and detrimental outcomes of metabolic diseases. Recent insights suggest that targeting macrophage metabolism itself might be a strategy to pharmacologically intervene in inflammation.

1.5 Metabolic rewiring of inflammatory macrophages

As described above, metabolic challenges can activate macrophages and result in various inflammatory pathologies. Likewise, macrophage activation itself is accompanied by changes in their metabolism. Upon LPS activation, macrophages rewire their metabolic pathways to provide energy, reducing equivalents and building blocks necessary for their response. Inflammatory macrophages increase glucose uptake and aerobic glycolysis, a process also termed Warburg metabolism after its initial description by Otto Warburg in cancer cells (Warburg, 1924). Additionally, macrophages also increase ATP production via oxidative phosphorylation during early hours of activation, whereas later on they change their mitochondrial metabolism to focus on the production of biosynthetic precursors and reactive oxygen species (ROS) (Nonnenmacher & Hiller, 2018). The interconnection between metabolic changes and the inflammatory response is still focus of intense research. However, an increasing body of studies provides evidence that metabolites of

the TCA-cycle are tightly integrated into the regulation of macrophage functions. This includes citrate, α-ketoglutarate, succinate and fumarate (Arts et al., 2016; Lampropoulou et al., 2016; Lauterbach et al., 2019; Netea et al., 2020; Tannahill et al., 2013). They were shown to modulate immune responses via different mechanisms, including post-translational modifications of immunoregulatory signaling proteins, as autocrine- and paracrine signals and as regulators of epigenetically controlled inflammatory gene transcription. Additionally, one of the best described metabolites with immunoregulatory and antimicrobial functions is itaconate. Itaconate is derived from the TCA-cycle intermediate cis-aconitate via LPS-inducible immune responsive gene 1 (IRG1) in macrophages. It decreases macrophage expression of pro-inflammatory cytokines and inhibits bacterial growth (Lampropoulou et al., 2016; Meiser et al., 2016; Michelucci et al., 2013). More recently, it was found that mesaconate is produced from itaconate in macrophages and exerts anti-inflammatory functions similar to its biosynthetic precursor (He et al., 2022). Importantly, while the production of some metabolites is increased early after inflammatory activation, others accumulate later on. Likewise, macrophage functions and their cytokine expression dynamically change throughout their activation (Hargreaves et al., 2009; Ramirez-Carrozzi et al., 2009). This suggests that specific metabolites affect the temporal shift in macrophage functions, and vice versa, thereby contributing to the successful clearance of an infection and/or re-establishment of tissue homeostasis.

A metabolite that was found to be increased early upon LPS activation of macrophages is citrate and it will be used to exemplify how metabolic rewiring of macrophages integrates into their inflammatory response (Lauterbach et al., 2019). Resting macrophages use metabolic products to regulate their homeostatic functions (Fig. I2 left). Early upon TLR4-activation with LPS, macrophages increase their glycolytic pathway. Concomitantly, the glycolytic end-product pyruvate is imported into the mitochondria to increase citrate production (Fig. I2 right). Cells have a mitochondrial- and a cytosolic citrate pool. Mitochondrial citrate gets exported into the cytosol and converted into acetyl-CoA by ATP-citrate lyase (ACLY). Among other functions, acetyl-CoA can then be used for the epigenetic modification of histones to license gene transcription.

In 2019, Lauterbach *et al.* demonstrated that LPS-activation of macrophages led to increased histone acetylation of LPS-response genes. Furthermore, they showed that glucose metabolism was a major supplier of the acetyl-CoA used for histone acetylation.

Intervention in this pathway regulated inflammatory macrophage functions. They showed that MPC inhibition by UK5099 prevented citrate accumulation in macrophages and reduced inflammatory cytokine secretion. Likewise, ACLY inhibition decreased carbon incorporation from glucose into acetylated histones and thereby regulated the transcription of LPS-response genes. Thus, pharmacological intervention of this metabolic-epigenetic axis promises to be useful in regulating inflammation that, as described above, contributes to a plethora of diseases. However, clinically applicable drugs targeting the metabolic pathways are still lacking. This warrants the identification and characterization of new small molecule inhibitors that modulate the metabolic changes underlying the inflammatory response of macrophages and potentially also other cell types.

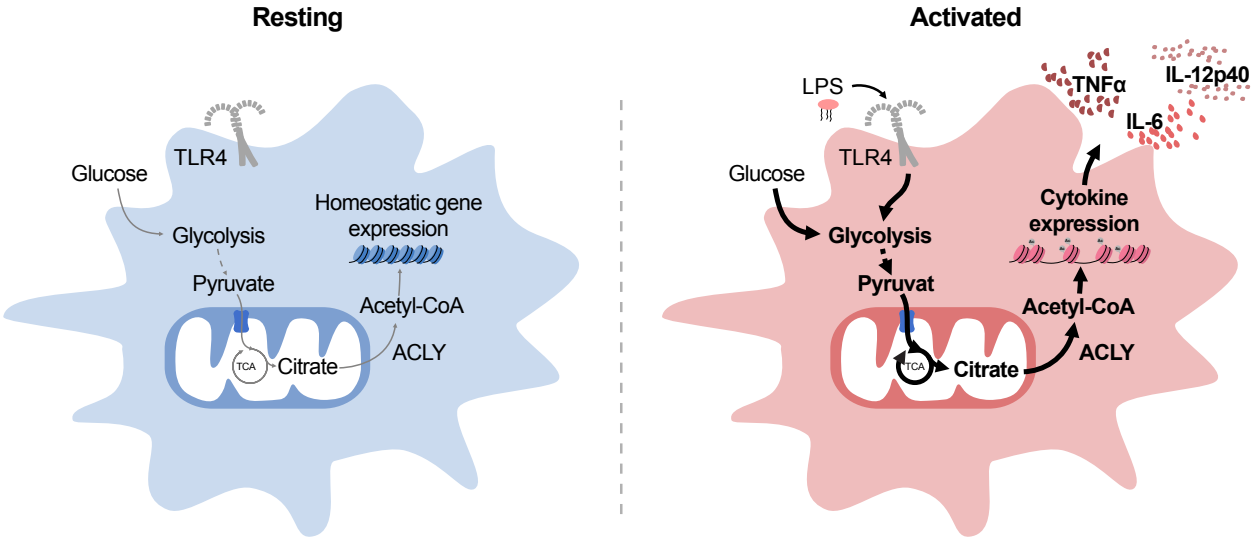

Fig. I2: Metabolic rewiring of macrophages upon TLR-activation regulates inflammatory gene transcription and cytokine secretion. Resting macrophages utilize glucose to sustain their homeostatic functions (left). In contrast, LPS-induced TLR4-activation (right) increases their glucose uptake and glycolysis. The glycolytic end-product pyruvate enters the mitochondria via the mitochondrial pyruvate carrier and is used to increase citrate production. Citrate gets exported from mitochondria and converted into acetyl-CoA via ATP-citrate lyase (ACLY). Histone acetyltransferases (HATs) use the acetyl-CoA to acetylate histones in regions encoding for inflammatory response genes. Consequently, chromatin-regions encoding for these genes and their regulatory elements open and transcription, e.g. of inflammatory cytokines, can be initiated. Ultimately, this enables macrophages to secret cytokines such as TNFα, IL-6 or IL-12p40 to initiate further immune responses.

1.6 Mitoglitazone promises to be a clinically applicable inhibitor of the MPC

A common hallmark of many metabolic diseases is a dysbalanced insulin system. This involves the impairment of both, cellular insulin resistance and sufficient insulin production to regulate cellular glucose uptake. Consequentially, blood glucose levels are chronically elevated (hyperglycemia), being at the root of deleterious outcomes (J. Colca, 2020; Soccio et al., 2014). This shows the importance of a balanced cellular- and organismal glucose metabolism to our health. Great efforts have gone into the development of drugs that continue to help ameliorate glucose imbalance, thereby treating metabolic diseases. Yet, use of these drugs comes with various side effects. Particularly since the prevalence of NCDs continues to rise in modern societies, further development of these drugs will be of significant importance.

Early in 1980, it was reported that thiazolidinediones, also called Glitazones, have insulin-sensitizing and glucose-balancing effects (Fujita et al., 1983). Later on, it was found that they are agonists of the transcription factor PPARɣ (Lehmann et al., 1995). The insulin-sensitizing effect of Glitazones was attributed to PPARɣ activation as it is a regulator of cellular lipid and glucose metabolism, among other functions (Hu et al., 2022). Three first-generation Glitazones were brought to the markets under FDA approval: Troglitazone, Rosiglitazone and Pioglitazone. However, a series of studies led to a decline in their clinical use as they are associated with side effects like fluid retention, weight gain, bone fractures and increased risk of cardiovascular events (Soccio et al., 2014). Troglitazone-intake elicited hepatotoxicity, which prompted its removal from the market (Kohlroser et al., 2000). Rosiglitazone was correlated with an increased risk of cardiovascular events (Nissen & Wolski, 2010; Singh et al., 2007), although later meta-analyses confuted these findings and led the FDA to re-approve its use (Home et al., 2009; Mahaffey et al., 2013). Nowadays, mainly Pioglitazone is used to treat T2DM and NASH as it exhibits significantly lower side effects than Rosiglitazone (Fig. I3). In fact, Pioglitazone is also suggested to mitigate cardiovascular diseases, certain cancers and neurodegenerative diseases (Dormandy et al., 2005; Erdmann et al., 2007; Heneka et al., 2015; Schmidt et al., 2004; Wilcox et al., 2007)). Rosiglitazone and Pioglitazone similarly balance blood glucose levels, yet Pioglitazone has approximately 15x less affinity for PPARɣ (Fig. I3) (Feinstein et al., 2005; Quansah et al., 2018). Intriguingly, reduced affinity for PPARɣ correlates with less side effects. In addition, the mitigating effects of Glitazones were shown to be partially PPARɣ-

independent (Chen et al., 2012; Feinstein et al., 2005; Jacques et al., 2021). Together, these disparities prompted a re-evaluation of the molecular mechanism underlying the beneficial effects of Glitazones.

Generation		Molecule	PPARɣ binding EC50 (µM)	Side effects	MPC binding IC50 (µM)	cmax / half life	Clinical use / Trial status
1st	Rosiglitazone	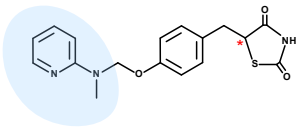	0.1	+++	1.1	1 µM / 3 – 4 h	+
1st	Pioglitazone	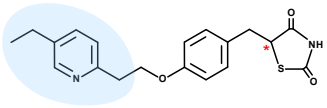	1.5	+	1.5	4 µM / 5 – 8 h	+++
2nd	Mitoglitazone (Mito)	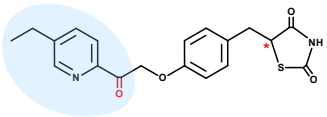	31.7	–	1.2	12 µM / 12 h	Phase 2b passed

Fig. I3: Mitoglitazone inhibits the MPC and exhibits reduced PPARɣ binding affinity. The first generation Glitazones, Rosiglitazone and Pioglitazone structurally differ in their hydrophobic moieties (highlighted in blue). While both show similar glucose-balancing effects in the clinics, increased PPARɣ affinity correlates with the severity of their side effects. Thus, Rosiglitazone is less frequently used than Pioglitazone. Yet, both first-generation Glitazones possess similar affinities for the MPC. Mitoglitazone (Mito) is a second-generation Glitazone with an additional keto-group (indicated in red) within the hydrophobic moiety compared to Pioglitazone. While having diminished PPARɣ affinity, it retains the affinity to the MPC, reaches higher blood concentrations with increased half life (cmax / half life) and showed no side effects in two successfully completed clinical phase 2b trials. Thus, Mito is a promising candidate drug for treating metabolic diseases with diminished side effects compared to currently used Glitazones. Asterisks indicate chiral centers.

Two studies demonstrated that Glitazones decrease mitochondrial pyruvate import by binding and inhibiting the MPC (J. R. Colca, McDonald, et al., 2013; Divakaruni et al., 2013). Interestingly, Pioglitazone and Rosiglitazone bind to the MPC with similar affinities. This suggests that the glucose-lowering effects of Glitazones might actually be facilitated through inhibition of the MPC rather than the activation of PPARɣ. Thus, a second-generation of Glitazones with reduced PPARɣ affinity, yet retained ability of MPC inhibition was developed. Mitoglitazone (Mito) belongs to these second-generation Glitazones (Fig. I3). It has approximately 300x less affinity for PPARɣ compared to Rosiglitazone, while retaining the ability to inhibit the MPC at concentrations similar to the first-generation Glitazones (Divakaruni et al., 2013; Quansah et al., 2018). Moreover, it reaches higher circulating

blood concentrations with a longer half-life than first-generation Gitazones and can be dosed effectively in rodents and humans (J. R. Colca, Vanderlugt, et al., 2013; Mallet et al., 2022; Shah et al., 2014). Its ability to pass the blood-brain barrier also suggests to reach cells associated with neurodegenerative diseases within the brain (Ghosh et al., 2016; Quansah et al., 2018). In fact, a successfully completed clinical phase 2b trial indicates that Mito can be used to ameliorate Alzheimer's disease progression (Shah et al., 2014). Moreover, another phase 2b trial showed similar glucose-balancing effects in T2DM patients compared to Pioglitazone (J. R. Colca, Vanderlugt, et al., 2013). Of note, none of these studies reported adverse effects. Together, these results suggest that Mito can be applied to the clinics, while circumventing the side effects of first-generation Glitazones.

As mentioned above, macrophages are key drivers of the chronic-inflammation accompanying metabolic diseases. PPARɣ regulates macrophage gene transcription and subsequent activation, generally suppressing their inflammatory response (Chawla, 2010; Gautier et al., 2012; Heming et al., 2018; Ricote et al., 1998). Hence, it came as no surprise that Glitazones exhibit anti-inflammatory effects. However, an ongoing debate about the anti-inflammatory mechanism of Glitazones was initiated by the findings that they can regulate immune cell functions, including macrophages and T cells, in time frames too early for transcription and independent of PPARɣ (Bolten et al., 2007; Brunmair et al., 2001; Chawla et al., 2001; Feinstein et al., 2005; Schmidt et al., 2004; Welch et al., 2003). For example, Chawla *et al.* (2001) demonstrated that Glitazones decrease LPS-induced IL-6 production and iNOS expression by ES cell-derived PPARɣ$^{wt/wt}$ and PPARɣ$^{-/-}$ macrophages, equally. Yet, the PPARɣ-independent mechanism of macrophage regulation by Glitazones remains elusive. As described earlier, mitochondrial pyruvate import is crucial for licensing the inflammatory response and inhibition of this intrinsic metabolic pathway decreases macrophage-facilitated inflammation. However, as described above, clinically applicable drugs specifically targeting the MPC were only recently developed. In light of the above-described new insights, the anti-inflammatory effects of Glitazones might originate from MPC inhibition rather than PPARɣ activation. Targeting the metabolic switch of inflammatory macrophages via MPC inhibition by Mito could be an efficient strategy to decrease their inflammatory response. Alongside lifestyle changes, Mito could help to

ameliorate the chronic-inflammation underlying NCDs and thereby contribute to decrease the burden posed upon societies through a rising prevalence of NCDs.

1.7 Aim of this thesis

Targeting macrophage metabolism promises new ways to pharmacologically intervene in inflammatory diseases. Inhibition of the mitochondrial pyruvate carrier (MPC) in macrophages using Mitoglitazone (Mito) might mitigate inflammation. However, to the present day, no study scrutinized the effects of MPC inhibition by Mito in macrophages.

This thesis aimed to investigate the potential of Mito to inhibit the MPC in macrophages and whether this inhibition could modulate the metabolic rewiring upon Toll-like receptor activation. Examining the changes of glycolysis and downstream metabolism upon Mito-facilitated MPC inhibition was intended to identify changes in general metabolic pathways and distinct metabolites with immunomodulatory function.

Furthermore, it was aimed to survey whether MPC inhibition by Mito modulates the inflammatory response of macrophages including the transcription and secretion of cytokines and other effector molecules.

To gain mechanistic insight, pharmacologic inhibition, genetic knock-out models and isotopic labeling of carbon sources in combination with mass-spectrometric analyses were used. Thereby, it was intended to delineate the effect of MPC inhibition by Mito in macrophages from potential off-targets.

Moreover, an acute sepsis mouse model was employed to identify whether the effects of Mito translate to inflammatory regulation in vivo.

2 Materials & Methods

2.1 Materials

2.1.1 Devices

Name	Supplier
-150°C freezer	SANYO Biomedical
-80°C freezer	Thermo Fisher Scientific
2950D Biochemistry Analyzer	YSI
BD LSR Fortessa	BD Biosciences
Blotting system Xcell II Blot Module	Invitrogen
Centrifuges	Eppendorf
Counting chamber Neubauer	Brand
Electronic E4 XLS+ multichannel pipets	Mettler-Toledo
Electrophoresis power supply Consort EV202	Merck
Epoch Microplate Spectrophotometer	BioTek
Freezing containers	True North
Gel electrophoresis chamber Novex mini cell	Invitrogen
Heatblock Thermomixer	Eppendorf
Incubator for tissue culture	SANYO Biomedical
LI-COR Odyssey® Infrared Imaging System	LI-COR Biosciences
MacBook Pro	Apple
MACS mix for rotation	Miltenyi Biotechnology
Magnet for magnetic bead immobilization	Invitrogen
MagPix Muliplex System	Luminex
nCounter MaxFlex System	Nanostring
Pipettes (0.1 µL – 1 mL)	Mettler-Toledo
Pipetting device Pipet boy acu	Integra Biosciences
Plate reader SpectraMax i3	Molecular Devices
Plate shaker DOS-10L	Neolab
Plate washer	Biotek
QuantStudio 6 Flex Real-Time PCR system	Thermo Fisher Scientific

Rotator for immunoblotting RM5	Ingenieurbüro CAT M. Zipperer
Seahorse XFe96 Analyzer	Agilent
Simple Western Wes/Jess	Simple Protein
SpectraMax i3 Multi-Mode Microplate Reader	Molecular Devices
Sterile tissue culture hood	Thermo Fisher Scientific
SW 41 Ti Swinging-Bucket Rotor	Beckman Coulter
Thermocycler T3000	Analytica Jena
Thermocycler Tadvanced (96-well)	Biometra
Vac-Man(R) 96 Vacuum Manifold	Promega
Vac-Man® Laboratory Vacuum Manifold	Promega
Vi-CELL BLU automatic cell counter	Beckman Coulter
Vortex Mixer VV3	VWR Collection
Waterbath WN7	Memmert
Wide-field fluorescent microscope Zeiss Observer.Z1	Carl Zeiss Jena

2.1.2 Disposables

Name	**Supplier**
15 mL, 50 mL falcon tubes	Eppendorf
384-well qRT-PCR plate	Greiner Bio-One
384-well small volume HTRF plate white	Greiner Bio-One
5 mL, 10 mL, 25 mL pipettes	Greiner Bio-One
70 µm cell strainer	Greiner Bio-One
Cell scrapers	Labomedic
Cell strainer 70 µm Nylon	Mettler Toledo
Cryotubes 2 mL	Sarstedt
Microcentrifuge tubes	Sigma
Mr. Frosty Freezing Container	VWR
Needles	ThermoFisher
Opti-Seal optical disposable adhesive	Falcon
PCR Stripes	Labomedic
Syringes	Perkin Elmer

Syringes	BD
Tissue culture plasticware (flasks, plates)	Beckman Coulter
0.1 µL – 1 mL pipette tips, filtered and unfiltered	Applied Biosystems
0.22 µm filters	BD Bioscience
Microfuge Tube Polypropylene, 1,5 mL	Thermo Fisher Scientific

2.1.3 Reagents and kits

Name	**Supplier**
10x PBS	Pan Biotech
10x Tris glycine	Thermo Fisher Scientific
12 – 230 kDa Jess or Wes Separation Module 25 capillary cartridge	ProteinSimple
20x MES buffer	Life Technologies
20x TBS (400 mM Tris, 3 M NaCl, pH = 7.4)	Santa Cruz Biotechnology
2329 L-Lactate Membranes	YSI
2365 Glucose Membranes	YSI
2747 Glucose/Lactate Standard	YSI
4 – 12% NuPAGE Bis-Tris gels	Life Technologies
Acetic acid	Roth
Adenosine diphosphate (ADP)	Sigma
Anti-Mouse Detection Module	ProteinSimple
Anti-Mouse NIR Detection Module	ProteinSimple
Anti-Rabbit Detection Module	ProteinSimple
Anti-Rabbit NIR Detection Module	ProteinSimple
Antimycin A	Sigma
Batyl alcohol 99%	Merck
Bovine serum albumin (BSA)	Roth
CellTiter-Blue® (CTB) Cell Viability Assay	Promega
Chloroform	Merck
cOmplete™ EDTA-free protease inhibitor cocktail	Roche Diagnostics
D-Mannitol	Sigma

DMSO	AppliChem
dNTP mix (10 mM)	Thermo Fisher Scientific
Dulbecco's Modified Eagle Medium (DMEM), high glucose, with L-glutamine	Life Technologies
Dulbecco's Modified Eagle Medium for flux analysis (DMEM A1443001), no glucose, no glutamine, no sodium pyruvate, no phenol red	Gibco
Dulbecco's Phosphate Buffered Saline (DPBS)	Life Technologies
Dynabeads™ Protein G	Life Technologies
ELISA mouse cytokines	R&D
Ethanol	Sigma
Ethylenediaminetetraacetic acid (EDTA) solution 0.5 M, pH = 8.0	Life Technologies
Ethyleneglycol-bis-(2-aminoethyl)-N,N,N',N'-tetraacetic acid (EGTA) solution 1 M, pH = 8.0	Boston Bioproducts
FCCP	Tocris
Fetal bovine serum (FBS)	Life Technologies
Glycerol	Roth
Goat serum	Life Technologies
Griess reagent system	Promega
GW9662	Selleckchem
HEPES 1 M pH = 7.0 – 7.6 cell culture grade	Sigma
Isopropanol	Roth
Jess RePlex Module	ProteinSimple
MagPix calibration kit (MPX-CAL-K25)	Millipore
MagPix performance verification kit (MPX-PVER-K25)	Millipore
Maxima SYBR Green/ROX qPCR Master Mix (2X)	Thermo Fisher Scientific
Methanol	Roth
Mitoglitazone (MSDC-0160)	Cayman Chemicals
Mouse Cytokine Magnetic Panel (MCYTOMAG-70K-09)	Milliplex
nCounter Master Prep Kit	Nanostring
nCounter XT PGX MmV2 Inflammation CodeSet panel	Nanostring

NIR live/dead stain	Thermo Fisher Scientific
Nonidet-P40 (NP-40)	AppliChem
NuPAGE LDS sample buffer (4x)	Life Technologies
NuPAGE sample reducing agent (10x)	LifeTechnologies
Oligo(dT)18 Primer	Thermo Fisher Scientific
Oligomycin A	Selleckchem
PageRuler™ Plus prestained protein ladder	Thermo Fisher Scientific
Penicillin-Streptomycin 100x	Thermo Fischer
Pentanedioic-d6 acid (d6 Glutaric acid)	CDN Isotopes
Phenylmethylsulfonyl fluoride (PMSF)	Applichem
PhosSTOP™ phosphatase inhibitor tablets	Roche Diagnostics
Pierce™ (BCA) Protein-Assay Kit	Thermo Fisher Scientific
Potassium monophosphate (KH_2PO_4)	Sigma
PVDF membrane Immobilon-FL	Millipore
Recombinant mouse IFNɣ	Immunotools
RNeasy mini kit	Quiagen
Rotenone	Sigma
RPMI-1640 (glucose-free; bi-carbonate free)	Sigma
Seahorse XF Calibrant Solution	Agilent
Seahorse XF96 cell culture microplates	Agilent
Seahorse XFe96 sensor cartidges	Agilent
Sodium chloride	Roth
Sodium dodecyl sulfate (SDS)	Sigma-Aldrich
Sucrose (cell culture grade)	Sigma
Superscript III reverse transcriptase	Thermo Fisher Scientific
tat-Cre enzyme (SCR508)	Merck Millipore
Trypan blue	Sigma-Aldrich
Trypsin 0.05% EDTA	Life Technologies
Tween 20	Roth
UK5099	Sigma
Ultrapure Lipopolysaccharide (LPS-EK) *E. coli* K12	Invivogen
Ultrapure Lipopolysaccharide (LPS) *E. coli* O111:B4	Invivogen

Water, nuclease-free	Thermo Fisher Scientific

2.1.4 Buffers and media

Name	Composition
ADP stock solution	400 mM, pH = 7.0 in 1x MAS buffer
Complete DMEM	DMEM supplemented with 10% FBS, 100 U/mL penicillin and 100 µg/ml streptomycin
FACS buffer	1x PBS, 0.5% FCS, 0.2% sodium azide
Freezing medium	90% FCS, 10% DMSO
Immunoprecipitation (IP) antibody binding buffer	0.02% Tween 20 in PBS
L929	Sterile filtered supernatants from NCTC L-929 cell cultures in complete DMEM; Self-supplied
MAS buffer (3x)	0.66 M Mannitol, 0.21 M Sucrose, 0.03 M KH_2PO_4, 0.015 M $MgCl_2$, 6 mM HEPES, 3 mM EGTA
PBS (1x)	137 mM NaCl, 2.7 mM KCl, 10 mM Na2HPO4, 1.8 mM KH2PO4 in water
RIPA lysis buffer	20 mM Tris-HCl (pH = 7.4), 150 mM NaCl, 1 mM EDTA, 1% Triton X-100, 0.5% deoxycholate, 0.1% SDS, 10% glycerol; add fresh: cOmplete protease inhibitor, PhosSTOP inhibitor, PMSF 0.2 mM
Seahorse Assay Medium	RPMI-1640 (2 mM L-glutamine; glucose-free; bi-carbonate free; pH = 7.4)
TBS (1x)	100 ml 10x TBS, water to 1 l
TBST (1x)	100 ml 10x TBS, 1 ml Tween 20, water to 1 l

2.1.5 Primary antibodies for western blot and simple western

Antigen	Source	Clone	Supplier	Dilution
Acetylated lysine	rabbit	Polyclonal (9441)	Cell Signaling	1:1000
MPC1	rabbit	Monoclonal (D2L9I)	Cell Signaling	1:1000
MPC2	rabbit	Monoclonal (D4I7G)	Cell Signaling	1:1000

PPARɣ	rabbit	Monoclonal (81B8)	Cell Signaling	1:20 Wes/Jess
β-actin	mouse	926-42212	LI-COR	1:2000
β-actin	rabbit	926-42210	LI-COR	1:2000 / 1:20 Jess
iNOS/NOS2	rabbit	polyclonal	Abcam	1:1000

2.1.6 Secondary antibodies

Antigen	**Fluorophore**	**Source**	**Supplier**	**Dilution**
mouse IgG	IRDye® 680RD	donkey	LI-COR	1:25000
mouse IgG	IRDye® 800CW	goat	LI-COR	1:25000
rabbit IgG	IRDye® 800CW	donkey	LI-COR	1:25000
rabbit IgG	IRDye® 680RD	goat	LI-COR	1:25000
Rabbit IgG	HRP coupled	/	Protein Simple	Undiluted

2.1.7 Antibodies for flow cytometry

Antigen	**Dye**	**Catalog #**	**Supplier**	**Dilution**
CD19	APC	115512	Biolegend	1:100
CD86	PE	105008	Biolegend	1:200
CD80	FITC	104706	Biolegend	1:200
HLA-DR	BV510	107635	Biolegend	1:200
F4/80	BV421	123132	Biolegend	1:100
CD11b	BV711	101242	Biolegend	1:100
Ly6C	PerCP-Cy5-5	128012	Biolegend	1:200
Ly6G	PE-Cy7	127618	Biolegend	1:200
CD45	BUV395	564279	Biolegend	1:100
CD16/CD32	/	101301	Biolegend	1:100

2.1.8 Oligonucleotides for qPCR

Target	Type	Sequence	Code	Supplier
mIl6	FWD primer	CAAAGCCAGAGTCCTTCAGAG	QM0147	K. Pelka, Latz Lab
mIl6	RV primer	GTCCTTAGCCACTCCTTCTG	QM0148	K. Pelka, Latz Lab
mIl10	FWD primer	GAAGCATGGCCCAGAAATCA	QM0001	L. Labzin, Latz Lab
mIl10	RV primer	TCACAGGGGAGAAATCGATGA	QM0002	L. Labzin, Latz Lab
mIl12b	FWD primer	GGAAGCACGGCAGCAGAATA	QM0059	L. Labzin, Latz Lab
mIl12b	RV primer	AACTTGAGGGAGAAGTAGGAATGG	QM0060	L. Labzin, Latz Lab
mHprt	FWD primer	TGAAGTACTCATTATAGTCAAGGGCA	QM0009	L. Labzin, Latz Lab
mHprt	RV primer	CTGGTGAAAAGGACCTCTCG	QM0010	L. Labzin, Latz Lab
mTnf	FWD primer	CCAAATGGCCTCCCTCTCAT	QM0007	L. Labzin, Latz Lab
mTnf	RV primer	TGGTGGTTTGCTACGACGTG	QM0008	L. Labzin, Latz Lab

2.1.9 Software

Name	Version	Supplier
Compass for Simple Western	4.0.0	ProteinSimple
FlowJo	10.8	FlowJo LLC
Image Studio Lite 2	5.2.5	LI-COR
Morpheus	2022	Broad Institute
Office for Mac	16.16.27	Microsoft
Prism 9	8.4.3	GraphPad LLC

QuantStudio Real-Time PCR System	1.3	Life Technologies
R Studio	1.4.1103	RSutio, PBC
ROSALIND®	3.35.12.0	ROSALIND, Inc. (San Diego, CA)
Seahorse Wave Desktop	2.6.3	Agilent
SoftMax Pro	6.3.0	Molecular Devices
xPONENT for MagPix®	4.2.1324.0	Luminex

2.2 Methods

2.2.1 Mouse work

Wildtype C57BL6/J and Ticam$^{-/-}$ mice were purchased from Charles River. Pparγ$^{fl/fl}$ mice (B6.129-Pparg^{tm2Rev}/J (He et al., 2003)) were generously provided by Prof. Christoph Wilhelm and bred inhouse. Littermates of Pparγ$^{fl/fl}$;LysM-Cre$^{-/-}$ and Pparγ$^{-/-}$;LysM-Cre$^{+/-}$ mice were obtained by crossing LysM-Cre$^{+/-}$ mice with Pparγ$^{fl/fl}$ mice inhouse.

2.2.2 Isolation and freezing of murine bone marrow

Mice were euthanized by cervical dislocation. All subsequent isolation steps were carried out under sterile conditions. Hind-legs were dissected and sterilized using ethanol (70%; AplliChem). Afterwards, the hind-legs were flushed using DPBS (RT; Life Technologies) and the resulting cell solution was homogenized using a 70 µm cell strainer and kept on ice. Following, the cells were centrifuged at 350 x g for 5 minutes at 4°C. The supernatant was discarded and the cells were either directly taken into culture for differentiation or resuspended in 1 mL freezing medium per leg and transferred to 2 mL cryotubes. To allow slow cooling rates of the cell solution, cells were frozen down at -80°C in a Mr. Frosty freezing container provided with isopropanol. One day after freezing, cell vials were transferred to a -150°C freezer for long-term storage.

2.2.3 Differentiation and cell culture of bone marrow derived macrophages (BMDMs)

For BMDM differentiation either freshly isolated bone marrow cells or frozen cells were used. Frozen cells were thawed rapidly in a water bath at 37°C and diluted gently in 10 mL complete DMEM. Following, the cells were centrifuged (350 x g, 5 minutes, RT) and the

supernatant was discarded. For BMDM differentiation, cells were resuspended and cultured in complete DMEM (15% L929 supernatant (Sigma: 85011425-1VL)) in 15 cm TC dishes for 6 days in a humidified incubator at 37°C with 5% CO_2. At day 6, the cells were washed once with DPBS (RT) and detached by incubation for 5 minutes in 2 ml DPBS (5 mM EDTA (Invitrogen)) at 4°C. After 5 minutes, 8 mL complete DMEM was added to the cells. The detached cells were homogenized by pipetting up and down and transferred into a 50 mL Falcon. The residually adherent cells were scraped from the culture dishes, homogenized by pipetting and pooled with the previously harvested cells. Following, only viable cells were counted using a hemocytometer and Trypan blue (Sigma) and afterwards seeded into the respective plates for experiments.

2.2.4 In vitro knockout via tat-Cre recombinase

For in vitro knockout of PPARɣ, bone marrow cells from C57BL6/J PPARɣ$^{fl/fl}$ mice (B6.129-Pparg^{tm2Rev}/J (He et al., 2003)) were used. Bone marrow cells were differentiated into BMDMs in 6-well plates following the protocol described in section 2.1.2. On day 5 of differentiation, the medium was exchanged to sterile filtered complete DMEM (15% L929 supernatant (Sigma: 85011425-1VL)) supplemented with tat-Cre enzyme (10 µM final; Millipore) to induce recombination of the floxed PPARɣ gene and obtain PPARɣ$^{-/-}$ BMDMs. On day 7, cells were harvested and seeded into the appropriate plates following the protocol as described in section 2.1.2. Cells were incubated overnight at 37°C with 5% CO_2 before they were used for experiments.

2.2.5 Nitric oxide measurements

For nitric oxide measurements, 8.0 x 10^4 cells per well were seeded in complete DMEM into 96-Well plates and incubated overnight in a humidified incubator at 37°C with 5% CO_2 for adherence. Next day, the medium was exchanged to complete DMEM containing the respective compounds at their final concentrations. The cells were incubated for 1 hour and subsequently stimulated with LPS (10 ng/mL) and recombinant mouse IFNɣ (100 µg/mL). After 24 hours, cells were spun down (350 x g, RT, 3 minutes) and the supernatants were collected into a fresh 96-Well plate. Nitrite concentrations were measured directly using the Griess reagent system (Promega).

2.2.6 Stimulation of BMDMs for cytokine measurements

For cytokine measurements, 8.0 x 10^4 cells per well were seeded in complete DMEM into 96-Well plates and incubated overnight in a humidified incubator at 37°C with 5% CO_2 for adherence. Next day, the medium was exchanged to complete DMEM containing the respective compounds at their final concentrations. For PPARɣ inhibition experiments, medium was exchanged to complete DMEM containing GW9962 (5µM) for 30 minutes and compounds were added to the wells directly to their respective final concnetrations. The cells were incubated for the indicated time points with the respective compounds and subsequently stimulated with inflammatory stimuli. After the indicated time points of inflammatory stimulation, the cells were spun down (350 x g, RT, 3 minutes) and the supernatants were collected into a fresh 96-Well plate. Supernatants were stored at -20°C.

2.2.7 Cytokine detection by ELISA

Concentrations of secreted mouse cytokines were measured in 96-Well format using the respective ELISA kits from R&D. Samples were either measured freshly or thawed on ice prior to the addition to the ELISA plates. Plates were coated with capture antibodies overnight at RT, washed three times with 300 µL washing buffer (PBS, 0.05% Tween20) and subsequently blocked for 1 hour with reagent solution (PBS, 1% BSA). Afterwards, 50 µL of serially diluted standard or respective dilutions of samples were added to the wells and incubated either 2 hours at RT or overnight at 4°C. Following, plates were washed three times with 300 µL washing buffer and incubated with 50 µL per well of detection antibodies for 2 hours at RT or overnight at 4°C. Plates were washed three times with 300 µL washing buffer, followed by the addition of 50 µL Streptavidin-HRP and incubation for 20 minutes in the dark. After washing of the plates 3 times with 300 µL washing buffer, 50 µL of substrate solution was added to the wells and incubated for 5 – 15 minutes in the dark until the reaction was stopped by the addition of 25 µL 2N H_2SO_4. The optical density of the wells was determined using the Spectramax i3 multi-mode detection platform. Readings at 570 nm were subtracted from readings at 450 nm for background correction. The cytokine concentrations were interpolated from the optical density values of the standard curve.

2.2.8 Multiplexed cytokine detection

Serum and peritoneal lavage concentrations of mouse cytokines were measured in 96-Well format using a 9-plex mouse cytokine magnetic panel (MCYTOMAG-70K-09; Milliplex) according to the manufacturer's instructions. Samples were thawed on ice, vortexed shortly and spun down at 1000 x g for 5 minutes at 4°C prior to the measurement. Serum samples were diluted 1:2 using the provided assay buffer while peritoneal lavage samples were measured undiluted. Throughout the assay, samples, standards and quality controls were protected from illumination. Samples, standards and quality controls were incubated with the provided beads overnight at 4°C on a plate shaker. Next day, beads were immobilized magnetically and washed 2x with 200 µL provided wash buffer. Beads were resuspended in 25 µL of detection antibody solution and incubated for 2 hours at RT on a plate shaker. Afterwards, 25 µL per well of streptavidin-phycoerythrin were added and incubated for 30 minutes at RT on a plate shaker. Beads were immobilized magnetically and washed 2x with 200 µL wash buffer and resuspended in 150 µL MagPix drive fluid (Millipore). Cytokine concentrations were measured on a MagPix instrument (Luminex).

2.2.9 Cell viability assay

Cell viability was measured in 96-Well plates using the CellTiter-Blue® (CTB) cell viability assay. As a negative control, cells were incubated for 2 minutes with 100% ethanol and washed once with DPBS prior to the assay. After removal of supernatants, 50 µL per well of the CTB solution was added to the cells. Cells were incubated in a humidified incubator at 37°C with 5% CO2 for approximately 40 min. Afterwards, the fluorescent signal was detected using the Spectramax i3 multi-mode detection platform using a 560/590 nm excitation/emission filter. For analysis, the mean of the signals derived from the negative controls was subtracted from the signals detected from the cells. The resulting values of the treated cells were compared to the untreated cells and depicted as the percentage of the relative fluorescence.

2.2.10 RNA isolation

For the RNA isolation, 1.0 x 10^6 cells per well were seeded into 12-well plates. For stimulation, the whole medium was exchanged and cells were incubated for the indicated time

frames with the respective compounds. Afterwards, the cells were washed once with DPBS and lysed in RLT Buffer (1% (v/v) β-Mercaptoethanol) for 5 minutes at RT. The resulting lysates kept at -80°C or directly used for RNA isolation. The RNA was isolated using the RNeasy Mini Kit (Qiagen) according to the manufacturer's instructions. RNA concentrations were assessed by measuring the absorbance at 260 nm using the Epoch Microplate Spectrophotometer (BioTek). RNA was stored at -80°C.

2.2.11 First strand cDNA synthesis

cDNA was reverse transcribed from mRNA using primers that bind to the poly(A) tail of the mRNA and a reverse transcriptase. For each sample, 500 ng of RNA was brought to a volume of 12.9 µL by addition of nuclease free water. 1 µL of oligo(dT)18 primer was added to the RNA and the mix was incubated at 65°C for 5 minutes to denature the mRNA secondary structure. Samples were then cooled down on ice for 1 minute to allow primer annealing to the mRNA. Sequentially, 4 µL of 5x first-strand buffer, 1 µL of 10 mM dNTPs, 1 µL of 0.1 M DTT and 0.1 µL of SuperScript III reverse transcriptase were added to the mix. Additionally, an RNA pooled control that did not contain the reverse transcriptase was prepared. Tubes were spun down and incubated for 50 minutes at 50°C to allow reverse transcription and subsequently heated up to 85°C for 5 minutes to denature the transcriptase. cDNA was diluted 1:5 with nuclease-free water and either freshly used for quantitative PCR (qPCR) or stored at -20°C for later use.

2.2.12 Quantitative PCR (qPCR)

qPCR was performed using the fluorescent DNA-binding dye SYBR Green in a 384-well format on a QuantStudio 6 Flex Real-Time PCR system. 2 µL of pre-diluted cDNA was mixed with 5 µL of SYBR® Green, 2 µL of a mix containing 2 µM of both forward and reverse primers and 1 µL of nuclease-free water. Each sample was run in duplicates, and no-template control reactions were also introduced. Samples underwent a 40-cycles program and each cycle consisted in three steps: a holding step at 95°C for 10 minutes, a denaturation step at 95°C for 15 s and an annealing/extension step at 60°C for 60 s. Following the thermal cycling protocol, a melting profile was obtained to confirm the specificity of the real-time qPCR reaction by melting curve analysis. The relative mRNA expression

to the housekeeping gene hypoxanthine-guanine phosphoribosyltransferase (Hprt) was calculated using the $\Delta\Delta C_t$ method and mRNA fold change data were presented as $2^{-\Delta\Delta Ct}$.

2.2.13 Nanostring multiplexed mRNA quantification

Multiplexed mRNA quantification of PPARγ$^{fl/fl}$;LysM-Cre$^{-/-}$ or PPARγ$^{fl/fl}$;LysM-Cre$^{+/-}$ BMDMs was performed on the nCounter MaxFlex system (Nanostring) using the XT mouse V2 inflammation panel according to the manufacturer. For each reaction, 100 ng of purified mRNA (protocol described in 2.1.7) was used as input material. For codeset hybridization of mRNA, 8 µL of the reporter probe was combined with 5 µL of RNA solution, followed by the addition of 2 µL of the capture probes. Samples were mixed by flicking, centrifuged shortly and incubated at 65°C (heated lid at 72°C) for 20 – 30 hours. After hybridization, the samples were immediately transferred to the MaxFlex liquid handling system for target mRNA purification and immobilization. Cartridges with immobilized mRNA were sealed directly after target immobilization and imaged on the MaxFlex imaging system for target mRNA quantification. Data was analyzed using ROSALIND® (https://rosalind.bio/), with a HyperScale architecture developed by ROSALIND, Inc. (San Diego, CA). Read Distribution percentages, violin plots, identity heatmaps, and sample MDS plots were generated as part of the QC step. Normalization, fold changes and p-values were calculated using criteria provided by Nanostring. ROSALIND® follows the nCounter® Advanced Analysis protocol of dividing counts within a lane by the geometric mean of the normalizer probes from the same lane. Housekeeping probes to be used for normalization are selected based on the geNorm algorithm as implemented in the NormqPCR R library (Perkins et al., 2012). Final heatmap was prepared using Morpheus (https://software.broadinstitute.org/morpheus) while Volcano plots were prepared using GraphPad Prism.

2.2.14 Extracellular flux analysis of BMDMs

Oxygen consumption rate (OCR) and extracellular acidification rate (ECAR) were measured on a Seahorse XFe96 analyzer using XF96 cell culture plates, XFe96 sensor cartidges and Seahorse XF Calibrant solution. Cells were seeded in complete DMEM at 8.0×10^4 per well and incubated in a humidified incubator at 37°C with 5% CO_2. In addition, a sensor cartridge was incubated in calibration buffer in a non-carbonated incubator

at 37°C overnight. Next day, the cells were stimulated by addition of LPS (*E. coli* O111:B4; 10 ng/mL final) and incubated for the indicated time frames in a humidified incubator at 37°C with 5% CO_2. Next, cells were washed three times with prewarmed 37°C Seahorse Assay medium (RPMI-1640; 2 mM L-glutamine; glucose-free; bi-carbonate free; pH = 7.4). Compounds were added to the cells in Seahorse assay medium (supplemented with LPS to 10 ng/mL final) at their final concentrations to a final volume of 180 µL. Cells were incubated for 1 hour in a non-carbonated incubator at 37°C. Meanwhile, the sensor cartridge was prepared for the injection of glucose (Port A; 20 µL to 10 mM final), oligomycin (Port B; 22 µL to 1 µM final), FCCP (Port C; 25 µL to 2 µM final), antimycin A (Port D; 28 µL to 0.5 µM final) and rotenone (Port D; 28 µL to 2.5 µM final) and transferred to the Seahorse XFe96 analyzer for equilibration. After incubation, the cells were transferred to the Seahorse XFe96 analyzer and measured. The assay was run using the Seahorse Wave Desktop Software.

2.2.15 Measurement of mitochondrial pyruvate utilization in permeabilized BMDMs

The oxygen consumption rate (OCR) and extracellular acidification rate (ECAR) of permeabilized BMDMs were measured on a Seahorse XFe96 analyzer using XF96 cell culture plates, XFe96 sensor cartridges and Seahorse XF Calibrant solution. Cells were seeded in complete DMEM at 8.0 x 10^4 per well and incubated overnight in a humidified incubator at 37°C with 5% CO_2. In addition, a sensor cartridge was incubated in calibration buffer in a non-carbonated incubator at 37°C overnight. Next day, the sensor cartridge was prepared for the injection of Mitoglitazone (50 µM final) or UK5099 (50 µM final) or the Vehicle (DMSO) control into Port A, FCCP (1 µM final) into Port B as well as Antimycin A and Rotenone (1 µM and 5 µM final) into Port C and placed into the Seahorse XFe96 analyzer. Following, the whole medium of the cells was removed and the cells were washed once with 1x MAS buffer (0.2 % BSA). The medium was removed and 1x MAS buffer (0.2 % BSA, 4 mM ADP, 0.5 mM Malate, 2 mM DCA, 5 mM Pyruvate, 2 µM Oligomycin, 1 nM rPFO) was added to the wells. Where appropriate, the 1x MAS buffer was supplemented with 10 mM MePyruvate prior to the addition to the cells. The cells were directly placed into the Seahorse XFe96 analyzer and measured. The assay was run using the Seahorse Wave Desktop Software (Baseline measurement 5x;

Ports A & C 3x, Port B 6x; Measure 0.5 minutes, Wait 0.5 minutes, Mix 2 minutes). An equilibration step was omitted to minimize a temporal delay.

2.2.16 Isotopic labeling, metabolite extraction, and mass-spectrometric analysis of metabolites

Isotopic labeling experiments were performed in collaboration with Antonia Henne and Wei He (Hiller lab Braunschweig). The day prior to the experiment, BMDMs were seeded into 6-well plates at 1.0 x 10^6 cells per well in complete DMEM and incubated for 3 hours at 37°C with 5% CO_2. Afterwards, the medium was exchanged to 1 mL DMEM (A1443001) supplemented with U-$^{13}C_6$-glucose (25 mM), U-$^{13}C_5$-glutamine (4 mM) or $^{13}C_1$-glutamine (4 mM). For carbon tracing from U-$^{13}C_6$-glucose or stable isotope labeled glutamine, medium was additionally supplemented with L-glutamine (4 mM) or D-glucose (25 mM), respectively. Cells were incubated overnight at 37°C with 5% CO_2 to equilibrate isotope labeling of cellular metabolites. Next day, the medium was exchanged to 1 mL stable isotope supplemented medium containing the respective compounds at their indicated concentrations. Cells were incubated for 1 hour with the respective compounds and subsequently activated with LPS (10 ng/mL) for 3 hours in technical triplicates for each biological replicate. Afterwards, cells were washed once with sterile filtered NaCl solution (0.9% (w/v)) and placed on ice. Following steps were carried out on ice or at 4°C. Sequentially, 250 µL methanol (precooled to -20°C) and 250 µL internal standard solution (MilliQ water, 1 µg/mL pentanedioic-d6 acid; precooled on ice) were added to each well. Cells were scraped thoroughly and the cellular lysates were transferred to new Eppendorf tubes containing 250 µL chloroform (precooled at -20°C). Cell lysates were mixed in a shaker at 1400 rpm for 20 min and subsequently centrifuged at 17,000 x g for phase separation. 300 µL of the upper (polar) phase was transferred into new Eppendorf tubes (precooled at -20°C) and stored at -80°C. Metabolite preparation and mass-spectrometric analysis were carried out in the Hiller lab. Samples were thawed on ice transferred to glas vials with micro inserts and evaporated under vacuum at 4°C. The dried metabolites were derivatized using equal amounts of methoxyamine hydrochloride (20 mg/ml in pyridin) and N-methyl-N-(tert-butyldimethylsilyl) trifluoroacetamide (MTBSTFA). After injection of the first derivatization reagent the vials were incubated at 55°C for 30 minutes, followed by injection of the second reagent and additional incubation

for 90 minutes at 55°C. For each sample, 1 µL was injected into a SSL injector at 270°C in splitless mode. Measurement was performed using a 7890A GC System from Agilent coupled to a 5975C inert XL MSD. The GC was equipped with a 30 m ZB-35 column from Zebron and helium was used as a carrier gas with a flow rate of 1 mL/minute. The intial oven temperature of 100°C was maintained for 2 min, followed by a temperature increase of 10°C/minute until reaching 300°C. The Agilent 5975C inert XL MSD was operating under electron ionization at 70 eV, the source was held at 230°C and the quadrupole at 150°C. The measurement was operated in selected ion monitoring mode. For normalization of recorded signals, pentanedioic-d6 acid was added during metabolite extraction as an internal standard. The software MetaboliteDetector (Hiller et al., 2009) was used to process all GC-MS chromatograms and to determine relative metabolite levels as well as their mass isotopomer distributions (MIDs) corrected for natural isotope abundance and normalized to the pentanedioic-d6 acid internal standard.

2.2.17 Glucose uptake and lactate secretion measurements

Glucose uptake of and lactate secretion by BMDMs were measured using the YSI Biochemistry Analyzer (YSI) in collaboration with Antonia Henne (Hiller lab, Braunschweig). Supernatants from U-$^{13}C_6$-glucose fed BMDMs treated as described in section 3.1.12 were used to measure lactate and glucose concentrations in technical duplicates. Glucose uptake was determined by subtracting supernatant glucose concentrations of cells treated with the respective compounds from glucose concentrations in control medium.

2.2.18 Immunoblot sample preparation from cells

Cells were lysed on ice in ice cold RIPA buffer, cell lysates were transferred into Eppendorf tubes and spun down at 16,000 x g for 10 minutes at 4°C.Supernatants were collected into fresh Eppendorf tubes and sample protein concentrations were measured using the Pierce™ BCA Protein Assay Kit. Samples were adjusted to the same protein concentration and prepared in LDS Sample buffer containing DTT for the reduction of di-sulfide bonds. Following, samples were heated up to 95°C for 10 min and either directly subjected to SDS-PAGE or stored at -20°C.

2.2.19 Immunoprecipitation of proteins from cell lysates

BMDMs were seeded into 6-Well plates on the day prior to the experiment and incubated at 37°C with 5% CO_2. Next day, medium was exchanged to complete DMEM and LPS (10 ng/mL) was added to the cells. After 3 hours, cells were lysed in ice cold RIPA buffer and lysates were prepared as described in 2.1.15. For input samples, 15 µL of lysates were transferred into new Eppendorf tubes and stored at -20°C. For pulldown of MPC1 or MPC2, 4 µL of α-MPC1 or α-MPC2 antibody were added to 200 µL of cell lysate (1:50 ratio) and incubated for 3 hours at 4°C on a rotator. 50 µL of protein G Dynabeads were washed twice with PBS and resuspended in the lysate-antibody solutions. Samples were incubated with the beads for 30 minutes at RT on a rotator. Beads were immobilized magnetically and 15 µL of supernatants were collected into new Eppendorf tubes for the flowthrough controls. Afterwards, beads were washed three times with PBS and resuspended in LDS buffer containing DTT. Samples were stored at -20°C until further use.

2.2.20 SDS-PAGE and immunoblotting of cell lysates

Separation of proteins by SDS-PAGE and transfer of separated proteins onto membranes was performed using the Mini Gel Tank system of Invitrogen. Samples were loaded onto 4 – 12% Bis-Tris-gels along with 3 µL of PageRuler^{TM} Plus prestained protein ladder. Proteins were separated under denaturing and reducing electrophoretic conditions at 150 V in MOPS or MES buffer. The separated proteins were transferred to an Immobilon-FL PVDF membrane using transfer buffer at 18 V for 1 hour. The membranes were blocked with TBS (3% BSA) for 1 hour at RT to prevent non-specific antibody binding and afterwards incubated with primary antibodies in TBST (3% BSA) overnight at 4°C. Following, the membranes were washed three times for 10 minutes with TBST and incubated with the secondary antibody in TBST (3% BSA) for 1 hour at RT. Afterwards, the membranes were washed twice with TBST and twice with TBS for 5 minutes. The resulting signals were detected using the LI-COR Odyssey Infrared Imaging System and the Image Studio Lite 2 software.

2.2.21 Immunoblotting of cell lysates by simple western (Wes and Jess)

Protein concentrations determined by BCA assay of each sample were adjusted to the same concentrations. Four parts of the lysates were combined with one part of the 5x Fluorescent Master Mix containing a fluorescently labeled standard, DTT and Sample Buffer, and were denatured by incubation at 95°C for 5 minutes. The samples, a biotinylated ladder, the primary antibodies, streptavidin-HRP, the secondary antibody, the chemiluminescent substrate, replex reagent (Jess) and wash buffer were loaded into a pre-filled microplate with Split Running Buffer, Wash Buffer and 10x Sample Buffer as indicated by the manufacturer. Samples were electrophoretically separated and detected in a 25-capillary cartridge (12 – 230 kDa) using the following protocol: 200 s loading time of the separation matrix, 15 s loading time of the stacking matrix, 9 s loading time of the sample, 25 minutes separation time of the sample at 375 V, 90 minutes incubation with the primary antibody and 30 minutes incubation with the secondary antibody. For capillary replexing the default protocol was used. Results were analyzed with the Compass for Simple Western software.

2.2.22 In vivo mouse work

In vivo mouse work was performed in collaboration with Prof. Zeinab Abdullah and Celia Kho. 8 weeks old male C57BL/6 mice (Charles River) were treated with 50 µL of Mitoglitazone (30 mg/kg) or Vehicle (1% (w/v) methyl-cellulose cP400, 0.01% (v/v) Tween80) via oral gavage. After 2 hours, mice were injected interperitoneally with a sublethal dose of LPS (5 mg/kg; LPS-EK Ultrapure) or PBS. Mice were monitored regularly in regards to their clinical score and weighed every two hours. After 8 hours, mice were sacrificed and blood as well as the peritoneal cells were collected. Blood was collected into Eppendorf tubes, centrifuged at 1000 x g for 10 minutes at 4°C and serum was transferred into a 96-Well plate for storage at -20°C until cytokine measurement. Peritoneal cells were collected in 4 mL of ice-cold PBS. Cells were centrifuged at 350 x g for 5 minutes at 4°C, supernatant (peritoneal lavage) was collected in a 96-Well plate and stored at -20°C until cytokines measurement. Peritoneal cells were resuspended in antibody master mix (FACS buffer containing NIR live dead 1:1000, anti-CD19-APC 1:100, anti-CD86-PE 1:200, anti-CD80-FITC 1:200, anti-HLA-DR-BV510 1:200, anti-F4/80-BV421 1:100, anti-CD11b-BV711 1:100, anti-Ly6C-PerCP-Cy5-5 1:200, anti-Ly6G-PE-Cy7 1:200, anti-CD45-BUV395

1:100, anti-CD16/CD32 1:100). Cells were stained for 20 minutes at 4°C, centrifuged at 350 x g for 5 minutes at 4°C and washed once with 200 µL cold PBS. Stained cells were incubated in fixation buffer (PBS containing 2% glucose, 0.02% sodium azide, 1% formaldehyde) for 15 minutes on ice. Afterwards, cells were washed twice with PBS, resuspended in FACS buffer and stored at 4°C overnight protected from illumination. Stained cells were measured on a BD LSR Fortessa (BD Biosciences) and results were analyzed using FlowJo.

3 Results

3.1 Mitoglitazone decreases glycolysis in inflammatory macrophages

Inhibition of the mitochondrial pyruvate carrier (MPC) with the tool compound UK5099 decreases mitochondrial respiration and the secretion of inflammatory cytokines from LPS activated macrophages (Lauterbach et al., 2019). To harness the potential of MPC inhibition, clinically applicable small molecule inhibitors are warranted to modulate macrophage-facilitated inflammation under pathological conditions. In 2013, it was shown that Glitazones inhibit the MPC (Divakaruni et al., 2013). Therefore, it was investigated whether Mitoglitazone (Mito), a newly developed Glitazone with reduced PPARɣ affinity but retained inhibitory MPC efficacy, can serve as a metabolic modulator of inflammatory macrophages.

Extracellular flux analysis was used to investigate the utilization of glucose in glycolysis and mitochondrial respiration of live cells. While glycolysis leads to the gradual acidification of the cellular environment, mitochondrial respiration is the primary consumer of cellular oxygen. Therefore, the extracellular acidification rate (ECAR) and the cellular oxygen consumption rate (OCR) were monitored after the sequential injection of glucose, specific electron transport chain inhibitors and the membrane uncoupling agent FCCP (Fig. 1 A). Each sequential injection allows to investigate differential aspects of cellular glycolysis (Fig. 1 B) and mitochondrial respiration (Fig. 2 A). It was first investigated whether Mito modulates glycolysis after LPS activation of macrophages. Therefore, BMDMs were stimulated with LPS for 2 hours, incubated with Mito or UK5099 for 1 hour and subjected to extracellular flux analysis (Fig. 1 C, D, E). Activation of BMDMs with LPS increased their basal glycolysis and their glycolytic capacity while the glycolytic reserve remained unchanged (Fig. 1 F, G, H). Inhibition of the MPC via UK5099 decreased the basal glycolysis and the glycolytic capacity of non-activated and LPS activated macrophages (Fig. 1 D, F, G). Simultaneously, UK5099 treatment did not affect the glycolytic reserve (Fig. 1 H). Treatment of BMDMs with Mito also showed a decrease of their glycolytic capacity regardless of their activation state (Fig. 1 G). In contrast to UK5099, Mito decreased the basal glycolysis of LPS activated macrophages, but did not affect the unstimulated cells (Fig. 1 E & F). Interestingly, Mito treatment also reduced the glycolytic reserve of the unstimulated and the LPS activated BMDMs (Fig. 1 H). It was further tested whether

UK5099 and Mito could modulate glycolysis in macrophages activated by other danger signals. Therefore, BMDMs were treated with the TLR7/8 agonist R848 (ssRNA mimicking a viral infection) for 2 hours and then incubated with UK5099 or Mito for 1 hour. As was previously demonstrated for dendritic cells and BMDMs (Everts et al., 2014; Tan & Kagan, 2019), stimulation with R848 also increased glycolysis in BMDMs (Fig. 1 I & J). As in LPS activated BMDMs, both UK5099 (Fig. 1 I) and Mito (Fig. 1 J) inhibited upregulation of glycolysis after the activation of BMDMs with R848. Regardless of Mito-facilitated glycolysis inhibition, cells remained viable in presence of all tested Mito concentrations (Fig. 1 K).

Mitochondrial respiration is upregulated within the first hours of inflammatory activation of macrophages, but is decreased after longer stimulation times. Instead, glycolysis and the conversion of pyruvate into lactate provide the necessary ATP and NAD^+ to sustain macrophage effector functions (Cameron et al., 2019; Rodríguez-Prados et al., 2010). Therefore, it was tested whether UK5099 and Mito decreases the glycolytic activity of macrophages after a prolonged inflammatory LPS stimulation for 24 hours (Fig. 1 L). Prolonged stimulation of macrophages with LPS showed the expected increase of glycolysis (Fig. 1 M & N). Of note, incubation of the cells with UK5099 showed no modulation of glycolysis (Fig. 1 M), whereas Mito sustained the inhibition of glycolysis in the long-activated BMDMs (Fig. 1 N).

Together, these findings demonstrate that Mito can acutely inhibit the glycolytic switch of inflammatory macrophages after recognizing different danger signals without negatively affecting cell viability. Moreover, Mito inhibits glycolysis even after long LPS activation, suggesting that glycolysis-dependent macrophage effector functions at later activation stages might be modulated by Mito treatment.

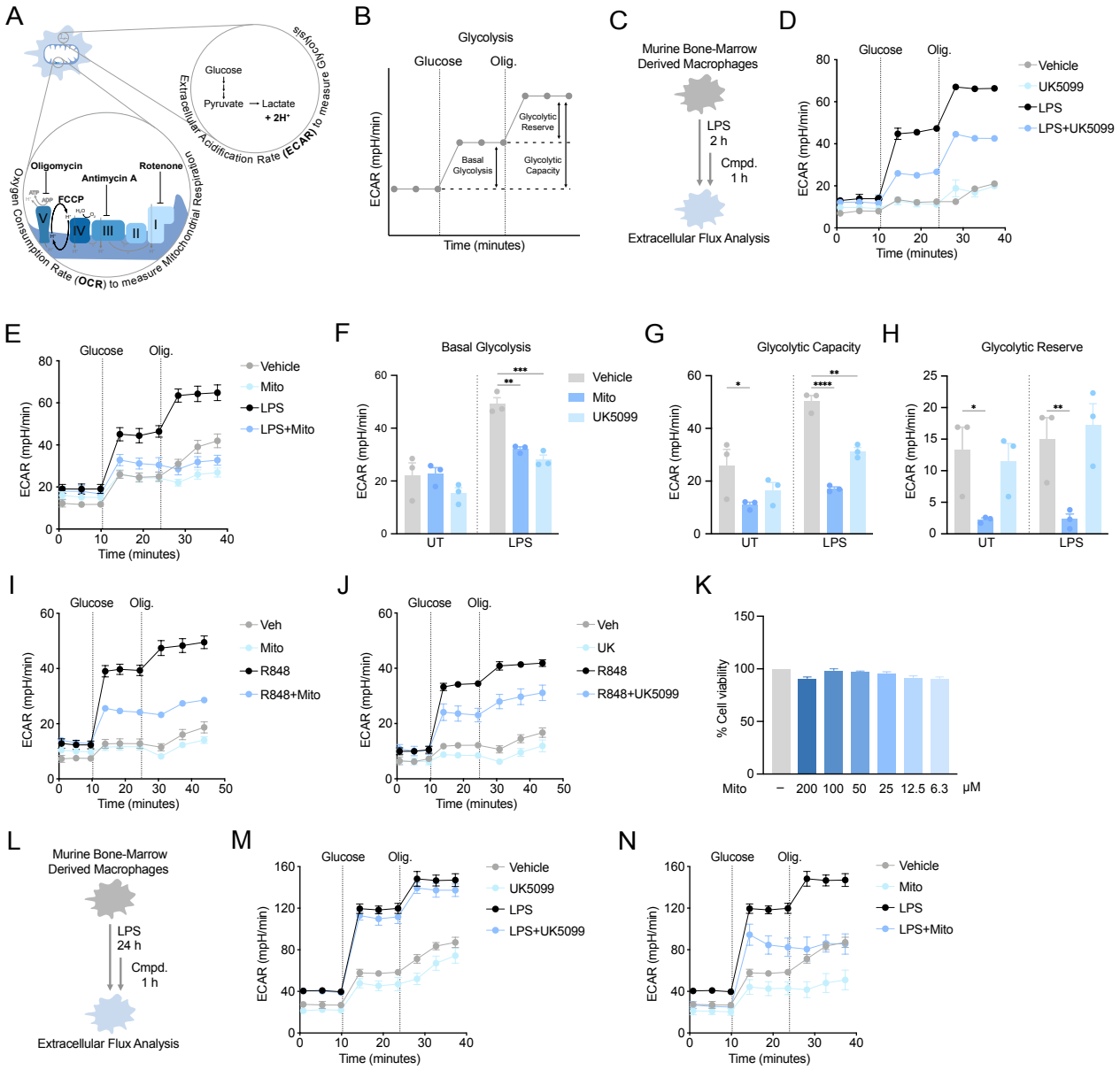

Fig. 1: Mitoglitazone inhibits the glycolytic burst of inflammatory macrophages. **A:** Scheme representing the measurement of the extracellular acidification rate (ECAR) indicating cellular glycolytic activity and oxygen consumption rate (OCR) indicating mitochondrial respiration. Treatment of cells with glucose, different inhibitors of the electron transport chain (ETC) or the uncoupling agent FCCP enables to monitor different components of cellular glycolysis and mitochondrial respiration. **B:** Exemplary graph of real-time ECAR measurement from live cells indicating the different measurable components of cellular glycolysis. **C:** Scheme representing the treatment of murine bone marrow-derived macrophages (BMDMs) to investigate the acute effect of Mito towards the metabolism of inflammatory macrophages via extracellular flux analysis. **D & E:** Representative graphs of ECAR measurements of Lipopolysaccharide (LPS; 10 ng/mL) activated BMDMs after injection of glucose and oligomycin (Olig.). Cells were treated with the covalent MPC inhibitor UK5099 (50 µM) or Mito (50 µM) as indicated in D. n = at least 5 biol. replicates from independent experiments. **F – H:** Basal glycolysis, glycolytic capacity and glycolytic reserve of BMDMs after activation with LPS and treatment with UK5099 or Mito as

indicated in D. Mean ± SD of n = 3 biol. replicates from independent experiments **I & J:** Representative ECAR measurements of BMDMs treated with the TLR7/8 agonist R848 (10 ng/mL) and UK5099 or Mito as indicated in D. n = 2 biol. replicates **K:** Cell viability of BMDMs upon incubation with increasing concentrations of Mito for 24 hours. **L:** Scheme representing the treatment of BMDMs to investigate the effect of Mito towards the metabolism of inflammatory macrophages after 24 hours of LPS stimulation. **M & N:** Representative graphs of ECAR measurements of inflammatory BMDMs treated with the covalent MPC inhibitor UK5099 or Mito as indicated in L (n = 1). Statistical significance was determined via 2-way ANOVA using Dunnett's multiple comparison test. Adjusted p-value: 0.03 (*), 0.0021 (**), 0.0002 (***), < 0.0001 (****)

3.2 Mitoglitazone decreases mitochondrial oxygen consumption of inflammatory macrophages

Within the first hours of inflammatory activation, macrophages increase their respiratory capacity to supply the necessary energy and building blocks required for their inflammatory response. A key step to enable increased mitochondrial respiration is the MPC-facilitated import of the glycolytic end product pyruvate into the mitochondria. Therefore, it was investigated whether Mito modulates the mitochondrial respiration of inflammatory activated macrophages. Sequential injection of oligomycin, FCCP and antimycin A together with rotenone were performed while monitoring the oxygen consumption rate (OCR) of cells in real-time (Fig. 2 A). These experiments provide insights into different parts of mitochondrial function and potential perturbations. BMDMs were treated with LPS for 2 hours, incubated with UK5099 or Mito for 1 hour and analyzed by extracellular flux analysis to assess their OCR (Fig. 2 B – D). Activation of the cells with LPS resulted in increased basal respiration, a moderate increase in ATP-linked respiration and increased maximal respiration (Fig. 2 E – G). While the treatment of the cells with UK5099 did not affect the basal- or ATP-linked respiration (Fig. 2 E & F), it decreased the spare respiratory capacity (SRC) and with it the maximal respiration of LPS activated BMDMs (Fig. 2 G & H). Similar to UK5099, the treatment of the cells with Mito decreased the SRC and maximal respiration of LPS activated BMDMs. Additionally, Mito treatment increased the basal- and ATP-linked respiration of LPS activated BMDMs (Fig. 2 D – F). Mito treatment of R848 activated BMDMs showed similar modulation of mitochondrial respiration compared to the LPS activated cells (Fig. 2 I – J).

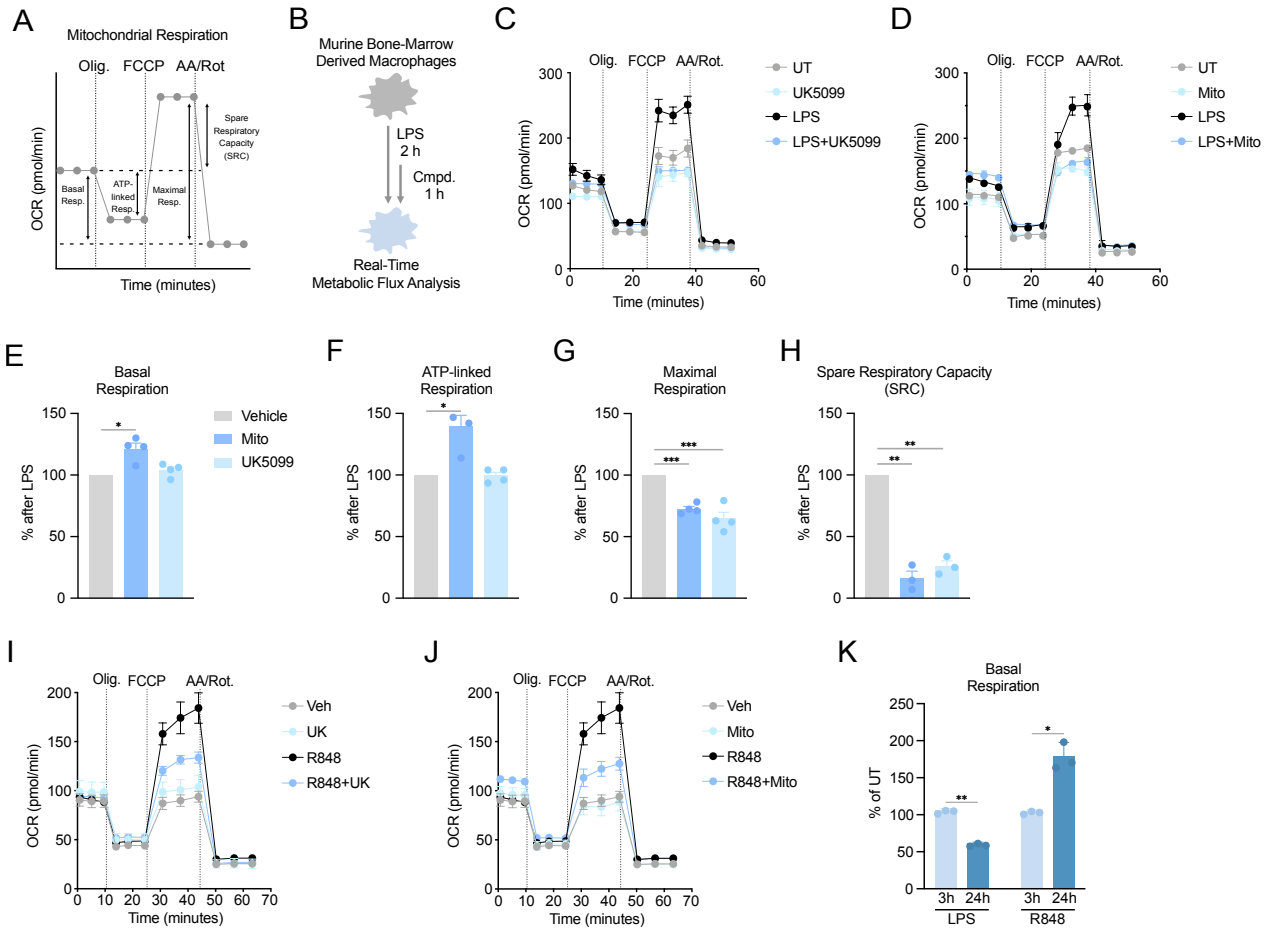

Fig. 2: Mitoglitazone inhibits the increased mitochondrial respiration of inflammatory macrophages. **A:** Exemplary graph indicating the different measurable components of mitochondrial metabolism by real-time oxygen consumption rate (OCR) measurement from live cells. Different components of mitochondrial metabolism can be investigated via sequential injection of oligomycin (Olig.), FCCP or antimycin A together with rotenone. **B:** Scheme representing the treatment of BMDMs to investigate the acute effect of Mito towards their mitochondrial respiration after inflammatory activation and treatment with UK5099 or Mito. **C & D:** Representative graphs of OCR measurements of LPS (10 ng/mL) activated BMDMs after injection of glucose and oligomycin. Cells were treated with the covalent MPC inhibitor UK5099 (50 µM) or Mito (50 µM) as indicated in B. n = at least 5 biol. replicates from independent experiments **E – H:** Basal respiration, ATP-linked respiration, maximal respiration and spare respiratory capacity of BMDMs after activation with LPS and treatment with UK5099 or Mito as indicated in B. Mean ± SD of n = 3 or 4 biol. replicates from independent experiments **I & J:** Representative OCR measurements of BMDMs treated with the TLR7/8 ligand R848 (10 ng/mL) and UK5099 or Mito as indicated in B. (n = 2 biol. replicates) **K:** Basal respiration of BMDMs treated for 3 or 24 hours with LPS or R848. Mean ± SD of n = 3 biol. replicates. Statistical significance was determined via 2-way ANOVA using Dunnett's multiple comparison test. Adjusted p-value: 0.03 (*), 0.0021 (**), 0.0002 (***), < 0.0001 (****)

Both, UK5099 and Mito inhibited the increase in SRC elicited by R848. Moreover, Mito increased the basal respiration of the cells while UK5099 showed no effect. The basal respiration of BMDMs stimulated with LPS for 24 hours was decreased compared to the cells that were stimulated for 3 hours (Fig. 2 K). Notably, BMDMs stimulated with R848 for 24 hours showed the opposite phenotype compared to the LPS treated cells. Treatment of the cells for 24 hours with R848 increased their basal respiration compared to 3 hours stimulation. This indicates a sustained metabolic dependency of the cells on mitochondrial respiration after prolonged TLR7/8 signaling (Fig. 2 K).
These findings demonstrate that Mito inhibits the increase in maximal mitochondrial respiration following short inflammatory stimulation of BMDMs with different TLR ligands in a similar manner to the MPC inhibitor UK5099. In addition, macrophages activated with TLR ligands resembling bacterial or viral infection showed time-dependent differences in their mitochondrial metabolism This suggests that their metabolism may change differentially dependent on their recognition of bacterial or viral danger signals.

3.3 Mitoglitazone inhibits the MPC in macrophages

Although Mito exhibited similar effects towards glycolysis and mitochondrial metabolism compared to UK5099, the earlier described differences raised the question whether Mito might affect processes downstream of mitochondrial pyruvate import. Therefore, it was investigated whether Mito directly inhibits the MPC or whether it targets the pyruvate to acetyl-CoA converting pyruvate dehydrogenase complex (PDH). As described by Divakaruni *et al.* (2013), perfringolysin O permeabilization and supplementation with a substrate of interest followed by the measurement of mitochondrial OCR allows investigating specific mitochondrial substrate utilization while circumventing the perturbation of mitochondrial integrity. Therefore, BMDMs were permeabilized with perfringolysin O and supplemented with pyruvate or methyl-pyruvate as carbon source (Fig. 3 A). Methyl-pyruvate can bypass the pyruvate import via the MPC and directly transfuse into the mitochondrial matrix. During extracellular flux analysis, cells were treated with vehicle, UK5099 or Mito, followed by the sequential injection of FCCP and antimycin A together with rotenone to investigate mitochondrial pyruvate utilization. Permeabilized BMDMs treated with the vehicle control could utilize pyruvate, as indicated by the increased OCR after FCCP injection. When the cells were treated with UK5099 (Fig. 3 B) or Mito (Fig. 3 C), FCCP injection

evoked no increase in mitochondrial OCR indicating diminished pyruvate utilization. In contrast, methyl-pyruvate supplementation of permeabilized cells treated with UK5099 or Mito rescued mitochondrial pyruvate metabolism (Fig. 3 B & C).

Overall, these findings demonstrate that Mito blocks the import of pyruvate into mitochondria and subsequent utilization of pyruvate in mitochondrial metabolism via inhibition of the MPC.

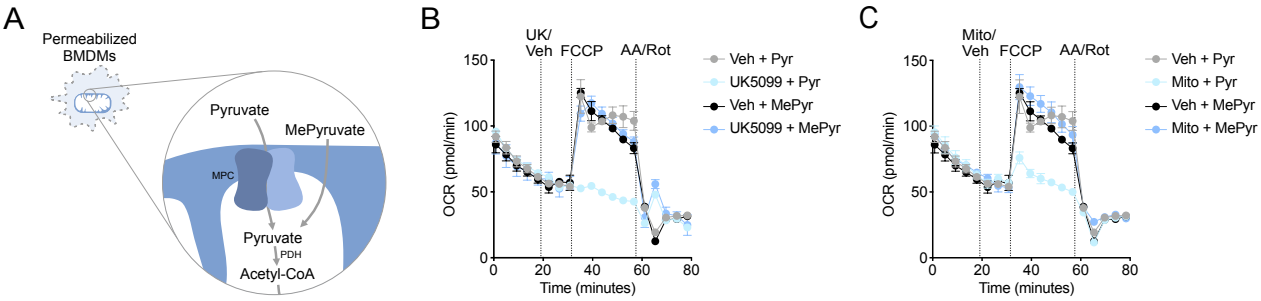

Fig. 3: Mitoglitazone blocks mitochondrial pyruvate utilization via inhibition of the MPC. **A:** Scheme representing specific substrate supplementation to mitochondria of perfringolysin O permeabilized BMDMs to investigate mitochondrial pyruvate utilization. Pyruvate entry into the mitochondria requires the MPC whereas methyl-pyruvate (MePyr) can bypass the MPC, transfuse directly into the mitochondrial matrix and be used in mitochondrial metabolism. PDH = Pyruvate dehyrogenase **B & C:** Representative OCR measurements of mitochondria from perfringolysin O permeabilized cells supplemented either with pyruvate or methyl-pyruvate. Vehicle (Veh), UK5099 (B) or Mito (C) were injected followed by the sequential injections of FCCP and antimycin A (AA) together with rotenone (Rot). (n = 3 biol. replicates of three independent experiments)

3.4 MPC expression or post-translational acetylation are independent of LPS activation or Mito treatment of BMDMs

To further exclude that Mito regulates the subunit expressions of the MPC and thereby modulates macrophage metabolism, BMDMs were incubated with Mito for different time periods and the protein abundance of MPC1 and MPC2 was investigated. Compared to the β-actin control, the expression levels of MPC1 or MPC2 remained unchanged at any of the investigated time points indicating that Mito does not control the expression of the MPC in BMDMs (Fig. 4 A). Furthermore, it was previously described that the pyruvate transport can be modulated via acetylation of the MPC (Liang et al., 2015; Vadvalkar et al., 2017). Inflammatory macrophages have a demand for pyruvate import into the mitochondria to supply their increased mitochondrial metabolism. Hence, it was investigated

whether LPS activation of BMDMs results in a change of the acetylation status of the MPC. To this end, MPC1 or MPC2 were immunoprecipitated from lysates of LPS activated BMDMs and immunostained for lysine acetylation. MPC1 and MPC2 were successfully immunoprecipitated from BMDM lysates (Fig. 4 B & C). However, neither the expression level of MPC1 or MPC2 nor their acetylation was changed upon LPS activation.
These data support the direct inhibition of the mitochondrial pyruvate import by Mito instead of an indirect effect through controlling MPC expression. Furthermore, LPS activation of BMDMs does not modulate the pyruvate import into mitochondria via lysine acetylation of the MPC.

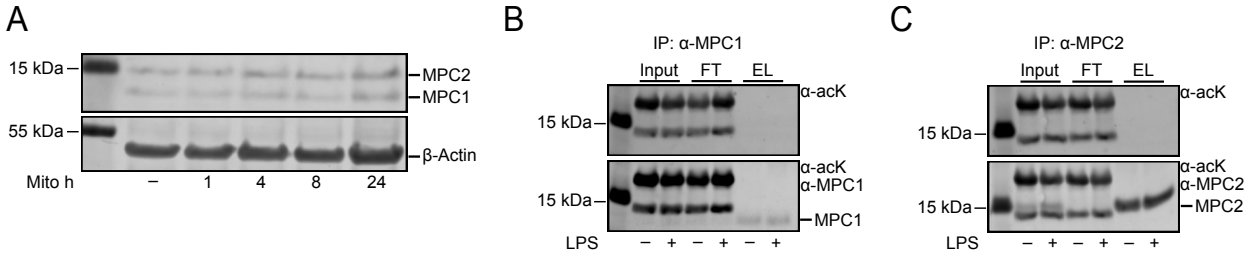

Fig. 4: MPC expression and acetylation remain unchanged after LPS activation or Mito treatment of BMDMs. A: BMDMs were incubated with Mito (100 µM) for the indicated time periods and cell lysates were investigated for the expression of MPC1 and MPC2 via western blotting. **B & C:** MPC1 or MPC2 were immunoprecipitated from BMDMs either unstimulated (UT) or after stimulation with LPS (10 ng/mL) for 3 hours. Whole lysates (Input), flow-through (FT) and immunoprecipitated protein eluates (EL) were subjected to SDS-PAGE and western blot. Membranes were stained against acetylated lysines (α-acK) and MPC1 or MPC2. (Pooled lysates from n = 3 biol. replicates)

3.5 MPC inhibition modulates glycolytic and TCA-cycle metabolites in macrophages

Indirect measurements of ECAR and OCR using extracellular flux analysis showed that MPC inhibition decreases glycolysis and mitochondrial respiration in BMDMs. It was hypothesized that the decrease of glycolysis and mitochondrial respiration via the Mito-facilitated inhibition of the MPC could directly affect the cellular metabolite levels associated with glycolysis and the mitochondrial TCA-cycle (Fig. 5 A). To test whether Mito facilitated inhibition of the MPC directly altered cellular metabolite levels, BMDMs were incubated with vehicle, Mito or UK5099 for 1 hour and activated with LPS for 3 hours or left untreated. Subsequently, the polar cellular metabolites were extracted and subjected to mass-spectrometric analysis (Fig. 5 B & C). Treatment of the cells with Mito or UK5099 increased

cellular pyruvate levels in the unstimulated cells (Fig. 5 B). In contrast, pyruvate levels were mainly increased after UK5099 treatment prior to LPS activation when compared to Mito or the vehicle control. Similarly, lactate levels were increased in LPS activated cells in both the vehicle control and UK5099 treated cells. Yet, Mito prevented cellular lactate accumulation in response to LPS (Fig. 5 B). Mito and UK5099 decreased cellular alanine levels, an amino acid mainly produced from pyruvate inside the mitochondria. Interestingly, glycine levels were increased upon treatment with Mito in unstimulated or LPS activated cells indicating a rerouting of glycolytic metabolites. Analysis of the TCA-cycle metabolites showed an increase of citrate and succinate levels following LPS stimulation of BMDMs (Fig. 5 C). Treatment with Mito or UK5099 decreased citrate levels in both unstimulated and LPS activated cells. Furthermore, Mito inhibited succinate accumulation following LPS activation, whereas UK5099 showed a decrease in both the unstimulated and LPS activated cells. The already well-described immunomodulatory metabolite itaconate was slightly reduced upon Mito or UK5099. Of note, treatment of BMDMs with Mito or UK5099 markedly increased cellular fumarate, malate and aspartate levels in both untreated and LPS stimulated cells indicating a reallocation of TCA-cycle metabolites due to the reduced citrate levels (Fig. 5 C). Upon activation, macrophages increase glucose uptake to sustain glycolysis. Thus, it was investigated whether Mito-facilitated inhibition of glycolysis in inflammatory macrophages resulted from reduced glucose uptake. BMDMs were treated with vehicle, Mito or UK5099 for 1 hour and subsequently activated with LPS for 3 hours. Measuring the glucose concentrations in the supernatants showed an increased uptake of glucose after LPS activation of BMDMs. However, Mito had no effect on glucose uptake while UK5099 only showed a slight reduction (Fig. 5 D). It was previously described that knockdown of either MPC1 or MPC2 in muscle cells results in increased lactate secretion (Vacanti et al., 2014). Since Mito prevented the accumulation of lactate inside the cells, lactate secretion into the supernatant was assessed as described for glucose uptake (Fig. 5 E). The untreated and LPS treated cells showed an increase in lactate secretion in presence of Mito compared with their vehicle controls. This correlated with the previously observed decrease in intracellular lactate levels in Mito treated and LPS activated BMDMs (Fig. 5 B). In contrast, treatment of the cells with UK5099 only showed an increase in lactate secretion in the unstimulated cells, whereas lactate secretion from LPS activated cells remained unchanged compared to the vehicle controls. This

finding correlated with the reduced cellular lactate levels in untreated cells, but increased levels in LPS stimulated cells in the presence of UK5099 (Fig. 5 B).

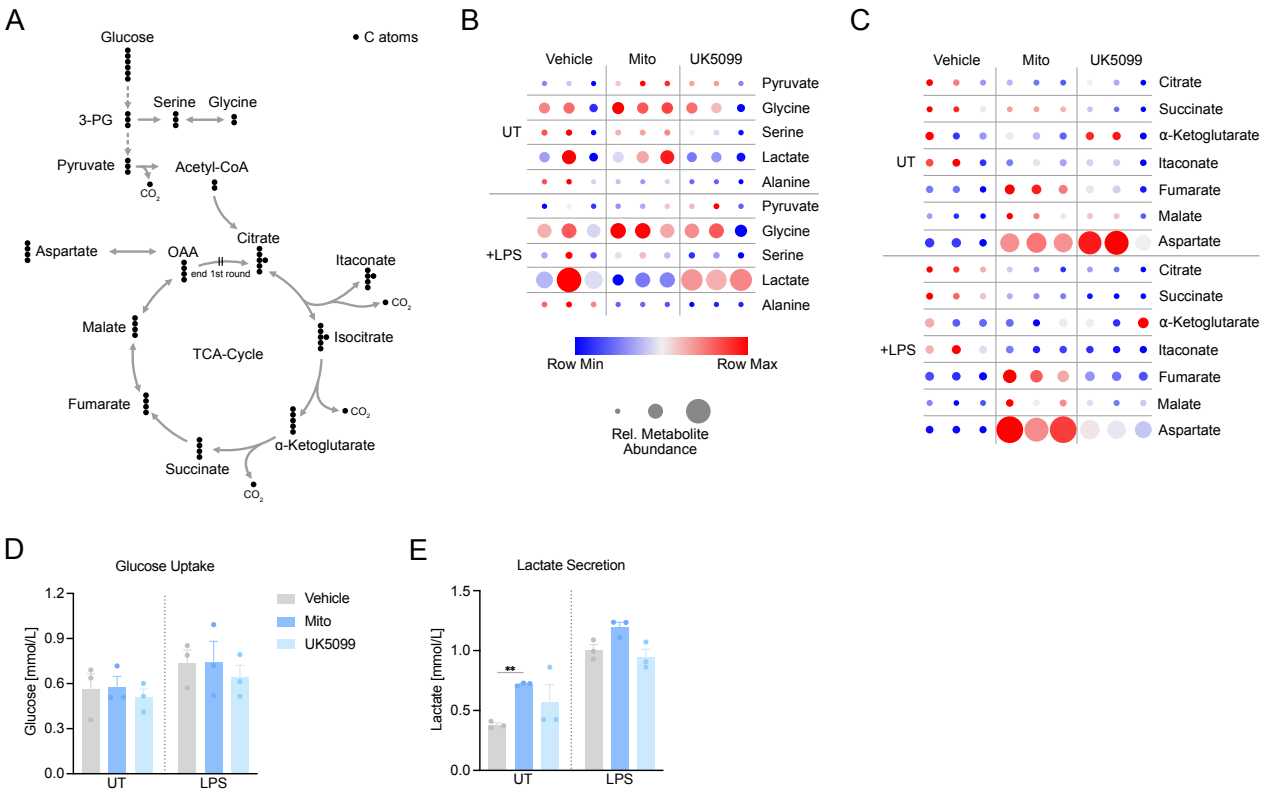

Fig. 5: Mitoglitazone modulates glycolytic metabolites and downregulates TCA-cycle metabolites. A: Scheme depicting the metabolic pathway and its related metabolites from glucose over glycolysis and the subsequent flux of pyruvate into the mitochondrial TCA-cycle. **B & C:** Heatmaps showing the relative levels of glycolysis and TCA-cycle as well as associated metabolites of U-$^{13}C_6$-glucose fed BMDMs incubated with Vehicle, UK5099 (100 µM) or Mito (100 µM) for 1 hour and subsequent stimulation with LPS (10 ng/mL) for 3 hours or left untreated (UT) (n = 3 biol. replicates representative of 3 independent experiments). Color coding represents metabolite levels scaled per row for each metabolite whereas circle sizes represent the relative metabolite levels over all metabolites. **D & E:** Glucose consumption and lactate secretion derived from glucose and lactate measurements in the supernatants from cells stimulated as described for B & C. n = 3 biol. replicates. Mean ± SD. Statistical significance was determined via 2-way ANOVA using Dunnett's multiple comparison test. Adjusted p-value: 0.03 (*), 0.0021 (**), 0.0002 (***)

These data demonstrate that MPC inhibition by Mito modulates metabolite levels of both glycolysis and the TCA-cycle in inflammatory macrophages, leaving glucose uptake unaffected. Furthermore, Mito evokes metabolic adaptations distinct from the covalent MPC inhibitor UK5099 in resting and LPS activated macrophages. Of note, increased lactate

secretion from BMDMs indicates that Mito treatment might also impact the cellular environment.

3.6 MPC inhibition by Mito decreases carbon flux from glucose into the TCA-cycle

Since both glycolytic and TCA-cycle associated metabolites were primarily downregulated by Mito treatment of BMDMs, it was hypothesized that Mito-facilitated MPC inhibition reduces carbon flux from glucose into the TCA-cycle. Feeding of isotopically labeled carbon sources combined with mass isotopomer distribution analysis of cellular metabolites can be used to investigate the carbon contribution from a specific carbon source (Fig. 6 A).
To investigate whether Mito reduced carbon contribution from glucose into cellular metabolites, BMDMs were fed U-$^{13}C_6$-glucose overnight to establish an equilibrium of ^{13}C-labeled cellular metabolites. Afterwards, cells were incubated with vehicle, UK5099 or Mito for 1 hour and subsequently activated with LPS for 3 hours or left untreated. The polar cellular metabolites were extracted and subjected to mass-spectrometric analysis to investigate metabolite mass isotopomer distributions. The relative contribution of glucose-derived carbons to the fully labeled isotopologues of pyruvate, lactate and alanine was increased when BMDMs were activated with LPS (Fig. 6 B – D). Treatment of the cells with Mito increased carbon labeling from glucose into pyruvate and lactate while it remained unaltered when cells were treated with UK5099 (Fig. 6 B & C). Corresponding to the total levels of pyruvate and lactate described earlier, relative M3 isotopomer abundances of pyruvate and lactate was decreased when LPS stimulated cells were treated with Mito. In contrast, UK5099 increased the carbon contribution from glucose into pyruvate and lactate in the LPS stimulated cells. Both unstimulated and LPS stimulated cells showed reduced M3 isotopomer abundance of alanine when treated with either Mito or UK5099 (Fig. 6 D). Carbon contribution from glucose into serine and glycine was increased by Mito or UK5099 treatment of unstimulated or LPS activated BMDMs (Fig. 6 E & F). Further investigation of TCA-cycle metabolites showed a decrease in the ^{13}C isotopologues of citrate, α-ketoglutarate, succinate, fumarate and malate as well as aspartate when BMDMs were left unstimulated or activated with LPS in presence of Mito or UK5099 (Fig. 6 G – L).

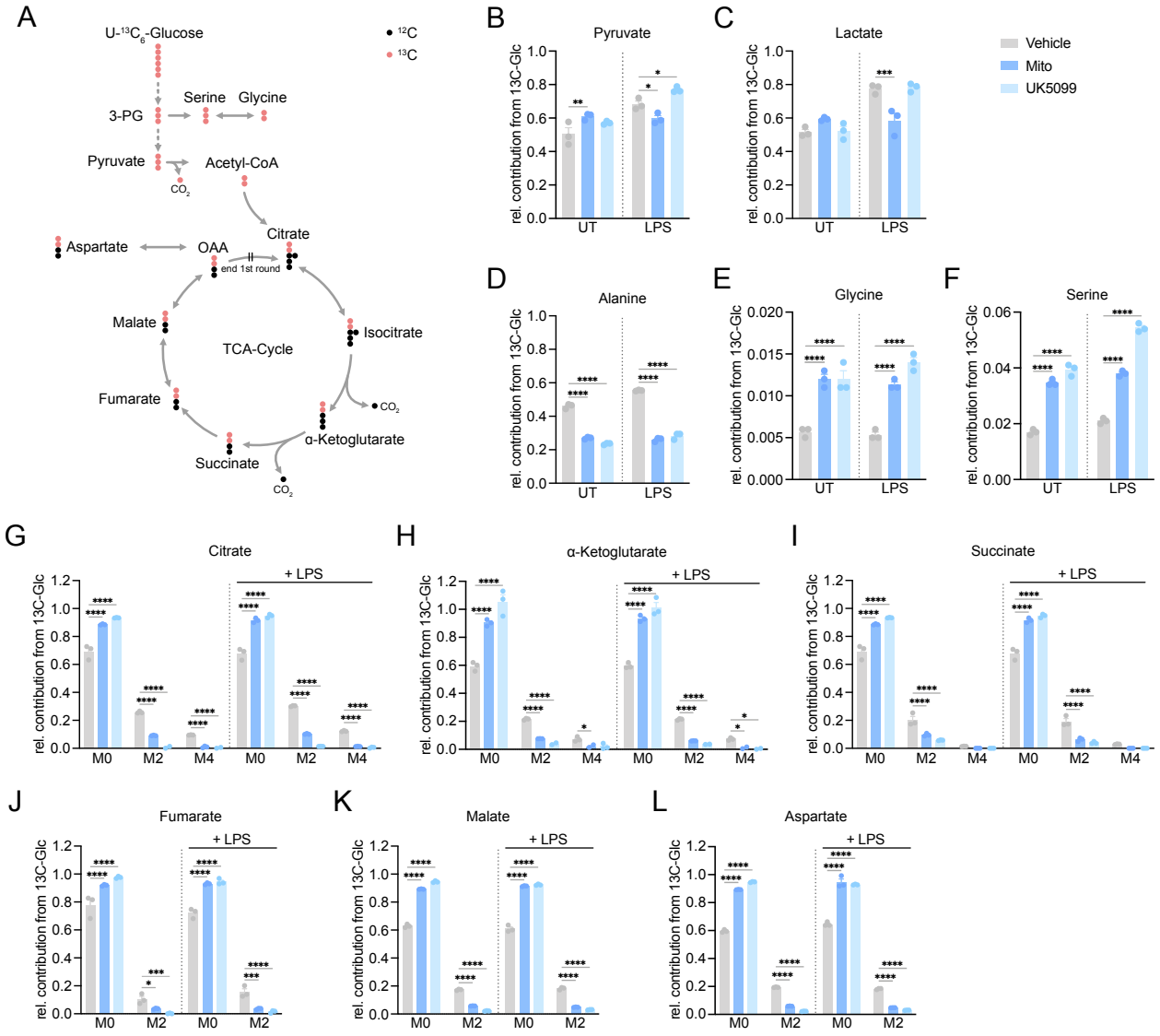

Fig. 6: MPC inhibition by Mito decreases carbon contribution from glucose to glycolytic and TCA-cycle metabolites. A: Schematic representation of carbon tracing from U-$^{13}C_6$-glucose in BMDMs. Black dots indicate ^{12}C carbons whereas red dots indicate ^{13}C carbons. **B – F:** Relative contributions of fully labeled (M3) isotopologues of pyruvate, lactate, alanine, serine and glycine from U-$^{13}C_6$-glucose fed BMDMs that were treated with vehicle, Mito (100 µM) or UK5099 (100 µM) for 1 hour and subsequently stimulated with LPS (10 ng/mL) for 3 hours or left unstimulated. Mean ± SD **G – L:** Relative contributions of isotopologues of Citrate, α-ketoglutarate, succinate, fumarate, malate and aspartate from U-$^{13}C_6$-glucose fed BMDMs that were treated as described for B – F. M# represent the isotopologues with the corresponding number of ^{13}C-labeled carbons. n = 3 biol. replicates representative of 3 independent experiments. Mean ± SD. Statistical significance was determined via 2-way ANOVA using Dunnett's multiple comparison test. Adjusted p-value: 0.03 (*), 0.0021 (**), 0.0002 (***), < 0.0001 (****)

Of note, while the reduced carbon labeling from glucose into citrate, α-ketoglutarate and succinate correlated with their decreased total metabolite changes, the decreased

labeling of fumarate, malate and aspartate was in contrast to their increased total cellular levels following Mito treatment (Fig. 5 C).
Together, these data demonstrate that Mito treatment of BMDMs reduces glucose utilization in glycolysis and downstream contribution to the TCA-cycle, likely resulting from the inhibition of mitochondrial pyruvate import.

3.7 Mitoglitazone increases glutaminolysis and alters TCA-cycle flux

As shown priorly, treatment of BMDMs with Mito resulted in decreased contribution of carbons from U-$^{13}C_6$-glucose to malate, fumarate and aspartate, whereas it increased their total cellular levels. Therefore, it was further investigated whether BMDMs switched to glutamine as an alternative carbon source for the TCA-cycle upon MPC inhibition with Mito or UK5099. To this end, U-$^{13}C_5$-glutamine fed BMDMs were treated with vehicle, Mito or UK5099 for 1 hour followed by their stimulation with LPS for 3 hours and carbon flux from glutamine into TCA-cycle metabolites was analyzed (Fig. 7 A). Glutamine is taken up into mitochondria, converted into glutamate and enters the TCA-cycle in the form of α-ketoglutarate. Treatment of BMDMs with Mito prior to LPS activation showed an increase in the M5 isotopologue of α-ketoglutarate while the isotopomer distribution remained unchanged in the unstimulated cells indicating an anaplerotic utilization of glutamine (Fig. 7 B). Activation of BMDMs with LPS showed no change of carbon flux from glutamine into TCA-cycle metabolites except for succinate as indicated by the increase in the M4 isotopologue of succinate when compared to the unstimulated cells (Fig. 7 C). This increase in M4 succinate upon LPS stimulation was inhibited by the treatment with Mito before LPS activation. Additionally, Mito treatment increased the M1 and M3 succinate isotopologues in LPS activated cells. Unexpectedly, not the M4, but the M3 isotopologues of fumarate, malate and aspartate were increased upon treatment of BMDMs with Mito and subsequent LPS activation hinting towards a deviation from the oxidative TCA-cycle flux (Fig. 7 D & E). In contrast, incorporation of carbons from glutamine into α-ketoglutarate, succinate, malate and aspartate remained unaltered upon UK5099 treatment compared to the vehicle controls.

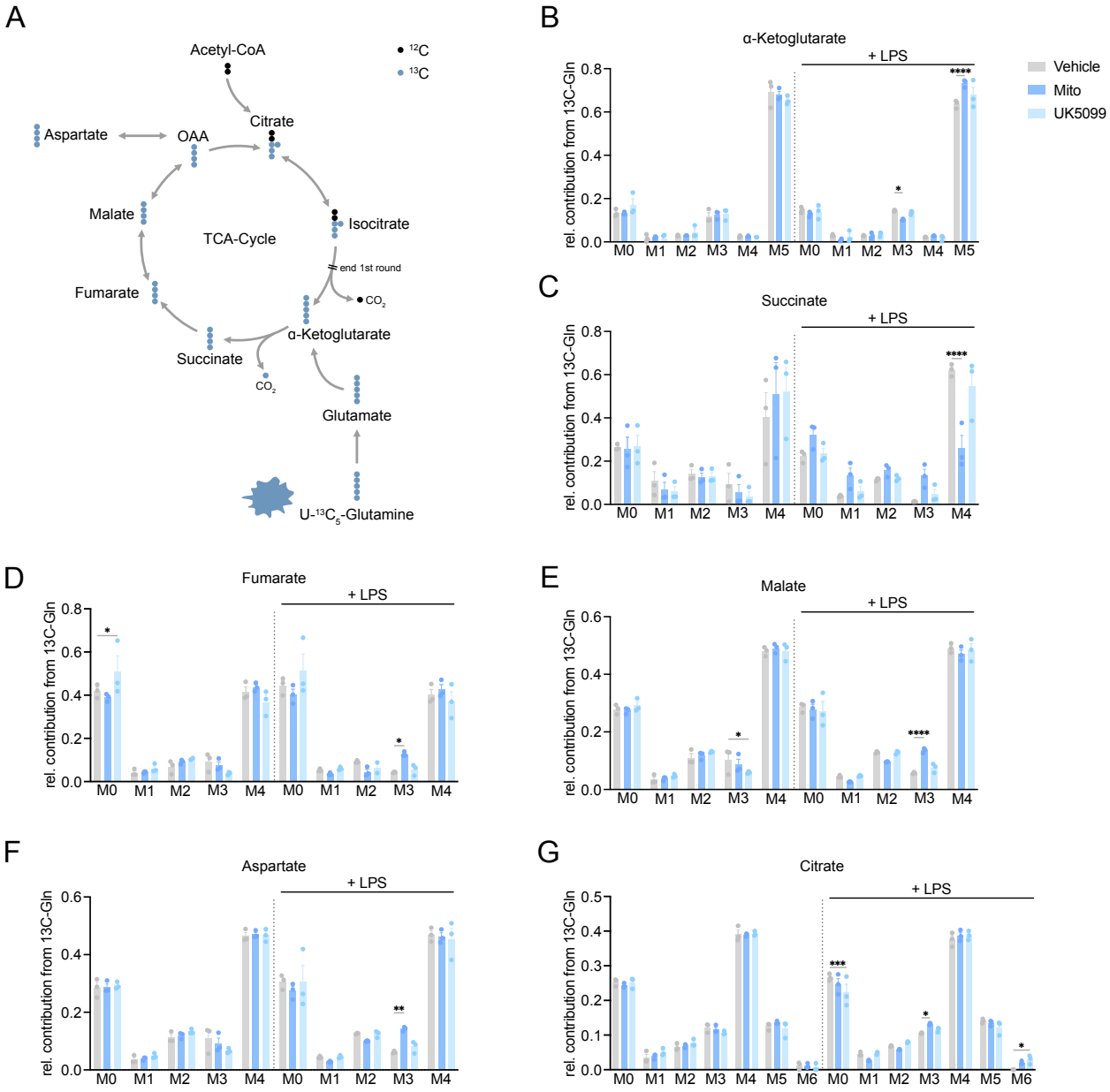

Fig. 7: Mitoglitazone increases carbon flux from glutamine into the TCA-cycle and alters TCA-cycle flux. A: Schematic representation of carbon tracing from U-$^{13}C_5$-glutamine in BMDMs. Black dots indicate ^{12}C carbons whereas blue dots indicate ^{13}C carbons. **B – G:** Relative contributions of isotopologues of Citrate, α-ketoglutarate, succinate, fumarate, malate and aspartate from U-$^{13}C_5$-glutamine fed BMDMs that were treated with vehicle, Mito (100 µM) or UK5099 (100 µM) for 1 hour and subsequently stimulated with LPS (10 ng/mL) for 3 hours or left unstimulated. M# represent the isotopologues with the corresponding number of ^{13}C-labeled carbons. n = 3 biol. replicates. Mean ± SD. Statistical significance was determined via 2-way ANOVA using Dunnett's multiple comparison test. Adjusted p-value: 0.03 (*), 0.0021 (**), 0.0002 (***), < 0.0001 (****)

Analysis of glutamine carbon contribution to citrate showed an increase for the M6 isotopologue after Mito or UK5099 treatment and an additional increase in the M3 isotopologue after the treatment with Mito but not with UK5099 (Fig. 7 G).
Collectively, these data indicate that treatment of BMDMs with Mito but not UK5099 prior to LPS activation evokes an increase in glutaminolysis and an adaptation of TCA-cycle flux.

3.8 The reductive TCA-cycle increases upon Mitoglitazone treatment

Isotopic labeling of glutamine hinted towards increased reductive rather than oxidative TCA-cycle flux when BMDMs were treated with Mito. Such adaptation might result from the inhibition of complex I of the electron transport chain (ETC) as it would elicit an increased succinate utilization by succinate dehydrogenase (SDH). The increased succinate turn-over would maintain complex III activity and thereby sustain the proton gradient over the inner mitochondrial membrane allowing for the continuation of oxidative phosphorylation (Fig. I1). Indeed, an inhibitory function towards complex I by Glitazones including Mito was suggested before (Brunmair et al., 2004; Divakaruni et al., 2013). To investigate the inhibitory effect of Mito towards complex I of the ETC, BMDMs were fed a glutamine tracer labeled with a ^{13}C carbon only at the first position ($^{13}C_1$-glutamine) and treated as described before for U-$^{13}C_5$-glutamine. Since the ^{13}C-labeled carbon originating from $^{13}C_1$-glutamine is excluded during the conversion of α-ketoglutarate into succinate following the oxidative TCA-cycle, investigation of the isotopomer distribution of TCA-cycle metabolites enables to monitor the carbon flux through the reductive TCA-cycle (Fig. 8 A). The LPS activation of BMDMs showed no alteration of carbon contribution from $^{13}C_1$-glutamine to glutamate and α-ketoglutarate when compared to the unstimulated vehicle control (Fig. 8 B & C). Yet, treatment of BMDMs with Mito resulted in a 2-fold and UK5099 in 1.6-fold increase of the $^{13}C_1$-labeled proportion of glutamate and α-ketoglutarate irrespective of LPS activation. As expected, there was no change in the labeling rate of succinate since the isotopically labeled carbon is eliminated during the conversion of $^{13}C_1$-α-ketoglutarate into succinate (Fig. 8 D). LPS activation of the cells increased the carbon contribution from $^{13}C_1$-glutamate to citrate as indicated by the slight increase of its M1 isotopologue indicating that LPS stimulation itself elicited an increase in carbon flux through the reductive TCA-cycle (Fig. 8 E). Importantly, the carbon contribution from $^{13}C_1$-

glutamate to citrate in both unstimulated and LPS activated BMDMs was increased approximately 4- or 2-fold upon Mito or UK5099 treatment, respectively. Moreover, the M1 isotopologues of malate and aspartate were increased mainly upon Mito treatment in both the unstimulated and LPS stimulated BMDMs (Fig. 8 F & G). In comparison, treatment of BMDMs with UK5099 only showed a slight increase of M1 malate or aspartate in the LPS activated cells.

Together, these data highlight that MPC inhibition by Mito or UK5099 increases the reductive TCA-cycle flux of resting and LPS activated BMDMs. However, the stronger increase in reductive TCA-cycle flux after Mito compared to UK5099 treatment might originate from a dual inhibition of both the MPC and complex I of the ETC.

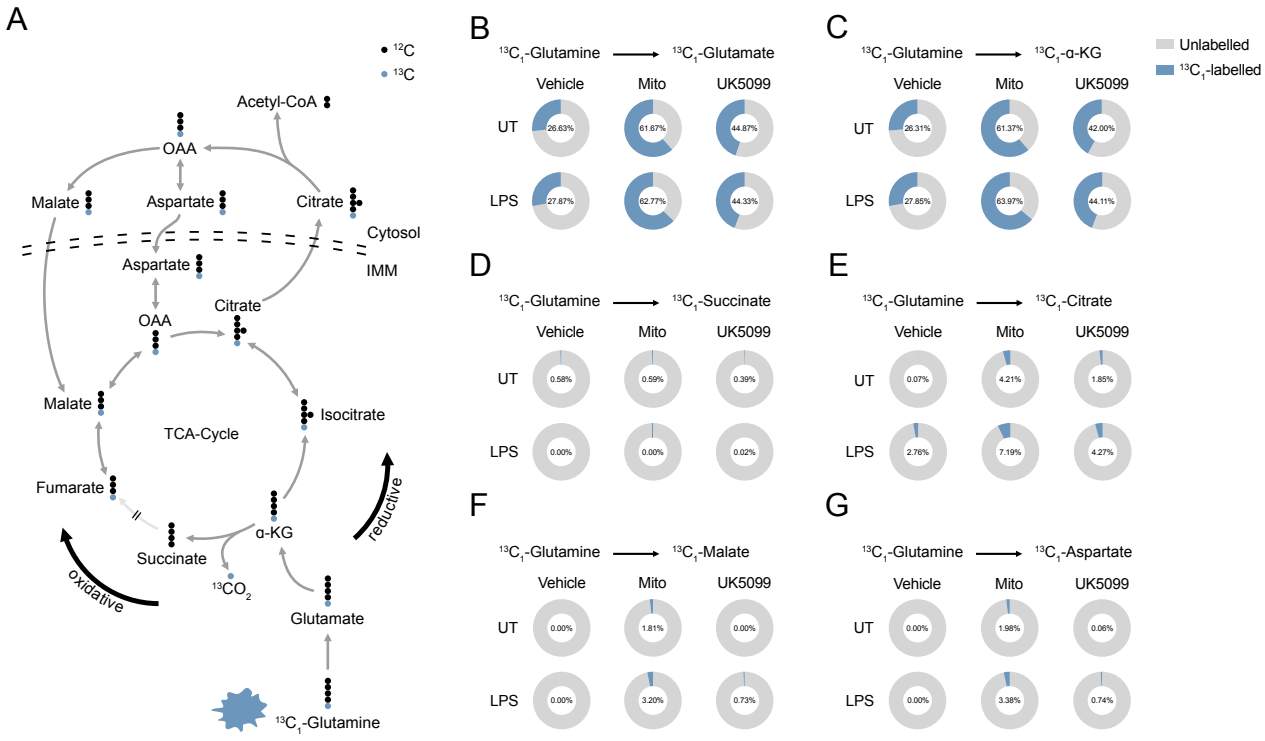

Fig. 8: MPC inhibition increases reductive TCA-cycle flux. A: Schematic representation of carbon tracing from U-$^{13}C_1$-glutamine through the reductive TCA-cycle in BMDMs. Black dots indicate ^{12}C carbons whereas blue dots indicate ^{13}C carbons. **B – G:** Relative contributions of the M1 isotopologues of glutamate, α-ketoglutarate, succinate, citrate, malate and aspartate from U-$^{13}C_1$-glutamine fed BMDMs that were treated with vehicle, Mito (100 µM) or UK5099 (100 µM) for 1 hour and subsequently stimulated with LPS (10 ng/mL) for 3 hours or left unstimulated. n = 3 biol. replicates representative of 2 independent experiments.

3.9 Mitoglitazone decreases nitric oxide release from inflammatory macrophages

One of the effector functions of macrophages is the production and release of nitric oxide through nitric oxide synthase 2 (iNOS or NOS2). iNOS converts L-arginine into L-citrulline and nitric oxide using NADPH and therefore is directly linked to the metabolic state of the cells. To investigate whether MPC inhibition through Mito affects the release of nitric oxide from BMDMs, cells were treated with vehicle, Mito or UK5099 for 1 hour and subsequently stimulated with LPS and IFNɣ overnight or left unstimulated (Fig. 9 A). The resulting supernatant was used to measure the concentrations of released nitric oxide via the Griess assay (Fig. 9 B). The treatment of BMDMs with Mito or UK5099 resulted in decreased nitric oxide release from LPS and IFNɣ stimulated cells compared to the vehicle control. It was further tested whether MPC inhibition by Mito might affect the expression of iNOS and thereby lead to a decrease in nitric oxide. To this end, cells were treated as described for the Griess assay and cell lysates were subjected to SDS-PAGE and western blotting against iNOS (Fig. 9 C). While iNOS was upregulated upon LPS and IFNɣ stimulation compared to the unstimulated cells, there was no observable change in iNOS expression in presence of Mito.

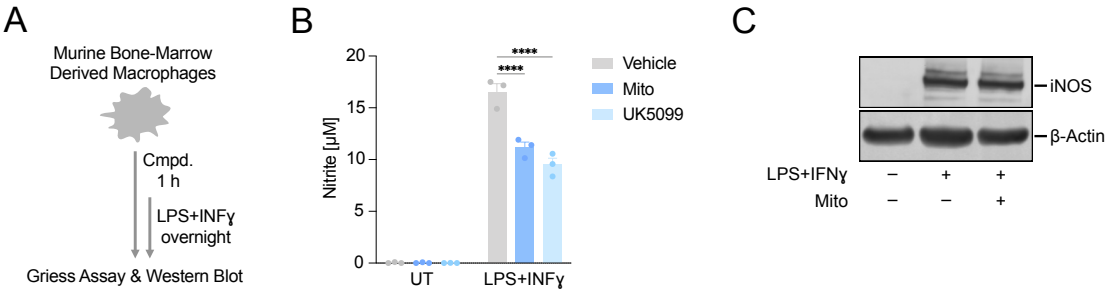

Fig. 9: MPC inhibition reduces nitric oxide release from inflammatory macrophages. A: Scheme representing the treatment of BMDMs to investigate the effect of MPC inhibition via Mito or UK5099 towards the iNOS facilitated nitric oxide production of inflammatory macrophages. **B & C:** BMDMs were treated with vehicle, Mito (100 µM) or UK5099 (100 µM) for 1 hour and subsequently stimulated with LPS (10 ng/mL) and IFNɣ overnight or left unstimulated. The resulting supernatants were used to determine nitric oxide release (**B**) whereas cell lysates were used to investigate iNOS expression via SDS-PAGE and western blotting (**C**). Bar graph showing Mean ± SD of n = 3 biol. replicates. Representative western blot of n = 3 biol. replicates is shown. Statistical significance was determined via 2-way ANOVA using Dunnett's multiple comparison test. Adjusted p-value: 0.03 (*), 0.0021 (**), 0.0002 (***), < 0.0001 (****)

Together, these data show that MPC inhibition via Mito or UK5099 modulates the effector function of macrophages in terms of nitric oxide release. This modulation is likely not related to iNOS regulation but might originate from the modulation of other involved factors in nitric oxide production such as L-arginine or NADPH abundance.

3.10 Mitoglitazone modulates cytokine secretion from inflammatory macrophages

It was previously shown that MPC inhibition by UK5099 in LPS activated BMDMs results in decreased inflammatory cytokine mRNA transcription and secretion (Lauterbach et al., 2019). As shown earlier, Mito inhibits the MPC as well as the metabolic shift in BMDMs after their inflammatory stimulation not just with LPS, but also with R848. Therefore, it was further tested whether MPC inhibition by Mito could regulate cytokines in a similar manner as UK5099. First, BMDMs were treated with vehicle, Mito or UK5099 for 1 hour and subsequently stimulated with LPS or R848 for 4 hours to test whether the transcription of cytokines was altered. Compared to the vehicle controls, Mito and UK5099 decreased transcription of Tnf, Il6 and Il12b in response to LPS or R848 activation (Fig. 10 A, B, C, E, F, G). Furthermore, the LPS induced upregulation of Il10 mRNA transcription remained unaltered by Mito or UK5099 treatment (Fig. 10 D). In contrast, the upregulation of Il10 after R848 stimulation of BMDMs was inhibited when cells were treated with Mito, but not UK5099 (Fig. 10 H). It was further inspected whether the observed changes in cytokine mRNA transcription after Mito treatment were also reflected on the secretion level of the respective cytokines. BMDMs were treated with vehicle, Mito or UK5099 for 1 hour and subsequently activated with LPS or R848 for 8 hours to allow for the translation and secretion of cytokines into the supernatants. Compared to their vehicle controls, the concentrations of secreted TNFα, IL-6, IL-12p40 and IL-10 were similarly affected by Mito and UK5099 as previously observed for their transcriptional levels (Fig. 10 I – P). BMDMs stimulated with LPS or R848 showed a decrease in TNFα, IL-6 and IL-12p40 when they were priorly treated with Mito or UK5099 (Fig. 10 I, J, K, M, N, O). Treatment of the cells with Mito decreased the secretion of IL-10 in response to R848, but not to LPS (Fig. 10 L & P). In contrast to the unaltered Il10 mRNA levels, UK5099 decreased the secretion of IL-10 after R848 stimulation of BMDMs (Fig. 10 H & P).

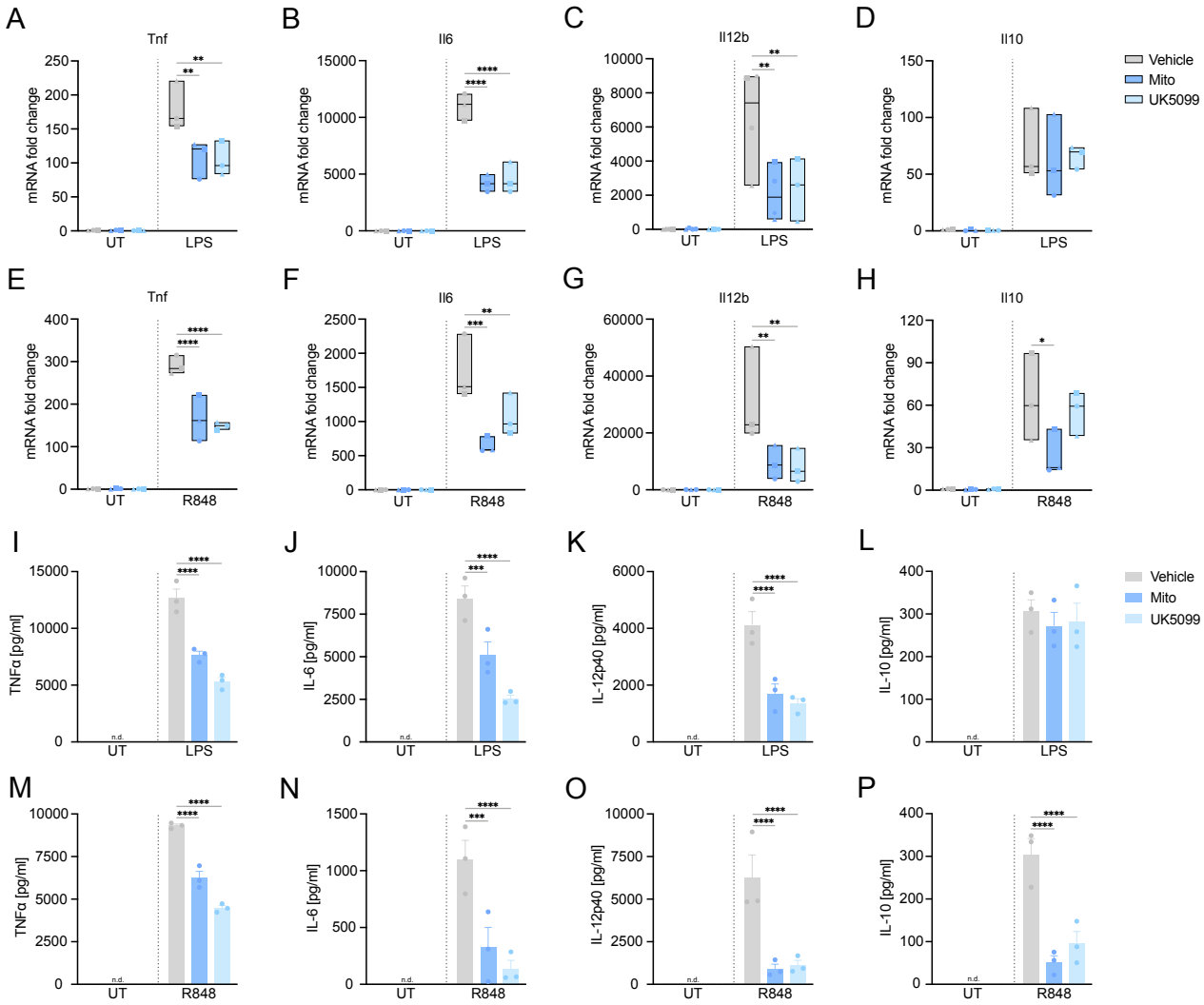

Fig. 10: Mitoglitazone decreases cytokine mRNA transcription and secretion by inflammatory BMDMs. A – H: BMDMs were treated with vehicle, Mito (100 µM) or UK5099 (100 µM) for 1 hour and subsequently stimulated with LPS (10 ng/mL) or R848 (10 ng/mL) for 4 hours or left unstimulated (UT). The resulting cytokine mRNA changes were detected by RT-qPCR and mRNA fold changes were calculated via the $\Delta\Delta C_t$-method. Data are represented by floating bar charts (min and max) with line indicating the median. n = 3 biol. replicates representative of at least 3 independent experiments **I – P:** BMDMs were treated with vehicle, Mito (100 µM) or UK5099 (100 µM) for 1 hour and subsequently stimulated with LPS (10 ng/mL) or R848 (10 ng/mL) for 8 hours or left unstimulated (UT). Supernatant concentrations of indicated cytokines were measured via ELISA. Mean ± SD of n = 3 biol. replicates representative of at least 3 independent experiments. n.d. = not detectable. Statistical significance was determined via 2-way ANOVA using Dunnett's multiple comparison test. Adjusted p-value: 0.03 (*), 0.0021 (**), 0.0002 (***), < 0.0001 (****)

Overall, these findings demonstrate that treatment of inflammatory BMDMs with Mito decreases the cytokine mRNA transcription and secretion of TNFα, IL-6 and IL-12p40 in a

similar manner as observed for MPC inhibition by UK5099. Moreover, a decreased expression of Il10 mRNA after Mito, but not UK5099, treatment of R848 activated macrophages indicates that Mito differentially regulates Il10 gene induction compared to UK5099.

3.11 Mitoglitazone decreases Il10 gene induction in a TRIF-independent manner

The recognition of LPS activates TLR4, a pattern recognition receptor that is unique compared to other TLRs as it signals via both, MyD88- and TRIF to induce inflammatory genes. In contrast, R848 gets recognized by TLR7/8 resulting in the activation of MyD88 signaling only. Interestingly, Mito treatment of BMDMs decreased the induction of Il10 mRNA in response to R848, but not to LPS. Therefore, it was investigated whether this differential regulation originated from a regulation of MyD88 signaling. To this end, Ticam1$^{-/-}$ BMDMs, devoid of the TLR adapter TRIF, were treated with Mito or UK5099 and activated with LPS or R848 for 4 or 8 hours to investigate mRNA transcription and secretion of cytokines, respectively. Treatment with Mito or UK5099 prior to LPS or R848 stimulation of Ticam1$^{-/-}$ BMDMs resulted in similar decreases of the induction of Tnf, Il6 and Il12b mRNA as previously observed in the WT cells (Fig. 11 A, B, C, E, F, G). Concomitantly, Mito and UK5099 decreased LPS or R848 induced secretion of IL-12p40 compared to the vehicle controls (Fig. 11 I & J). Interestingly, Mito slightly increased the mRNA expression of Il10 in the LPS stimulated Ticam1$^{-/-}$ BMDMs whereas it decreased Il10 in the R848 stimulated cells compared to the vehicle controls (Fig. 11 D & H). In contrast, treatment of Ticam1$^{-/-}$ BMDMs with UK5099 and subsequent stimulation with LPS or R848 resulted in unaltered Il10 expression compared to the vehicle control. Furthermore, LPS induced secretion of IL-10 was not changed by prior treatment with Mito, yet it was slightly increased when Ticam1$^{-/-}$ BMDMs were pretreated with UK5099 (Fig. 11 K). Mito decreased the release of IL-10 by Ticam1$^{-/-}$ BMDMs after R848 stimulation in a similar manner as seen previously in wildtype cells (Fig. 11 L; Fig. 10 P). In contrast to wildtype cells, UK5099 treatment of Ticam1$^{-/-}$ BMDMs did not change the secretion of IL-10 after R848 stimulation.

These data demonstrate that regulation of Il10 mRNA expression and IL-10 secretion by Mito in BMDMs is not MyD88-specific and TRIF-independent. Moreover, differences in IL-

10 regulation on both transcriptional and protein secretion level indicate that Mito at least partly regulates the induction of cytokines differentially from UK5099.

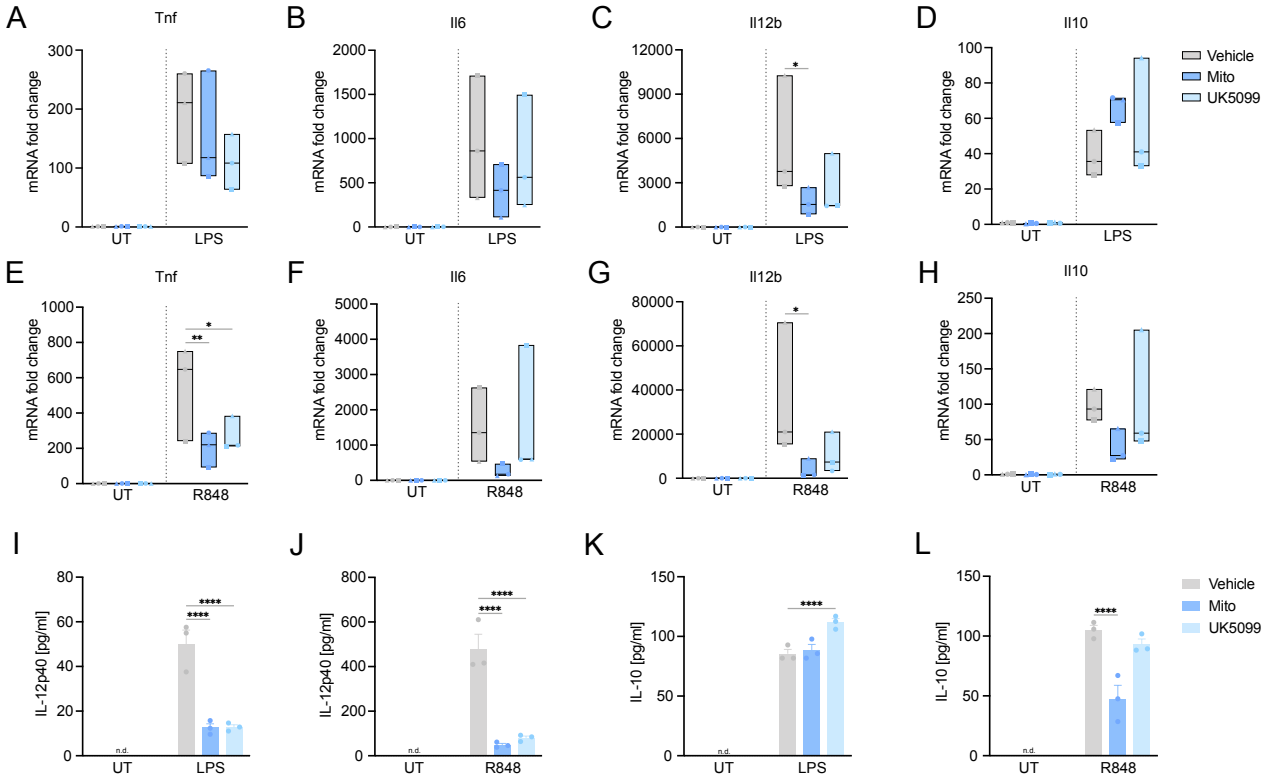

Fig. 11: Mitoglitazone modulates cytokine mRNA transcription and secretion independent of TRIF signaling. A – H: Ticam$^{-/-}$ BMDMs were treated with vehicle, Mito (100 µM) or UK5099 (100 µM) for 1 hour and subsequently stimulated with LPS (10 ng/mL) or R848 (10 ng/mL) for 4 hours or left unstimulated (UT). The resulting cytokine mRNA changes were detected by RT-qPCR and mRNA fold changes were calculated via the $\Delta\Delta C_t$-method. Data are represented by floating bar charts (min and max) with line indicating the median. n = 3 biol. replicates from one experiment **I – L:** Ticam$^{-/-}$ BMDMs were treated with vehicle, Mito (100 µM) or UK5099 (100 µM) for 1 hour and subsequently stimulated with LPS (10 ng/mL) or R848 (10 ng/mL) for 8 hours or left unstimulated (UT). Supernatant concentrations of indicated cytokines were measured via ELISA. Mean ± SD of n = 3 biol. replicates from one experiment. n.d. = not detectable. Statistical significance was determined via 2-way ANOVA using Dunnett's multiple comparison test. Adjusted p-value: 0.03 (*), 0.0021 (**), 0.0002 (***), < 0.0001 (****)

3.12 Mitoglitazone regulates cytokine secretion independent of PPARɣ

Glitazones were initially designed to activate the nuclear receptor PPARɣ, thereby modulating cellular metabolism and aiding in the treatment of type 2 diabetes. Macrophages express PPARɣ at low levels and LPS was shown to further downregulate its expression

(Welch et al., 2003; Zhou et al., 2008). Although Mito has a significantly reduced binding affinity for PPARɣ, it was necessary to exclude that prolonged Mito treatment regulated cytokine secretion from LPS activated macrophages via PPARɣ activation. Therefore, it was determined at which time points LPS stimulation downregulates PPARɣ expression in BMDMs. While PPARɣ was expressed in unstimulated cells, it was downregulated after 3 and 6 hours and undetectable after 24 hours of LPS stimulation (Fig. 12 A). Hence, PPARɣ was still present in stimulated macrophages during the earlier observations of cytokine regulation by Mito treatment. To further exclude the potential mechanistic cytokine regulation via PPARɣ, BMDMs were preincubated with the PPARɣ inhibitor GW9662 before treatment with Mito or UK5099 and subsequent stimulation with LPS. The treatment of BMDMs with GW9662 resulted in decreased IL-12p40 secretion when comparing the vehicle controls of the untreated and GW9662 incubated cells (Fig. 12 B). Nevertheless, Mito and UK5099 still reduced the LPS induced secretion of IL-12p40 in the presence of GW9662. Furthermore, PPARɣ inhibition by GW9662 had no effect on the Mito-facilitated regulation of IL-10 secretion in response to LPS or R848 (Fig. 12 C & D).

In addition to pharmacologic inhibition, it was sought to investigate the effect of Mito on IL-12p40 secretion in a genetic PPARɣ knockout model. As unspecific knockout of PPARɣ results in embryonal lethality, an in vitro knockout system using PPARɣ$^{fl/fl}$ BMDMs was established (Fig. 12 O). Bone-marrow cells from PPARɣ$^{fl/fl}$ mice were differentiated into BMDMs as done for previous experiments. During the last two days of BMDM differentiation, cells were either left untreated (PPARɣ$^{fl/fl}$) or treated with purified tat-Cre recombinase to induce the recombination of the PPARɣ$^{fl/fl}$ allele and obtain PPARɣ$^{-/-}$ BMDMs. Analysis of PPARɣ expression showed an almost complete knockout of PPARɣ in the tat-Cre treated PPARɣ$^{-/-}$ BMDMs while PPARɣ was still expressed in the PPARɣ$^{fl/fl}$ cells (Fig. 12 P). Similar to the GW9662 treated cells, Mito or UK5099 treatment prior to LPS activation of BMDMs resulted in the decreased secretion of IL-12p40 independent of PPARɣ expression (Fig. 12 Q).

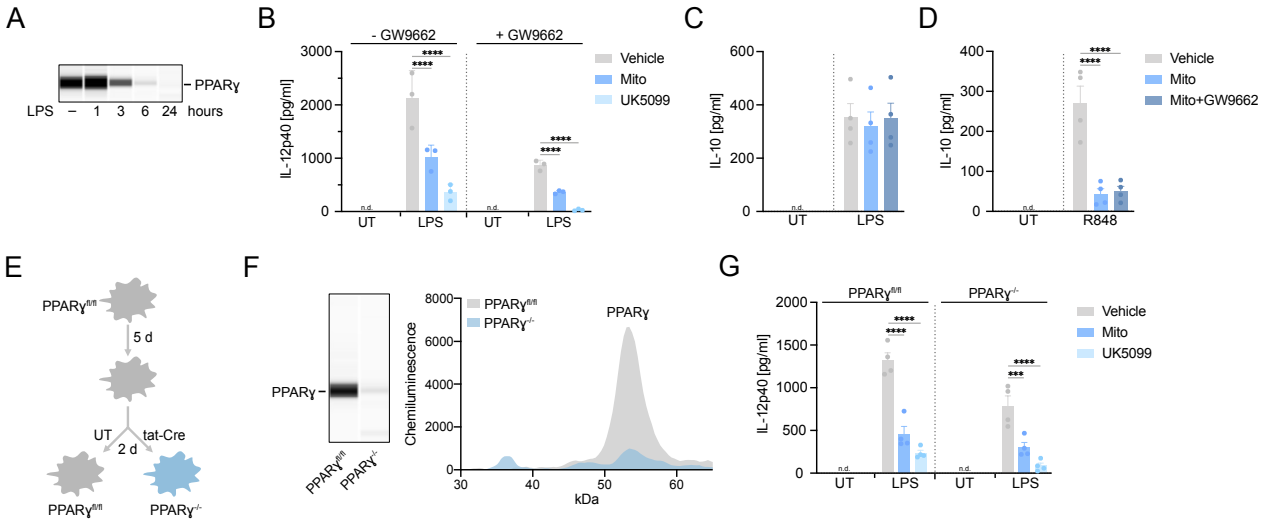

Fig. 12: Mitoglitazone modulates cytokine mRNA transcription and secretion under pharmacologic PPARγ inhibition as well as in an in vitro PPARγ knockout. **A:** BMDMs were stimulated with LPS (10 ng/mL) for the indicated time points and the cell lysates were used to investigate PPARγ expression using the Wes chemiluminescence western blotting system. n = 2 biol. replicates **B:** BMDMs were incubated with the PPARγ inhibitor GW9662 (5 µM) for 30 minutes, treated with vehicle, Mito (100 µM) or UK5099 (100 µM) for 1 hour and subsequently activated with LPS (10 ng/mL) for 8 hours. The resulting supernatants were used to measure the concentrations of secreted IL-12p40 via ELISA. Mean ± SD of n = 3 biol. replicates from 2 independent experiments. n.d. = not detectable. **C & D:** BMDMs were incubated with the PPARγ inhibitor GW9662 (5 µM) for 30 minutes, treated with vehicle, Mito (100 µM) or UK5099 (100 µM) for 1 hour and subsequently activated with LPS (10 ng/mL) or R848 (10 ng/mL) for 8 hours. The resulting supernatants were used to measure the concentrations of secreted IL-10 via ELISA. Mean ± SD of n = 4 biol. replicates from 2 independent experiments. **O:** Scheme depicting the in vitro knockout system used to obtain PPARγ$^{-/-}$ BMDMs. Bone-marrow cells from PPARγ$^{fl/fl}$ mice were differentiated with L929 supernatant into BMDMs for 7 days. On day 5 of differentiation, cells were either left untreated or treated with purified tat-Cre recombinase (10 µM) for 2 days to obtain PPARγ$^{-/-}$ BMDMs. **P:** Cell lysates PPARγ$^{fl/fl}$ and tat-Cre induced PPARγ$^{-/-}$ BMDMs were tested for PPARγ expression via Wes chemiluminescence western blotting. **Q:** PPARγ$^{fl/fl}$ or PPARγ$^{-/-}$ BMDMs were treated with vehicle, Mito (100 µM) or UK5099 (100 µM) for 1 hour, stimulated with LPS (10 ng/mL) for 8 hours and the secreted IL-12p40 was measured via ELISA. Mean ± SD of n = 4 biol. replicates representative of independent experiments. n.d. = not detectable. Statistical significance was determined via 2-way ANOVA using Dunnett's multiple comparison test. Adjusted p-value: 0.03 (*), 0.0021 (**), 0.0002 (***), < 0.0001 (****)

To further validate the finding of PPARγ independent regulation of cytokines in BMDMs by Mito treatment, a macrophage-specific PPARγ knockout was used. PPARγ$^{fl/fl}$ mice were crossed to LysM-Cre mice and PPARγ$^{fl/fl}$;LysM-Cre$^{+/-}$ (PPARγ$^{-/-}$) as well as PPARγ$^{fl/fl}$;LysM-Cre$^{-/-}$ (PPARγ$^{fl/fl}$) littermates were used for experiments (Fig. 13 A). Analysis of PPARγ$^{fl/fl}$ and PPARγ$^{-/-}$ BMDMs showed a substantial reduction in PPARγ

expression in PPARγ$^{-/-}$ compared to the PPARγ$^{fl/fl}$ cells (Fig. 13 B). To investigate the effect of Mito treatment on the inflammatory activation of BMDMs a multiplexed mRNA expression profiling was used. Both PPARγ$^{fl/fl}$ and PPARγ$^{-/-}$ BMDMs generally increased their expression of inflammatory genes 4 hours after LPS or R848 stimulation when compared to unstimulated cells treated with Mito or vehicle (Fig. 13 C). Hierarchical cluster analysis resulted in clustering of PPARγ$^{fl/fl}$ and PPARγ$^{-/-}$ into their different treatments indicating that the knockout of PPARγ did not affect the general gene sets regulated by inflammatory activation of BMDMs with LPS or R848. Of note, some genes showed a higher expression level in the PPARγ$^{-/-}$ BMDMs compared to the PPARγ$^{fl/fl}$ cells with Tnf, Il6, Il10 and Il12b among them (Fig. 13 C indicated by asterisks). Further analyzing the effect of Mito treatment on the LPS induced gene expression in PPARγ$^{fl/fl}$ BMDMs showed significant downregulation of Il12a, Il12b, Nos2 and Nox1 (encoding a NADPH oxidase) (Fig. 13 D). Of note, Mito treatment of LPS activated PPARγ$^{-/-}$ BMDMs resulted in the regulation of similar genes compared to the PPARγ$^{fl/fl}$ cells (Fig. 13 E). PPARγ$^{fl/fl}$ cells also showed a significant decrease in expression of Il12a, and Nox1 as well as a, albeit statistically non-significant, decreased expression of Il12b and Nos2. In addition, Ccl24 – a chemotactic factor for resting T-cells as well as for neutrophils – was decreased in LPS stimulated BMDMs priorly treated with Mito. Concomitantly, Mito treatment of PPARγ$^{fl/fl}$ or PPARγ$^{-/-}$ BMDMs prior to their activation with R848 also showed a significant decrease in Il12b and Nos2 expression (Fig. 13 F & G). Both PPARγ$^{fl/fl}$ and PPARγ$^{-/-}$ BMDMs additionally showed significant downregulation of Il6. Moreover, Mito treatment decreased the expression of Cxcl10 and Il10 in both PPARγ$^{fl/fl}$ and PPARγ$^{-/-}$ BMDMs activated with R848, although not statistically significant in the PPARγ$^{-/-}$ cells. The treatment of PPARγ$^{fl/fl}$ BMDMs with Mito significantly inhibited the R848 induced upregulation of Il1b whereas this effect was absent in the PPARγ$^{-/-}$ BMDMs. Interestingly, Mito treatment resulted in the upregulation of Cxcl5 in LPS or R848 stimulated BMDMs irrespective of PPARγ expression (Fig. 13 D – G). Further investigation of the cytokine secretion after treatment with Mito or UK5099 and subsequent activation with LPS or R848 showed a decrease in both IL-6 and IL-12p40 secretion by both PPARγ$^{fl/fl}$ and PPARγ$^{-/-}$ BMDMs (Fig. 13 H – K). Hence, the previous observations of Mito or UK5099 facilitated regulation of cytokines under pharmacological PPARγ inhibition and in an in vitro knockout of PPARγ in BMDMs were further validated using an in vivo macrophage-specific PPARγ knockout. Overall,

these data demonstrate that Mito and UK5099 regulate the expression and secretion of inflammatory cytokines from BMDMs independent of PPARɣ.

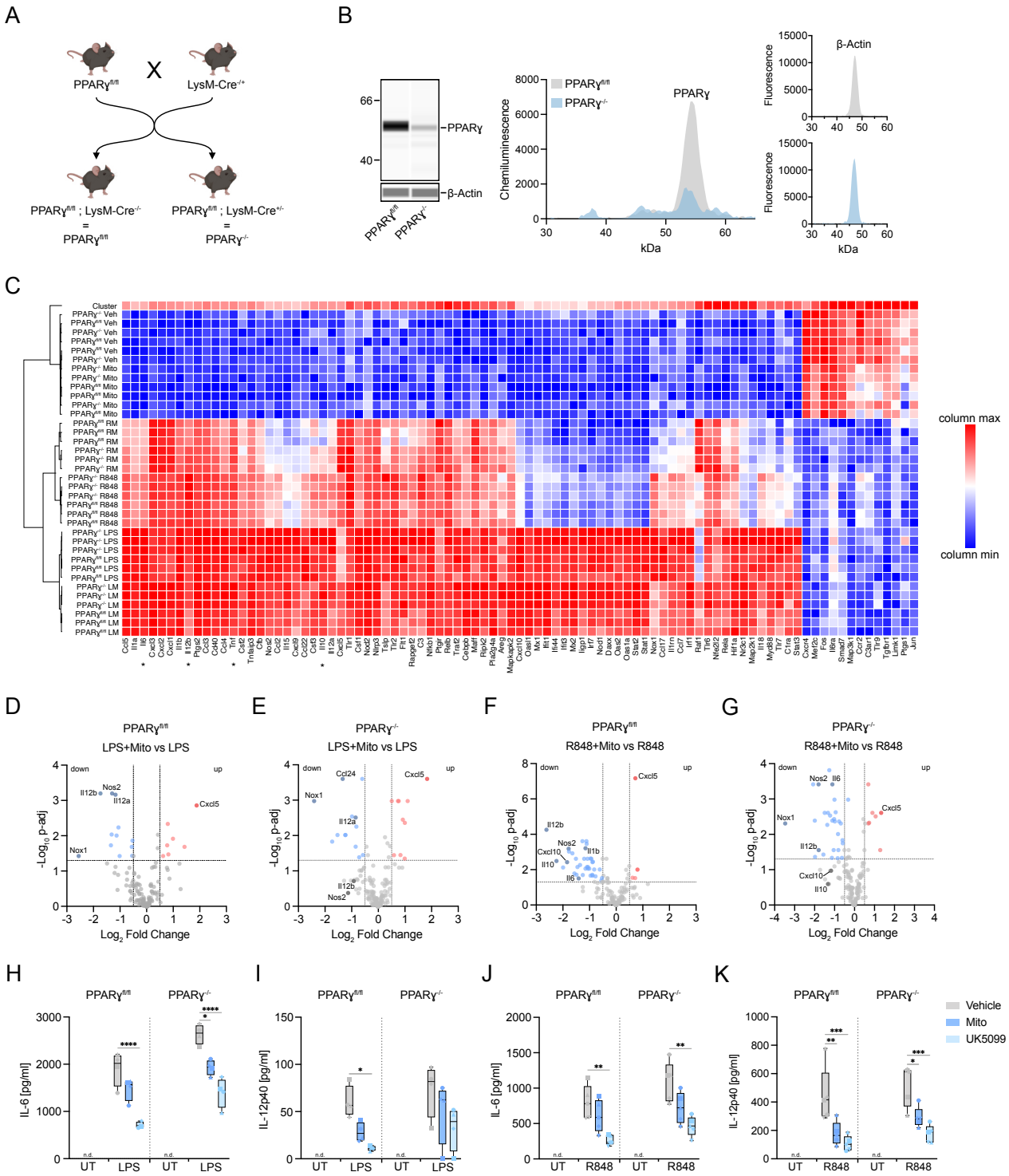

Fig. 13: Mitoglitazone modulates cytokine transcription and secretion independent of PPARɣ. A: PPARɣ$^{fl/fl}$ mice were crossed to LysM-Cre$^{+/-}$ mice yielding PPARɣ$^{fl/fl}$;LysM-Cre$^{-/-}$ (PPARɣ$^{fl/fl}$ control mice) and PPARɣ$^{fl/fl}$;LysM-Cre$^{+/-}$ (PPARɣ$^{-/-}$) littermates. **B:** Cells

lysates of PPARγ$^{fl/fl}$ and PPARγ$^{-/-}$ BMDMs were tested for PPARγ expression via Jess chemiluminescence western blotting. Capillaries were stripped, re-stained for β-actin as loading control and visualized via fluorescence detection. Mouse cartoon provided by BioRender **C:** PPARγ$^{fl/fl}$ or PPARγ$^{-/-}$ BMDMs were treated with vehicle or Mito (100 µM) for 1 hour, stimulated with LPS (10 ng/mL) or R848 (10 ng/mL) for 4 hours and purified mRNA was used for multiplexed mRNA profiling of inflammatory genes using the nCounter platform (Nanostring). Differentially expressed genes (Fold changes of ≤ -2 and ≥ 2; FDR adjusted-p value threshold = 0.05) were analyzed via hierarchical clustering analysis. Log_2-scaled fold changes were displayed in a heatmap with individual genes (columns) scaled from min to max. RM = R848+Mito; LM = LPS+Mito; n = 3 biological replicates **D – E:** Data obtained as described in C was analyzed for the effect of Mito treatment on LPS (LPS+Mito vs LPS) or R848 (R848+Mito vs R848) stimulation of PPARγ$^{fl/fl}$ and PPARγ$^{-/-}$ BMDMs. Differentially expressed genes (Fold changes of ≤ -1.5 and ≥ 1.5; FDR adjusted p-value threshold = 0.05) are displayed as volcano plots. Selected genes were highlighted. Blue dots = significantly downregulated genes; Red dots = significantly upregulated genes. **H – K:** PPARγ$^{fl/fl}$ or PPARγ$^{-/-}$ BMDMs were treated with vehicle or Mito (100 µM) for 1 hour, stimulated with LPS (10 ng/mL) or R848 (10 ng/mL) for 8 hours and the secreted cytokines were analyzed via ELISA. Mean ± SD of n = 4 or 5 biol. replicates from three independent experiments. n.d. = not detectable. Statistical significance was determined via 2-way ANOVA using Dunnett's multiple comparison test. Adjusted p-value: 0.03 (*), 0.0021 (**), 0.0002 (***), < 0.0001 (****)

3.13 Mitoglitazone improves macrophage viability and decreases serum cytokine levels in an acute sepsis mouse model

Since Mito inhibited inflammatory cytokine mRNA transcription and secretion from LPS activated macrophages, it was tested if Mito also modulated cytokine secretion in vivo using an acute sepsis mouse model. Aged matched male C57BL6/J mice were orally administered with Mito (30 mg/kg) or vehicle 2 hours prior to intraperitoneal injection with PBS or a sublethal dose of LPS (5 mg/kg) (Fig. 14 A). Mice were regularly monitored and clinically scored. Intraperitoneal injection of mice with LPS markedly deteriorated their clinical score (Fig. 14 B). Compared to the vehicle control, the oral administration of Mito showed no difference in the scoring of the mice within the first 4 hours post LPS injection. Yet, mice showed a delayed worsening of their clinical score between 5 to 8 hours post LPS injection when treated with Mito compared to the vehicle control. While LPS injection of mice increased overall weight loss, there was no observable difference in weight loss between the vehicle or Mito-treated groups (Fig. 14 C). Mice were euthanized 8 hours post LPS injection and their peritoneal cells (PECs) were isolated along with peritoneal lavage fluid. Additionally, serum was taken for multiplexed cytokine measurements. PECs

were stained for flow cytometric analysis of neutrophil ($CD19^-$ $CD11b^+$ $Ly6G^+$), B cell ($CD19^+$) and macrophage ($CD11b^+$ $F4/80^+$) populations, their viability and their respective surface expression of MHC-II, CD80 and CD86. While there was only a small population of neutrophils within the viable immune cells, Mito administration of mice showed no difference in the number of viable neutrophils compared to the vehicle-treated PBS or LPS injected groups (Fig. 14 D). Likewise, the number of viable B cells remained unchanged irrespective of Mito or vehicle administration compared to the PBS or LPS injected groups (Fig. 14 E). The surface expression of MHC-II (Fig. 14 F) and CD86 (Fig. 14 H) on B cells increased according to the total increase of viable B cells (Fig. 14 E). Moreover, Mito administration showed similar increases in B cell MHC-II and CD86 expression when compared to the LPS injected group administered with the vehicle control (Fig. 14 F & H). The presentation of CD80 on B cells remained unchanged irrespective of Mito administration or LPS injection compared to the control groups (Fig. 14 G). Although Mito did not change the number of viable macrophages in the PBS injected groups, Mito administration of the mice prior to LPS injection resulted in an increase of viable macrophages within the peritoneum compared to the LPS and vehicle treated group (Fig. 14 I). In contrast to the surface expression of MHC-II and CD80 on B cells, LPS injection of mice increased the expression of CD80, but not of MHC-II on macrophages (Fig. 14 J & K). Similar to the B cells, macrophage expression of both MHC-II and CD80 remained unchanged by Mito treatment compared to the control groups. In addition, while there was a slight decrease in CD86 on the surface of macrophages in the Mito administered and PBS injected group, this change was not observed for macrophages isolated from LPS injected mice (Fig. 14 L).

In order to investigate whether Mito regulates inflammatory cytokines in vivo, the sera and peritoneal lavage fluid were analyzed via multiplexed cytokine measurement. Importantly, Mito administration prior to LPS injection resulted in a slight reduction in IL-6 and a significant reduction in IL-12p40 serum concentrations (Fig. 14 N & O). There were no differences in TNFα, MCP-1, IL-10 or IP-10 serum concentrations irrespective of Mito treatment (Fig. 14 M, P, Q, R). Similarly, IL-6, IP-10 and MCP-1 concentrations in the peritoneal lavage of the mice remained unchanged regardless of Mito treatment (Fig. 14 S – U).

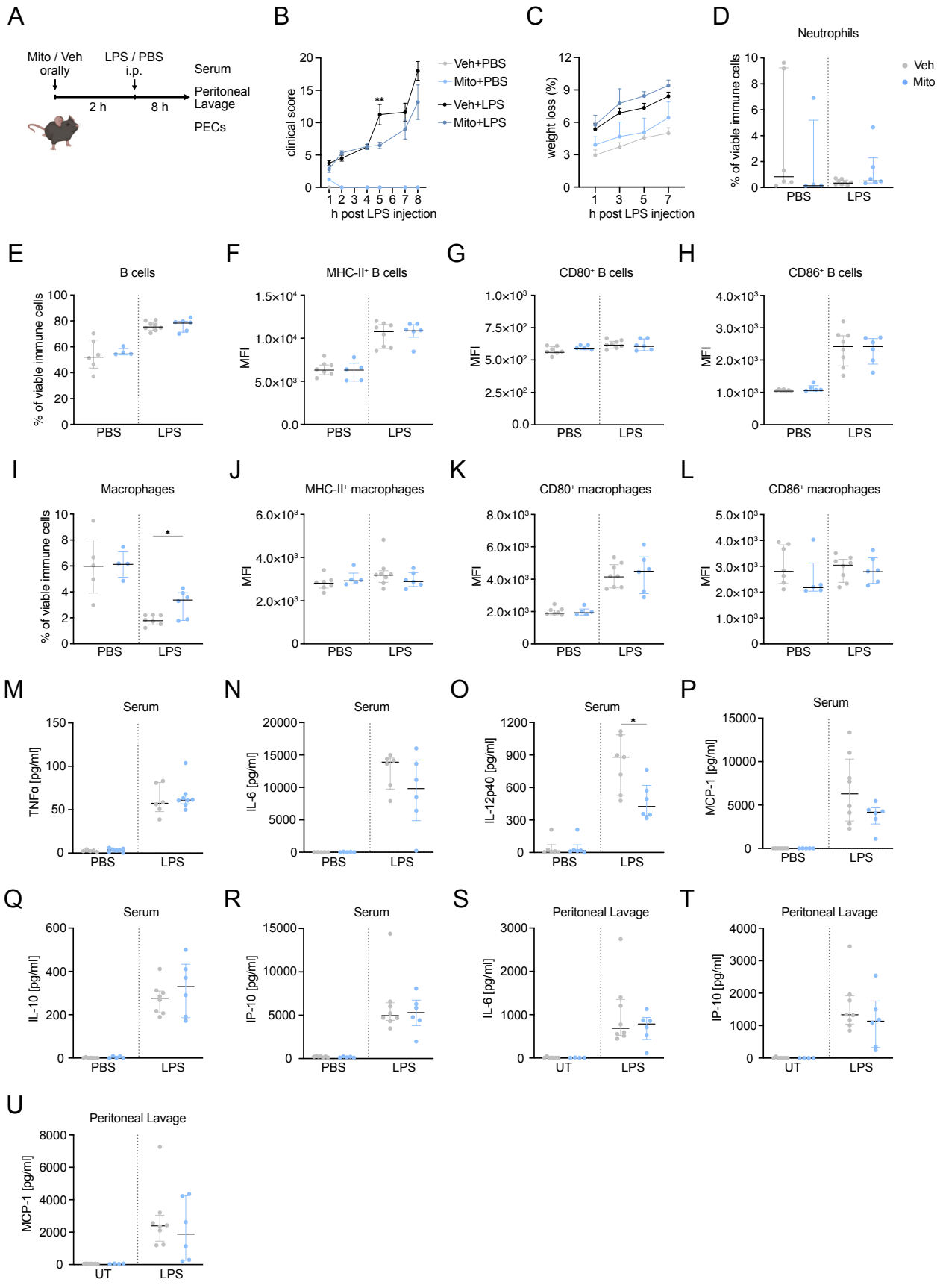
A
Mito / Veh orally
LPS / PBS i.p.
2 h
8 h
Serum
Peritoneal Lavage
PECs
B
clinical score
h post LPS injection
Veh+PBS
Mito+PBS
Veh+LPS
Mito+LPS
C
weight loss (%)
h post LPS injection
D
Neutrophils
% of viable immune cells
Veh
Mito
E
B cells
% of viable immune cells
F
MHC-II+ B cells
MFI
G
CD80+ B cells
MFI
H
CD86+ B cells
MFI
I
Macrophages
% of viable immune cells
J
MHC-II+ macrophages
MFI
K
CD80+ macrophages
MFI
L
CD86+ macrophages
MFI
M
Serum
TNFα [pg/ml]
N
Serum
IL-6 [pg/ml]
O
Serum
IL-12p40 [pg/ml]
P
Serum
MCP-1 [pg/ml]
Q
Serum
IL-10 [pg/ml]
R
Serum
IP-10 [pg/ml]
S
Peritoneal Lavage
IL-6 [pg/ml]
T
Peritoneal Lavage
IP-10 [pg/ml]
U
Peritoneal Lavage
MCP-1 [pg/ml]
PBS
LPS
UT

Fig. 14: The inflammatory response in an acute sepsis mouse model is decreased by Mitoglitazone. A: Aged matched (8 weeks) C57BL6/J male mice were administered Mito (30 mg/kg) or vehicle 2 hours prior to intraperitoneal (i.p.) injection with LPS (5 mg/kg). Mice were monitored regularly and euthanized 8 hours post LPS injection to isolate their sera, peritoneal cells (PECs) and peritoneal lavage fluid. Mouse cartoon provided by BioRender **B & C:** Mice were weighed and their clinical score was assessed regularly throughout the experiment. Data points are mean ± SEM of n = 5 – 8 biol. replicates. **D – L:** Peritoneal cells were isolated and stained for flow cytometric analysis of neutrophils ($CD19^-$ $CD11^+$ $Ly6G^+$), macrophages ($CD11b^+$ $F4/80^+$) and B cells ($CD19^+$) and their presentation of MHC-II, CD80 and CD86. Median ± interquartile of n = 4 – 8 biol. replicates. **M – S:** Sera and peritoneal lavage were analyzed for their cytokine concentrations via multiplexed cytokine measurement (Luminex). IL-12p40 concentrations were measured via ELISA. Median ± interquartile of n = 6 – 8 biol. replicates. Statistical significance was determined via an unpaired multiple t-test using Welch's correction. Adjusted p-value: 0.03 (*), 0.0021 (**), 0.0002 (***), < 0.0001 (****)

Together, these data show that oral administration of Mito delays the septic response to intraperitoneal injection of LPS, increases peritoneal macrophage viability and decreases IL-6 and IL-12p40 serum concentrations in an acute sepsis model in vivo.

4 Discussion

4.1 Inhibiting mitochondrial pyruvate import in macrophages regulates inflammation

Within the first hours of activation, macrophages undergo a metabolic remodeling with increased glycolysis and mitochondrial metabolism (Lauterbach et al., 2019; Rodríguez-Prados et al., 2010; Tannahill et al., 2013). In 2019, Lauterbach *et al.* demonstrated that intervention in macrophage metabolism can regulate their inflammatory response. They showed that inhibition of pyruvate import via MPC inhibition by UK5099 reduces mitochondrial metabolism and, concomitantly, the inflammatory response of BMDMs. However, UK5099 displays pharmacochemical properties unfit for clinical use. This warrants the identification of new small molecule inhibitors of the MPC that could aid in treating inflammatory diseases.

While developed as PPARɣ agonists, later reports showed that Glitazones also inhibit the MPC (Divakaruni et al., 2013). A new, PPARɣ-sparing generation of Glitazones is now being investigated for their potential to treat T2DM, NASH and neurodegenerative diseases like Alzheimer's disease or Parkinson's disease (Chen et al., 2012; J. R. Colca, Vanderlugt, et al., 2013; Jacques et al., 2021; Mallet et al., 2022; Shah et al., 2014). However, as of today there are no reports specifically investigating whether MPC inhibition via these new Glitazones can regulate inflammation. Hence, it was investigated whether Mito – a clinically applicable MPC inhibitor with reduced PPARɣ affinity – can regulate the metabolically governed inflammatory response of macrophages.

4.1.1 Mitoglitazone inhibits the MPC and evokes metabolic adaptations in macrophages

Using permeabilized BMDMs, it was demonstrated that Mito inhibits the mitochondrial pyruvate import and subsequent pyruvate metabolism similar to the covalent MPC inhibitor UK5099. Decreased total levels of alanine – produced via pyruvate transamination – and its reduced carbon labeling from glucose further validated that Mito inhibits mitochondrial pyruvate import and metabolism. These results align with a previous report in which Pioglitazone or Mito inhibited the MPC in permeabilized human skeletal muscle cells (Divakaruni et al., 2013). Furthermore, isotopic labeling showed that Mito or UK5099 inhibition of the MPC reduces carbon integration from U-$^{13}C_6$-glucose into all TCA-cycle metabolites. Most notably, Mito treatment reduced the citrate levels in BMDMs via blocking

pyruvate entry into the mitochondria. Citrate can be converted into acetyl-CoA via ATP-citrate lyase (ACLY) and subsequently be used for acetylation of histones to foster inflammatory gene transcription (Lauterbach et al., 2019). Upon macrophage activation, histones in regions of LPS-responsive genes undergo de novo acetylation by histone acetyltransferases (HATs) using acetyl-CoA. This opens the chromatin structure to allow for gene transcription. Blocking acetyl-CoA production from citrate via direct inhibition of ACLY reduces acetylation of histones of LPS response genes such as Il12b. Likewise, reduced citrate-availability in BMDMs upon Mito-facilitated MPC inhibition during inflammatory stimulation might regulate transcription of inflammatory response genes similar to ACLY inhibition. Furthermore, histone acetylation is a dynamic process that occurs even without an inflammatory stimulus (Escoubet-Lozach et al., 2011). Poised chromatin – determined by the simultaneous presence of histone modifications with both positive and negative regulation of gene transcription – allows to rapidly switch on transcription of genes. Citrate reduction in unstimulated BMDMs might reduce acetylation of histones in these poised regions and delay the transcription of inflammatory response genes. As Mito reduced citrate levels independent of inflammatory macrophage activation, it might very well be that it can evoke changes in the epigenetic landscape of macrophages before their activation, thereby influencing inflammatory response dynamics.

In 2013, Divakaruni *et al.* showed that acute inhibition of the MPC using Pioglitazone results in increased glucose uptake of myotubes, yet they did not show the effects of Mito. Here, acute MPC inhibition via Mito treatment of BMDMs did not change their glucose uptake. Indeed, it was shown that knockdown of MPC1 or MPC2 in C2C12 myoblasts did not affect glucose uptake of cells (Vacanti et al., 2014). This suggests that the cellular response to Mito-facilitated MPC harbors differences to Pioglitazone treatment and may better reflect the loss of pyruvate import via the MPC. Differences between Mito and Pioglitazone might originate from their different PPARɣ affinities. It was shown that PPARɣ activation increases glucose uptake of cells by increasing the expression of the glucose transporter GLUT4 (Armoni et al., 2003). However, another study found that Pioglitazone can increase glucose utilization of astrocytes without upregulating glucose transporters (dello Russo et al., 2003). The exact mechanism of how Glitazones regulate glucose uptake within different cell types remains to be understood. However, Mito seems to generally downregulate cellular glucose metabolism, without affecting glucose uptake.

To cope with changes in nutrient availability, cellular metabolism can adapt metabolic pathways via rerouting of metabolites and thereby sustain supply of energy- and reducing equivalents and biosynthetic precursors. It was shown that pharmacologic MPC inhibition and knockdown as well as knockout of the MPC subunits can result in anaplerosis of the TCA-cycle via increased glutaminolysis and β-oxidation of fatty acids in different cell types (Lauterbach et al., 2019; Vacanti et al., 2014; Wenes et al., 2022). Concomitantly, Mito inhibition of the MPC resulted in increased glutaminolysis as indicated by the increase of glutamate and α-ketoglutarate labeling in $^{13}C_1$- or $^{13}C_5$-glutamine fed BMDMs. Although it was not investigated during the course of this work, it is likely that macrophages that were treated with Mito also adapted their fatty acid utilization for anaplerosis of the TCA-cycle. The metabolism of LPS activated macrophages ultimately shifts towards glycolysis and downregulates mitochondrial respiration after longer activation times. However, the TCA-cycle keeps being utilized to produce and accumulate distinct metabolites at later stages of activation. Some of these metabolites were shown to modulate and fine-tune the immune responses of macrophages. Well-described examples are succinate and itaconate. Succinate accumulation at later stages of macrophage activation can stabilize hypoxia-inducible factor 1-α (HIF1-α), a transcription factor that directly drives the transcription of Il1b and glycolytic genes to boost the inflammatory response (McGettrick & O'Neill, 2020; Tannahill et al., 2013; Wang et al., 2017). As initially described, itaconate is produced from cis-aconitate (directly subsequent to citrate in the TCA-cycle) via the LPS-inducible IRG1. Itacconate accumulates and decreases the expression of pro-inflammatory cytokines such as IL-12p70, IL-6 and IL-1β (Lampropoulou et al., 2016; Meiser et al., 2016; Michelucci et al., 2013). Mito reduced glycolysis in macrophages even after long LPS stimulation indicating its potential to regulate the accumulation of TCA-cycle products from glucose. Hence, it should be investigated whether reduced carbon flux from glucose into TCA-cycle metabolites after MPC inhibition by Mito can regulate the accumulation of immunomodulatory metabolites such as succinate or itaconate at later activation stages. Inhibition of the MPC further increased fumarate, malate and aspartate hinting towards an increased aspartate-argininosuccinate shunt to replenish the TCA-cycle. Indeed, it was shown before that the aspartate-argininosuccinate shunt contributes to TCA-cycle anaplerosis in macrophages (Jha et al., 2015). Fumarate itself was shown to inhibit histone demethylases, thereby regulating the epigenetic landscape and gene transcription of

macrophages (Arts et al., 2016; Netea et al., 2020). Whether the increased fumarate levels upon Mito treatment affects methylation of histones within macrophages is currently investigated. Together with changes in histone acetylation upon Mito treatment, these findings could help to delineate how MPC inhibition gets integrated into the metabolic-epigenetic axis of macrophages.

Overall, the observed metabolic changes in BMDMs upon Mito treatment are in line with current literature reporting on the metabolic adaptations in the absence of MPC-facilitated mitochondrial pyruvate import. This supports the putative use of Mito in regulating inflammation via rerouting of macrophage metabolism.

4.1.2 Inhibition of the MPC increases reductive TCA-cycle flux

In 2004, it was shown that Rosiglitazone and Pioglitazone can inhibit complex I of the ETC in a similar manner as Metformin, albeit less efficiently (Brunmair et al., 2004). Metformin is the most prescribed drug to treat T2DM and also has anti-inflammatory effects. Moreover, Metformin is often given as a combination anti-diabetic medication including its combination with Pioglitazone (e.g. Actoplus Met). Therefore, it was speculated whether some of the anti-diabetic effects of Glitazones originate from complex I inhibition. Indeed, in 2013 Divakaruni *et al.* showed that high concentrations of Glitazones, including Mito, can inhibit complex I in C2C12 myoblasts. A consequence of complex I inhibition is the increase of reductive TCA-cycle flux, as was shown by using the complex I inhibitor rotenone in myoblasts (Vacanti et al., 2014). One way to investigate reductive TCA-cycle flux is to trace stable isotope labeled $^{13}C_1$-glutamine (only the first carbon labeled) as the single labeled carbon will be excluded immediately from the normal oxidative TCA-cycle. Using $^{13}C_1$-glutamine fed immortalized murine embryonic fibroblasts (MEFs) from MPC1$^{-/-}$ mice, it was shown that loss of the MPC increases the M1 isotopologue of citrate (Vanderperre et al., 2016). Importantly, this demonstrated that loss of mitochondrial pyruvate import via the MPC can result in increased reductive TCA-cycle flux without direct complex I inhibition. In line with these findings, Mito or UK5099 increasd the M1 isotopologues of citrate, malate and aspartate in $^{13}C_1$-glutamine labeled BMDMs. This demonstrates that pharmacologic inhibition of the MPC in BMDMs increases the reductive TCA-cycle. Of note, Mito treatment showed a greater increase of the reductive TCA-cycle when compared to UK5099. It is unclear whether this qualitative difference between UK5099 and Mito

originates from their covalent and non-covalent MPC inhibition, respectively, or a potential dual inhibition of both the MPC and complex I by Mito. However, when tracing the carbon integration into TCA-cycle metabolites coming from U-$^{13}C_5$-glutamine, an increase of the reductive TCA-cycle after complex I inhibition would result in the increase in the M5 isotopologue of citrate. This was shown in U-$^{13}C_5$-glutamine fed myoblasts that were treated with the complex I inhibitor rotenone (Vacanti et al., 2014). In the same study, MPC inhibition by UK5099 only showed an increase in M6 citrate whereas MPC1 or MPC2 knockdown resulted in increased labeling of both M5 and M6 citrate. The increase in the M6 isotopologue of citrate was attributed to increased flux through malic enzymes (MEs; malate conversion to pyruvate) and pyruvate dehydrogenase (PDH; pyruvate conversion to acetyl-CoA) (Fig. D1). Furthermore, the authors used an alternative labeling approach feeding $^{13}C_3$-labeled glutamine (only the third carbon labeled) in combination with MPC1 or MPC2 knockdown and reported an increase in M2 labeled citrate (flux through MEs), but not in M1 labeled citrate (reductive flux). They concluded that loss of the MPC results in increased reductive TCA-cycle flux and alternative flux through MEs whilst attributing a higher proportion of metabolic adaptation to MEs. Furthermore, Mito treatment of U-$^{13}C_5$-glutamine labeled and LPS activated BMDMs showed increases in the M3 and M6 isotopologues of citrate, but not of the M5 isotopologue (Fig. 7 G). This argues against a complex I inhibition whilst indicating an increased flux through MEs and subsequently pyruvate dehydrogenase (PDH) (Fig. D1 A) and potentially pyruvate carboxylase (PC) after Mito treatment (Fig. D1 B). While these results showed that metabolic adaptation can be more complex than just upregulation of one metabolic route, they were overall in line with both pharmacologic MPC inhibition by Mito or UK5099 and the results obtained from MPC1 knockout in MEFs by Vanderperre *et al.* (2016) described earlier. Nevertheless, a future investigation using extracellular flux analysis of permeabilized cells supplied with either glutamate and malate to assess complex I activity or succinate and rotenone to assess complex II activity in presence or absence of Mito is necessary to ultimately resolve its inhibitory function towards complex I in BMDMs.

Conclusively, treatment of BMDMs with Mito elicits mitochondrial adaption by simultaneously increasing reductive TCA-cycle flux and metabolism through MEs. These changes likely originate from Mito inhibition of the MPC rather than an inhibition of complex I.

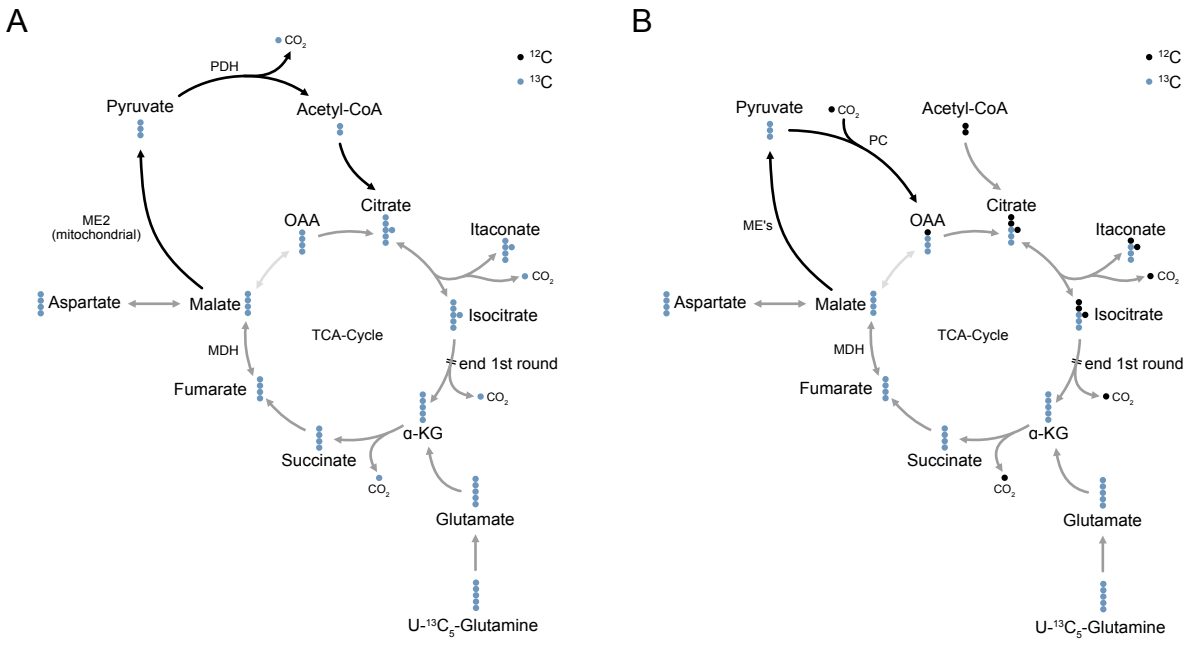

Fig. D1: Increased carbon flux through malic enzymes as metabolic adaptation to maintain mitochondrial metabolism. A: Scheme following carbon labeling from U-$^{13}C_5$-glutamine after rerouting of metabolites through mitochondrial malic enzyme (ME2) and pyruvate dehydrogenase (PDH). **B:** Scheme following carbon labeling from U-$^{13}C_5$-glutamine after rerouting of metabolites through malic enzymes (MEs) and pyruvate carboxylase (PC).

4.1.3 Mitoglitazone regulates the metabolic switch of inflammatory macrophages

Here, it was demonstrated that Mito treatment acutely inhibits the glycolytic shift and the increased mitochondrial respiration of inflammatory macrophages early after LPS activation. Mito-elicited effects were similar to the results obtained by MPC inhibition using UK5099. These results are in line with previous reports demonstrating the inhibition of both glycolysis and mitochondrial respiration by UK5099 in LPS activated macrophages (Lauterbach et al., 2019; Ran et al., n.d.). Together, these results strongly suggest that the inhibitory effects towards the metabolic switch of macrophages originate from Mito-facilitated inhibition of the MPC.

Qualitatively, Mito inhibited glycolysis to an even greater extent than UK5099 as it also completely ablated the glycolytic reserve of the cells. Both, Mito and UK5099 treatment of BMDMs already reduced their glycolytic capacity and glycolytic reserve without LPS activation. Similarly, total levels of glycolytic and TCA-cycle metabolites were regulated by Mito or UK5099 treatment independent of inflammatory macrophage activation. Hence,

MPC inhibition regulates macrophage metabolism independent of their activation status. Accordingly, Mito treatment might affect the metabolism of other cell types that either heavily depend on glucose such as cancer cells. Moreover, adipocytes of obese visceral adipose tissue have an increased oxygen consumption that, together with a dysbalanced vascularity of hypertrophic adipose tissue, results in hypoxia. As a consequence, adipocytes can release cytokines to recruit and activate monocytic cells into the adipose tissue, resulting in increased numbers of inflammatory adipose tissue macrophages (Lumeng, Bodzin, et al., 2007; Soccio et al., 2014). Future studies should scrutinize whether Mito can reduce adipose tissue inflammation by reducing adipocyte hypoxia, concurrent recruitment of immune cells and inflammatory macrophage responses.

In addition to the well-described metabolic shift after TLR4 activation by LPS, it was also demonstrated that a similar metabolic shift occurs in BMDMs activated with the TLR7/8 ligand R848 (Tan & Kagan, 2019). Interestingly, MPC inhibition by both Mito and UK5099 also decreased the glycolytic and mitochondrial metabolism in R848 activated macrophages. This highlights the similarities of the metabolic shift of macrophages after activation of different TLRs and suggests that the MPC might be a common denominator of pharmacologic intervention. As such, MPC inhibition may harbor the potential to treat aberrant inflammation in a multitude of diseases.

4.1.4 Basal MPC expression is sufficient to supply mitochondrial metabolism of LPS activated macrophages

The activation of macrophages with LPS increases their mitochondrial respiration at early time points. While this increased mitochondrial demand for carbon sources might have been fueled by the upregulation of the MPC subunits, LPS activation of BMDMs had no effect on the expression levels of either MPC1 or MPC2. Moreover, it was suggested that MPC activity might get regulated via the acetylation of MPC1 or MPC2 (Liang et al., 2015; Vadvalkar et al., 2017). Immunoprecipitating either MPC1 or MPC2 from LPS stimulated or unstimulated BMDMs and investigating their acetylation status demonstrated that TLR4 activation does not affect the post-translational acetylation of the MPC. Together, this suggests that the increased demand for carbon sources of mitochondrial metabolism early after macrophage activation is already sufficiently covered by the transport rate of the MPC or that macrophages regulate MPC activity in an alternative manner.

4.1.5 Mitoglitazone regulates the inflammatory response of macrophages via MPC inhibition and PPARγ-independently

Further looking into the effector functions of BMDMs showed that Mito and UK5099 treatment of LPS and IFNγ activated BMDMs reduced secretion of nitric oxide and inhibited the induction of Nos2 mRNA transcription in both PPARγ$^{fl/fl}$ and PPARγ$^{-/-}$ BMDMs stimulated with LPS or R848. However, the LPS and IFNγ induced expression of iNOS (also termed NOS2) protein remained unchanged when the cells were pretreated with Mito. This indicates that Mito delays nitric oxide production as Nos2 mRNA expression was measured 4 hours after LPS stimulation, whereas protein expression was tested after 24 hours of stimulation. Moreover, iNOS levels were tested after stimulation with both LPS and IFNγ, whereas Nos2 mRNA levels were changed only upon stimulation with LPS. Therefore, Mito-facilitated regulation of Nos2 mRNA expression should be investigated after stimulation with both LPS and IFNγ to investigate its nitric oxide inhibitory mechanism. Moreover, Mito modulated amino acid metabolism as seen by decreased alanine and increased aspartate levels. In fact, it was reported that MPC1 or MPC2 knockdown results in altered amino acid metabolism in muscle cells (Vacanti et al., 2014). Thus, it is possible that iNOS production of nitric oxide was reduced due to a decreased substrate supply of iNOS with L-arginine and/or its reducing factor NADPH.

Earlier it was reported that LPS-induced secretion of IL-12p40 depends on glucose availability to BMDMs (Lauterbach et al., 2019). Furthermore, the same study demonstrated that inhibition of the MPC by UK5099 decreases the LPS-induced secretion of IL-6 and IL-12p40. In both experiments, the early induced cytokine Cxcl1 was not affected, leading the authors to conclude that specifically cytokines of the late LPS response may be affected by blockage of mitochondrial pyruvate import. Of note, the late cytokine IL-12p40 was found to be particularly susceptible to the inhibition of the MPC or ACLY in both BMDMs and human macrophages. Here, it was shown that Mito decreases Il6 and Il12b mRNA transcription and IL-6 and IL-12p40 secretion similar to UK5099 treatment of LPS activated BMDMs. Similar to what was shown for ACLY inhibition, IL-12p40 was the most susceptible cytokine to Mito inhibition of the MPC throughout my investigations. MPC inhibition by Mito or UK5099 also regulated cytokine transcription and secretion after

activation of BMDMs with the TLR7/8 ligand R848. This indicates that the MPC might not only be a target to modulate the inflammatory responses to bacterial, but also viral infections.

As described earlier, Glitazones were developed as agonists for PPARɣ. Mito has a decreased PPARɣ binding affinity compared to the first generation Glitazones Rosiglitazone or Pioglitazone while retaining the affinity for the MPC (Bolten et al., 2007; Quansah et al., 2018). Nevertheless, it had to be excluded that Mito-facilitated PPARɣ activation resulted in the observed cytokine regulation. Results from pharmacologic PPARɣ inhibition and in vitro as well as in vivo PPARɣ$^{-/-}$ BMDMs demonstrate that Mito regulates LPS and R848 induced cytokines independently of PPARɣ. Similar to wildtype- and PPARɣ$^{fl/fl}$ cells, Mito decreased the expression of IL-6 and IL-12p40 in LPS- and R848 activated BMDMs even in the absence of PPARɣ. Moreover, Mito also decreased the mRNA transcription of Cxcl10 in R848 activated PPARɣ$^{fl/fl}$ and PPARɣ$^{-/-}$ BMDMs indicating a regulation of antiviral responses. Of note, IL-12p40 seemed to be the most susceptible cytokine to MPC inhibition also in the absence of PPARɣ, matching the results observed in wildtype BMDMs. Both, IL-12p40 and CXCL10 bridge the innate and adaptive immune response by recruiting and activating neutrophils and T cells. Indeed, Lauterbach *et al.* (2019) suggested that ACLY regulation might hold therapeutic potential regarding viral infections, vaccine approaches and T cell driven inflammatory pathologies. They based their claim on the up- or downregulation of specific LPS responsive gene sets linked to adaptive immune activation after ACLY inhibition. In addition, Welch *et al.* (2003) reported that treatment of peritoneal macrophages with rosiglitazone decreased the expression of IFN-ɣ response genes including Nos2, Cxcl10 and Il12b. These findings greatly overlap with the inflammatory gene regulation I observed in the context of Mito treatment of LPS or R848 activated BMDMs. Therefore, mitochondrial pyruvate import might be of similar importance to mediate immune responses compared to downstream acetyl-CoA production by ACLY. In fact, MPC inhibition might regulate the immune response of macrophages in a similar manner as ACLY inhibition. As mentioned earlier, the reduced citrate production observed after Mito treatment might result in reduced acetyl-CoA production and subsequently modulate histone acetylation and expression of similar TLR signaling response genes as reported for ACLY. Whether Mito affects histone acetylation of inflammatory macrophages is currently undergoing investigation.

In vitro observations of Mito-regulated IL-6 and IL-12p40 secretion were also reflected in an acute sepsis mouse model as both cytokine levels were decreased systemically in the serum of mice pretreated with Mito prior to i.p. injection with LPS. Moreover, Mito seems to have a protective effect against endotoxemia-induced macrophage exhaustion as it decreased loss of macrophages in the peritoneal cavity. These findings demonstrate that Mito facilitates anti-inflammatory effects by modulating macrophage functions in vivo. However, it should be pointed out that Mito might also regulate functions of other immune cells. A recent publication showed that MPC inhibition affects memory T cell differentiation and anti-tumor functions of CAR T cells (Wenes et al., 2022). It should be further investigated whether Mito treatment can regulate innate immune crosstalk to adaptive immune cells such as T cells and whether Mito inhibition of the MPC can regulates T cell functions directly. Overall, these results highlight that targeting the MPC might hold therapeutical value to treat inflammatory diseases involving not just the innate- but also the adaptive immune system.

In contrast to Il6 and Il12b, Tnf expression is induced early after LPS activation of BMDMs. Mito or UK5099 treatment of LPS or R848 activated BMDMs also reduced Tnf mRNA expression and TNFα secretion. However, administration of Mito and subsequent LPS injection of mice showed no alterations of TNFα levels. Therefore, while the early response cytokine TNFα may be affected by MPC inhibition in vitro, these data suggest that Mito treatment does not affect TNFα in vivo.

4.1.6 IL-10 regulation via MPC inhibition by Mito is TLR-specific and correlates with maximal respiration of mitochondria

Mitochondrial citrate export and its conversion into acetyl-CoA via ACLY happen downstream of mitochondrial pyruvate import. Pharmacologic inhibition of ACLY in LPS activated BMDMs increased the transcription of IL-10 mRNA (Lauterbach et al., 2019). However, MPC inhibition by Mito or UK5099 did not change Il10 mRNA transcription or IL-10 secretion after LPS activation of wildtype BMDMs. In contrast, Mito decreased Il10 transcription and IL-10 secretion of R848 activated wildtype and PPARɣ$^{-/-}$ BMDMs. These findings indicate that MPC inhibition upstream of ACLY at least partially exerts different immunomodulatory functions than direct inhibition of acetyl-CoA production from citrate. Indeed, modulation of IL-10 after ACLY inhibition was already suggested to result from

metabolic alterations upstream of ACLY rather than from direct inhibition of citrate production from acetyl-CoA (Lauterbach et al., 2019). However, the mechanism of IL-10 modulation after ACLY inhibition remains to be clarified.

Ligand binding of TLR7/8 activates myeloid differentiation primary response protein 88 (MyD88) whereas ligand activation of TLR4 evokes TIR-domain-containing adapter-inducing interferon-β (TRIF) and MyD88 signaling cascades. Since Mito regulated IL-10 induction by R848 but not LPS, Ticam$^{-/-}$ BMDMs – that are devoid of TRIF signaling – were used to look into the putative differential regulation of TRIF- and MyD88 signaling by Mito. Mito treatment of Ticam$^{-/-}$ BMDMs activated with LPS showed similar downregulation of cytokines compared to the wildtype cells. Also, LPS induced IL-10 production still remained unchanged when Ticam$^{-/-}$ BMDMs were treated with Mito. This demonstrates that the difference in Mito regulated IL-10 regulation after LPS or R848 activation of BMDMs is not solely dependent on MyD88 signaling. It is likely, that Mito affects signaling downstream of TRIF- or MyD88 signaling. Of note, mitochondrial respiration rates of BMDMs showed significant differences after prolonged activation for 24 hours when comparing LPS and R848. LPS activation of BMDMs for prolonged time frames results in reduced mitochondrial respiration and a strong dependence on aerobic glycolysis. However, prolonged activation of BMDMs with R848 showed an increase in mitochondrial respiration compared to shorter activation. This suggests, that macrophage responses to TLR7/8 activation (e.g. after viral infections) might have a higher dependency on mitochondrial respiration than after the recognition of bacterial LPS. Production of IL-10 in R848 activated BMDMs might therefore be more susceptible to mitochondrial perturbation than LPS activated BMDMs. This is further indicated by the generally greater downregulation of cytokines after Mito treatment of R848 compared to LPS activated cells. Future experiments should investigate whether Mito can downregulate mitochondrial respiration after prolonged R848 activation of macrophages. Additionally, it should be investigated whether Mito regulates the response of macrophages to viral infections.

4.2 Current state and future prospects of MPC inhibition

While Glitazones were successfully used to treat T2DM, their clinical application declined due to their side effects such as weight gain, fluid retention, bone fractures and, in the case of troglitazone, hepatotoxicity (Soccio et al., 2014). As mentioned earlier, nowadays

mainly Pioglitazone is being used to treat T2DM; Often in combination with Metformin. Moreover, Pioglitazone is the only drug that is being recommended by both the American Association for the Study of Liver diseases (AASLD) and the European Association for the Study of Liver diseases (EASL) to treat biopsy-proven NASH, albeit without FDA approval (Cusi et al., 2016). A growing body of research is now looking into the potential of second generation Glitazones to treat inflammatory diseases including T2DM, NASH and neurodegenerative diseases. The overarching hypothesis for these newly developed drugs is to no longer aim for PPARɣ activation, but to inhibit the MPC as this seems to retain the drugs' positive effects while simultaneously diminishing side effects. In fact, a clinical trial investigated whether Mito treatment improved glucose metabolism in T2DM (J. R. Colca, Vanderlugt, et al., 2013). Treatment of T2DM patients with Mito showed similar glucose-lowering effects compared to Pioglitazone. In contrast to Pioglitazone, Mito showed no fluid retention and no expansion of adipocytes.

Metabolic dysregulation is now being considered as one of the key factors contributing to neurodegenerative disorders. Alzheimer's disease is associated with insulin resistance and recessed glucose metabolism in certain brain regions. Treatment of mild Alzheimer's disease patients showed improvement of glucose metabolism in these regions suggesting that MPC inhibition could reverse AD-related metabolic changes within the brain (Shah et al., 2014). Furthermore, in vitro and in vivo studies suggest beneficial effects of Mito in the context of Parkinson's disease (Ghosh et al., 2016; Mallet et al., 2022; Quansah et al., 2018). In 2016, Ghosh *et al.* demonstrated reduced secretion of TNFα, IL-6 and IL-1β from a microglia cell line upon Mito treatment. Since microglia are considered specified macrophages of the brain, Mito treatment of these cells might have similar effects on their activation compared to the results in BMDMs demonstrated in this study.

Developed by the same company (Metabolic Solutions Development Company) as Mito and structurally very similar, MSDC-0602K was tested for its efficacy in treating NASH patients in the Phase 2b EMMINENCE trial (NCT02784444). While MSDC-0602K treatment did not significantly change liver histology of the patients, it improved glucose and insulin regulation as well as serum levels of liver enzymes and the nonalcoholic fatty liver disease (NAFLD) activity score (NAS). Yet, no side effects were displayed by the intake of the drug. This prompted a follow-up Phase 3 clinical trial (NCT03970031) that will investigate the efficacy of MSDC-0602K in patients afflicted by both NASH and T2DM as

both diseases often occur in the same patients. Moreover, several in vivo mouse studies suggest that MPC inhibition by MSDC-0602K can be used to increase liver physiology in NASH and ameliorate adverse effects of obesity such as adipose tissue inflammation (Chen et al., 2012; J. Colca, 2020; Mccommis et al., 2016; Rauckhorst et al., 2017).

Both, Mito and MSDC-0602K are structurally very similar to Pioglitazone. Pioglitazone is usually given as a racemic mixture of its (R)- and (S)-stereoisomer. Interestingly, a recent clinical Phase 1a study demonstrated that while both enantiomers display efficacy in treating NASH, the (R)-stereoisomer shows none of the side effects ascribed to Pioglitazone intake (Jacques et al., 2021). Moreover, while both the (R)- and (S)-stereoisomer of Pioglitazone inhibited the MPC, the (R)-stereoisomer does not activate PPARɣ. This again strongly supports the hypothesis that the beneficial effects of Glitazones can be ascribed to a substantial degree to MPC inhibition rather than PPARɣ activation. A deuterium-stabilized (R)-Pioglitazone enantiomer is now being developed by Poxel SA under the name PXL065. In addition to its application in NASH, it will soon undergo further clinical investigation (NCT05200104) regarding the treatment of X-linked adrenoleukodystrophy (ALD); A rare disease caused by impaired peroxisomal metabolism of very long-chain fatty acids and concomitant inflammation and mitochondrial dysfunction. However, enantiomeric stabilization of PXL065 is achieved via deuteriation, making its upscaled production difficult. Interestingly, another study showed that double-bond stabilization of the chiral center of a truncated Glitazone (5-(4-hydroxybenzylidene)thiaolidine-2,4-dione) can further reduce PPARɣ affinity while further increasing MPC affinity compared to Mitoglitazone or MSDC-0602K (Touaibia et al., 2021). Whether this compound affects macrophage metabolism and their inflammatory response is currently under investigation.

Recent research identified several other MPC inhibitors, with partially significantly higher affinity for the MPC compared to Mito or UK5099 (Corbet et al., 2018; Du et al., 2013; Hegazy et al., 2022; Hodges et al., 2022; Liu et al., 2021; Tavoulari et al., 2022). Yet, the pharmacokinetic properties of most of these inhibitors render them unfit for their use in vivo (Yiew & Finck, 2022). Exceptions are entacapone and nitrofurantoin, two clinically used drugs for treating Parkinson’s disease or bacterial bladder infections, respectively (Tavoulari et al., 2022). However, entacapone has a higher affinity for its intended target catechol-O-methyltransferase compared to the MPC and nitrofurantoin is an antibiotic, making them unfit to specifically target the MPC without risking side effects.

Overall, current studies indicate a promising future for the development and clinical application of MPC inhibitors for the treatment of metabolic- and inflammatory diseases.

4.3 Conclusion

A growing body of studies suggest the MPC to be a promising drug target in the treatment of metabolic and inflammatory diseases. MPC inhibition seems especially beneficial in the context of neurodegenerative disorders, but also to the treatment of non-communicable diseases such as T2DM or NASH. It is now widely accepted that many of the pathologies on the rise in modern societies have an underlying inflammatory component that is connected to metabolic dysregulation. Pharmacologic intervention in both the inflammatory and metabolic components of these diseases is therefore of great interest to remedy the socio-economic burden placed upon society.

In accordance with current literature, this study showed that Mitoglitazone can be used to pharmacologically inhibit the MPC in macrophages. Mito-facilitated MPC inhibition modulated the adaptations of both, glycolysis and mitochondrial metabolism necessary for the inflammatory response of macrophages. The inhibition of the MPC by Mito generally decreased the utilization of glucose and the downstream production of immunomodulatory metabolites by inflammatory macrophages. Furthermore, it modulated the effector functions of macrophages by decreasing the production of nitric oxide and inflammatory cytokines. Of note, MPC inhibition by Mito most prominently affected the pro-inflammatory cytokines IL-6 and IL-12p40 in vitro and in vivo. Together with its proven clinical safety, these findings suggest that Mito could be used as an anti-inflammatory drug. Moreover, the persistent downregulation of inflammatory cytokines by Mito in presence and absence of PPARɣ strongly suggest that the so far undefinable anti-inflammatory effects of Glitazones originate from MPC inhibition. Not only the LPS-evoked, but also the TLR7/8-facilitated inflammatory response was modulated by MPC inhibition. This further suggests that Mito could be used to treat erroneous inflammation not only in the context of metabolic dysregulation or bacterial infections, but also viral diseases. While the mechanism of how Mito-facilitated MPC inhibition decreases the pro-inflammatory response of macrophages is currently under investigation, it is likely that it involves an integration of the metabolic-epigenetic axis that licenses the transcription of inflammatory response genes.

Mito-facilitated MPC inhibition promises to be useful to further understand the interplay between metabolic dysregulation and pathologic inflammation. Together with lifestyle changes, pharmacologic MPC inhibition could aid in treating non-communicable diseases that are sure to place increasing burdens upon modern societies.

5 Abstract

Upon Toll-like receptor (TLR) activation, macrophages rapidly change their transcriptional- and translational network and rewire their metabolism. Mitochondrial pyruvate import via the mitochondrial pyruvate carrier (MPC) is essential to the metabolic changes controlling inflammatory responses. Thus, the MPC is a promising target to pharmacologically intervene in inflammatory diseases. Mitoglitazone is an MPC inhibitor currently under clinical investigation for insulin sensitization and amelioration of neurodegeneration. Yet, its effects on macrophage metabolism and inflammation remain undescribed.

Here, it is reported that Mitoglitazone inhibits the MPC in macrophages and decreases their inflammatory response following TLR4- or TLR7/8 activation. Metabolic analyses showed rerouting of glucose metabolism and, concomitantly, inhibition of the glycolytic switch and maximal respiration of inflammatory macrophages. Accordingly, Mitoglitazone decreased inflammatory cytokine transcription and release as well as nitric oxide production. Sustained effects of Mitoglitazone under pharmacologic inhibition or in the absence of the nuclear receptor PPARɣ emphasize its mode of action via MPC inhibition. In an acute sepsis mouse model Mitoglitazone decreased LPS-induced cytokines, demonstrating its immunomodulatory effect also in vivo.

These findings give new insights into the integrative network of macrophage metabolism and their inflammatory response, and highlight the potential of MPC inhibition by Mitoglitazone as a strategy to ameliorate erroneous inflammation.

6 List of figures

7 References

Armoni, M., Kritz, N., Harel, C., Bar-Yoseph, F., Chen, H., Quon, M. J., & Karnieli, E. (2003). Peroxisome proliferator-activated receptor-γ represses GLUT4 promoter activity in primary adipocytes, and rosiglitazone alleviates this effect. *Journal of Biological Chemistry*, *278*(33), 30614–30623. https://doi.org/10.1074/jbc.M304654200

Arts, R. J. W., Novakovic, B., ter Horst, R., Carvalho, A., Bekkering, S., Lachmandas, E., Rodrigues, F., Silvestre, R., Cheng, S. C., Wang, S. Y., Habibi, E., Gonçalves, L. G., Mesquita, I., Cunha, C., van Laarhoven, A., van de Veerdonk, F. L., Williams, D. L., van der Meer, J. W. M., Logie, C., … Netea, M. G. (2016). Glutaminolysis and Fumarate Accumulation Integrate Immunometabolic and Epigenetic Programs in Trained Immunity. *Cell Metabolism*, *24*(6), 807–819. https://doi.org/10.1016/j.cmet.2016.10.008

Berg, J. M., Tymoczko J. L., Stryer L., Stryer Biochemie 7. Auflage. Heidelberg: Springer Verlag, 2013

Bolten, C. W., Blanner, P. M., Mcdonald, W. G., Staten, N. R., Mazzarella, R. A., Arhancet, G. B., Meier, M. F., Weiss, D. J., Sullivan, P. M., Hromockyj, A. E., Kletzien, R. F., & Colca, J. R. (2007). Insulin Sensitizing Pharmacology of Thiazolidinediones Correlates with Mitochondrial Gene Expression rather than Activation of PPARγ. In *Gene Regulation and Systems Biology*. http://www.la-press.com/copyright.htm

Bricker, D. K., Taylor, E. B., Schell, J. C., Orsak, T., Boutron, A., Chen, Y. C., Cox, J. E., Cardon, C. M., van Vranken, J. G., Dephoure, N., Redin, C., Boudina, S., Gygi, S. P., Brivet, M., Thummel, C. S., & Rutter, J. (2012). A mitochondrial pyruvate carrier required for pyruvate uptake in yeast, Drosophila, and humans. *Science*, *336*(6090), 96–100. https://doi.org/10.1126/science.1218099

Brunmair, B., Gras, F., Neschen, S., Roden, M., Wagner, L., Waldhä, W., & Fü, C. (2001). *Direct Thiazolidinedione Action on Isolated Rat Skeletal Muscle Fuel Handling Is Independent of Peroxisome Proliferator-Activated Receptor-Mediated Changes in Gene Expression*. http://diabetesjournals.org/diabetes/article-pdf/50/10/2309/366424/db1001002309.pdf

Brunmair, B., Staniek, K., Gras, F., Scharf, N., Althaym, A., Clara, R., Roden, M., Gnaiger, E., Nohl, H., Waldhä Usl, W., & Fü Rnsinn, C. (2004). *Thiazolidinediones, Like*

Metformin, Inhibit Respiratory Complex I A Common Mechanism Contributing to Their Antidiabetic Actions?

Cameron, A. M., Castoldi, A., Sanin, D. E., Flachsmann, L. J., Field, C. S., Puleston, D. J., Kyle, R. L., Patterson, A. E., Hässler, F., Buescher, J. M., Kelly, B., Pearce, E. L., & Pearce, E. J. (2019). Inflammatory macrophage dependence on NAD + salvage is a consequence of reactive oxygen species–mediated DNA damage. *Nature Immunology*, *20*(4), 420–432. https://doi.org/10.1038/s41590-019-0336-y

Canevari, L., & Clark, J. B. (2007). Alzheimer's Disease and Cholesterol: The Fat Connection. *Neurochemical Research*, *32*(4), 739–750. https://doi.org/10.1007/s11064-006-9200-1

Charles-Messance, H., & Sheedy, F. J. (2021). Train to Lose: Innate Immune Memory in Metaflammation. In *Molecular Nutrition and Food Research* (Vol. 65, Issue 1). Wiley-VCH Verlag. https://doi.org/10.1002/mnfr.201900480

Chawla, A. (2010). Control of macrophage activation and function by PPARs. In *Circulation Research* (Vol. 106, Issue 10, pp. 1559–1569). https://doi.org/10.1161/CIRCRESAHA.110.216523

Chawla, A., Barak, Y., Nagy, L., Liao, D., Tontonoz, P., & Evans, R. M. (2001). PPAR-γ dependent and independent effects on macrophage-gene expression in lipid metabolism and inflammation. *Nature Medicine*, *7*(1), 48–52. https://doi.org/10.1038/83336

Chen, Z., Vigueira, P. A., Chambers, K. T., Hall, A. M., Mitra, M. S., Qi, N., McDonald, W. G., Colca, J. R., Kletzien, R. F., & Finck, B. N. (2012). Insulin resistance and metabolic derangements in obese mice are ameliorated by a novel peroxisome proliferator-activated receptor γ-sparing thiazolidinedione. *Journal of Biological Chemistry*, *287*(28), 23537–23548. https://doi.org/10.1074/jbc.M112.363960

Christ, A., Günther, P., Lauterbach, M. A. R., Duewell, P., Biswas, D., Pelka, K., Scholz, C. J., Oosting, M., Haendler, K., Baßler, K., Klee, K., Schulte-Schrepping, J., Ulas, T., Moorlag, S. J. C. F. M., Kumar, V., Park, M. H., Joosten, L. A. B., Groh, L. A., Riksen, N. P., … Latz, E. (2018). Western Diet Triggers NLRP3-Dependent Innate Immune Reprogramming. *Cell*, *172*(1–2), 162-175.e14. https://doi.org/10.1016/j.cell.2017.12.013

Christ, A., & Latz, E. (2019). The Western lifestyle has lasting effects on metaflammation. In *Nature Reviews Immunology* (Vol. 19, Issue 5, pp. 267–268). Nature Publishing Group. https://doi.org/10.1038/s41577-019-0156-1

Christ, A., Lauterbach, M., & Latz, E. (2019). Western Diet and the Immune System: An Inflammatory Connection. *Immunity*, *51*(5), 794–811. https://doi.org/10.1016/J.IMMUNI.2019.09.020

Colca, J. (2020). NASH (nonalcoholic steatohepatitis), diabetes, and macrovascular disease: multiple chronic conditions and a potential treatment at the metabolic root. In *Expert Opinion on Investigational Drugs* (Vol. 29, Issue 2, pp. 191–196). Taylor and Francis Ltd. https://doi.org/10.1080/13543784.2020.1715940

Colca, J. R., McDonald, W. G., Cavey, G. S., Cole, S. L., Holewa, D. D., Brightwell-Conrad, A. S., Wolfe, C. L., Wheeler, J. S., Coulter, K. R., Kilkuskie, P. M., Gracheva, E., Korshunova, Y., Trusgnich, M., Karr, R., Wiley, S. E., Divakaruni, A. S., Murphy, A. N., Vigueira, P. A., Finck, B. N., & Kletzien, R. F. (2013). Identification of a Mitochondrial Target of Thiazolidinedione Insulin Sensitizers (mTOT)-Relationship to Newly Identified Mitochondrial Pyruvate Carrier Proteins. *PLoS ONE*, *8*(5). https://doi.org/10.1371/journal.pone.0061551

Colca, J. R., Vanderlugt, J. T., Adams, W. J., Shashlo, A., McDonald, W. G., Liang, J., Zhou, R., & Orloff, D. G. (2013). Clinical proof-of-concept study with MSDC-0160, a prototype mTOT-modulating insulin sensitizer. *Clinical Pharmacology and Therapeutics*, *93*(4), 352–359. https://doi.org/10.1038/clpt.2013.10

Corbet, C., Bastien, E., Draoui, N., Doix, B., Mignion, L., Jordan, B. F., Marchand, A., Vanherck, J.-C., Chaltin, P., Schakman, O., Becker, H. M., Riant, O., & Feron, O. (2018). Interruption of lactate uptake by inhibiting mitochondrial pyruvate transport unravels direct antitumor and radiosensitizing effects. *Nature Communications*, *9*(1), 1208. https://doi.org/10.1038/s41467-018-03525-0

Cusi, K., Orsak, B., Bril, F., Lomonaco, R., Hecht, J., Ortiz-Lopez, C., Tio, F., Hardies, J., Darland, C., Musi, N., Webb, A., & Portillo-Sanchez, P. (2016). Long-term pioglitazone treatment for patients with nonalcoholic steatohepatitis and prediabetes or type 2 diabetes mellitus a randomized trial. *Annals of Internal Medicine*, *165*(5), 305–315. https://doi.org/10.7326/M15-1774

dello Russo, C., Gavrilyuk, V., Weinberg, G., Almeida, A., Bolanos, J. P., Palmer, J., Pelligrino, D., Galea, E., & Feinstein, D. L. (2003). Peroxisome proliferator-activated receptor γ thiazolidinedione agonists increase glucose metabolism in astrocytes. *Journal of Biological Chemistry*, *278*(8), 5828–5836. https://doi.org/10.1074/jbc.M208132200

Divakaruni, A. S., Wiley, S. E., Rogers, G. W., Andreyev, A. Y., Petrosyan, S., Loviscach, M., Wall, E. A., Yadava, N., Heuck, A. P., Ferrick, D. A., Henry, R. R., McDonald, W. G., Colca, J. R., Simon, M. I., Ciaraldi, T. P., & Murphy, A. N. (2013). Thiazolidinediones are acute, specific inhibitors of the mitochondrial pyruvate carrier. *Proceedings of the National Academy of Sciences of the United States of America*, *110*(14), 5422–5427. https://doi.org/10.1073/pnas.1303360110

Dormandy, J. A., Charbonnel, B., Eckland, D. J. A., Erdmann, E., Massi-Benedetti, M., Moules, I. K., Skene, A. M., Tan, M. H., Lefèbvre, P. J., Murray, G. D., Standl, E., Wilcox, R. G., Wilhelmsen, L., Betteridge, J., Birkeland, K., Golay, A., Heine, R. J., Korányi, L., Laakso, M., … Tatoň, J. (2005). Secondary prevention of macrovascular events in patients with type 2 diabetes in the PROactive Study (PROspective pioglitAzone Clinical Trial In macroVascular Events): a randomised controlled trial. *The Lancet*, *366*(9493), 1279–1289. https://doi.org/10.1016/S0140-6736(05)67528-9

Du, J., Cleghorn, W. M., Contreras, L., Lindsay, K., Rountree, A. M., Chertov, A. O., Turner, S. J., Sahaboglu, A., Linton, J., Sadilek, M., Satrústegui, J., Sweet, I. R., Paquet-Durand, F., & Hurley, J. B. (2013). Inhibition of Mitochondrial Pyruvate Transport by Zaprinast Causes Massive Accumulation of Aspartate at the Expense of Glutamate in the Retina *. *Journal of Biological Chemistry*, *288*(50), 36129–36140. https://doi.org/10.1074/jbc.M113.507285

Erdmann, E., Dormandy, J. A., Charbonnel, B., Massi-Benedetti, M., Moules, I. K., & Skene, A. M. (2007). The Effect of Pioglitazone on Recurrent Myocardial Infarction in 2,445 Patients With Type 2 Diabetes and Previous Myocardial Infarction: Results From the PROactive (PROactive 05) Study. *Journal of the American College of Cardiology*, *49*(17), 1772–1780. https://doi.org/https://doi.org/10.1016/j.jacc.2006.12.048

Escoubet-Lozach, L., Benner, C., Kaikkonen, M. U., Lozach, J., Heinz, S., Spann, N. J., Crotti, A., Stender, J., Ghisletti, S., Reichart, D., Cheng, C. S., Luna, R., Ludka, C.,

Sasik, R., Garcia-Bassets, I., Hoffmann, A., Subramaniam, S., Hardiman, G., Rosenfeld, M. G., & Glass, C. K. (2011). Mechanisms Establishing TLR4-Responsive Activation States of Inflammatory Response Genes. *PLOS Genetics*, *7*(12), e1002401-. https://doi.org/10.1371/journal.pgen.1002401

Everts, B., Amiel, E., Huang, S. C. C., Smith, A. M., Chang, C. H., Lam, W. Y., Redmann, V., Freitas, T. C., Blagih, J., van der Windt, G. J. W., Artyomov, M. N., Jones, R. G., Pearce, E. L., & Pearce, E. J. (2014). TLR-driven early glycolytic reprogramming via the kinases TBK1-IKKε supports the anabolic demands of dendritic cell activation. *Nature Immunology*, *15*(4), 323–332. https://doi.org/10.1038/ni.2833

Feinstein, D. L., Spagnolo, A., Akar, C., Weinberg, G., Murphy, P., Gavrilyuk, V., & dello Russo, C. (2005). Receptor-independent actions of PPAR thiazolidinedione agonists: Is mitochondrial function the key? In *Biochemical Pharmacology* (Vol. 70, Issue 2, pp. 177–188). Elsevier Inc. https://doi.org/10.1016/j.bcp.2005.03.033

Fujita, T., Sugiyama, Y., Taketomi, S., Sohda, T., Kawamatsu, Y., Iwatsuka, H., & Suzuoki, Z. (1983). Reduction of Insulin Resistance in Obese and/or Diabetic Animals by 5-[4-(1-Methylcyclohexylmethoxy)benzyl]-thiazolidine-2,4-dione (ADD-3878, U-63,287, Ciglitazone), a New Antidiabetic Agent. *Diabetes*, *32*(9), 804–810. https://doi.org/10.2337/diab.32.9.804

Gao, D., Madi, M., Ding, C., Fok, M., Steele, T., Ford, C., Hunter, L., & Bing, C. (2014). Interleukin-1β mediates macrophage-induced impairment of insulin signaling in human primary adipocytes. *American Journal of Physiology - Endocrinology and Metabolism*, *307*(3). https://doi.org/10.1152/AJPENDO.00430.2013

Gautier, E. L., Chow, A., Spanbroek, R., Marcelin, G., Greter, M., Jakubzick, C., Bogunovic, M., Leboeuf, M., van Rooijen, N., Habenicht, A. J., Merad, M., & Randolph, G. J. (2012). Systemic Analysis of PPARγ in Mouse Macrophage Populations Reveals Marked Diversity in Expression with Critical Roles in Resolution of Inflammation and Airway Immunity. *The Journal of Immunology*, *189*(5), 2614–2624. https://doi.org/10.4049/jimmunol.1200495

Ghosh, A., Tyson, T., George, S., Hildebrandt, E. N., Steiner, J. A., Madaj, Z., Schulz, E., Machiela, E., Mcdonald, W. G., Galvis, M. L. E., Kordower, J. H., van Raamsdonk, J. M., Colca, J. R., & Brundin, P. (2016). *Mitochondrial pyruvate carrier regulates*

autophagy, inflammation, and neurodegeneration in experimental models of Parkinson's disease. https://doi.org/10.1126/scitranslmed.aag2210

Halestrap, A. P. (1975). The Mitochondrial Pyruvate Carrier KINETICS AND SPECIFICITY FOR SUBSTRATES AND INHIBITORS. In *Biochem. J* (Vol. 148).

Halestrap, A. P., & Denton, R. M. (1974). Specific Inhibition of Pyruvate Transport in Rat Liver Mitochondria and Human Erythrocytes by a-Cyano-4-hydroxycinnamate. In *Biochem. J* (Vol. 138).

Hargreaves, D. C., Horng, T., & Medzhitov, R. (2009). Control of Inducible Gene Expression by Signal-Dependent Transcriptional Elongation. *Cell*, *138*(1), 129–145. https://doi.org/10.1016/j.cell.2009.05.047

He, W., Barak, Y., Hevener, A., Olson, P., Liao, D., Le, J., Nelson, M., Ong, E., Olefsky, J. M., & Evans, R. M. (2003). *Adipose-specific peroxisome proliferator-activated receptor knockout causes insulin resistance in fat and liver but not in muscle*. www.pnas.orgcgidoi10.1073pnas.2536828100

He, W., Henne, A., Lauterbach, M., Geißmar, E., Nikolka, F., Kho, C., Heinz, A., Dostert, C., Grusdat, M., Cordes, T., Härm, J., Goldmann, O., Ewen, A., Verschueren, C., Blay-Cadanet, J., Geffers, R., Garritsen, H., Kneiling, M., Holm, C. K., … Hiller, K. (2022). Mesaconate is synthesized from itaconate and exerts immunomodulatory effects in macrophages. *Nature Metabolism*, *4*(5), 524–533. https://doi.org/10.1038/s42255-022-00565-1

Hegazy, L., Gill, L. E., Pyles, K. D., Kaiho, C., Kchouk, S., Finck, B. N., McCommis, K. S., & Elgendy, B. (2022). Identification of Novel Mitochondrial Pyruvate Carrier Inhibitors by Homology Modeling and Pharmacophore-Based Virtual Screening. *Biomedicines*, *10*(2). https://doi.org/10.3390/biomedicines10020365

Heming, M., Gran, S., Jauch, S. L., Fischer-Riepe, L., Russo, A., Klotz, L., Hermann, S., Schäfers, M., Roth, J., & Barczyk-Kahlert, K. (2018). Peroxisome proliferator-activated receptor-γ modulates the response of macrophages to lipopolysaccharide and glucocorticoids. *Frontiers in Immunology*, *9*(MAY). https://doi.org/10.3389/fimmu.2018.00893

Heneka, M. T., Fink, A., & Doblhammer, G. (2015). Effect of pioglitazone medication on the incidence of dementia. *Annals of Neurology*, *78*(2), 284–294. https://doi.org/10.1002/ana.24439

Herzig, S., Raemy, E., Montessuit, S., Veuthey, J. L., Zamboni, N., Westermann, B., Kunji, E. R. S., & Martinou, J. C. (2012). Identification and functional expression of the mitochondrial pyruvate carrier. *Science*, *336*(6090), 93–96. https://doi.org/10.1126/science.1218530

Hiller, K., Hangebrauk, J., Jäger, C., Spura, J., Schreiber, K., & Schomburg, D. (2009). Metabolite detector: Comprehensive analysis tool for targeted and nontargeted GC/MS based metabolome analysis. *Analytical Chemistry*, *81*(9), 3429–3439. https://doi.org/10.1021/ac802689c

Hodges, W. T., Jarasvaraparn, C., Ferguson, D., Griffett, K., Gill, L. E., Chen, Y., Ilagan, Ma. X. G., Hegazy, L., Elgendy, B., Cho, K., Patti, G. J., McCommis, K. S., & Finck, B. N. (2022). Mitochondrial pyruvate carrier inhibitors improve metabolic parameters in diet-induced obese mice. *Journal of Biological Chemistry*, *298*(2). https://doi.org/10.1016/j.jbc.2021.101554

Home, P. D., Pocock, S. J., Beck-Nielsen, H., Curtis, P. S., Gomis, R., Hanefeld, M., Jones, N. P., Komajda, M., & McMurray, J. J. v. (2009). Rosiglitazone evaluated for cardiovascular outcomes in oral agent combination therapy for type 2 diabetes (RECORD): a multicentre, randomised, open-label trial. *The Lancet*, *373*(9681), 2125–2135. https://doi.org/10.1016/S0140-6736(09)60953-3

Hosseini, Z., Whiting, S. J., & Vatanparast, H. (2016). Current evidence on the association of the metabolic syndrome and dietary patterns in a global perspective. *Nutrition Research Reviews*, *29*(2), 152–162. https://doi.org/10.1017/S095442241600007X

Hotamisligil, G. S. (2017). Inflammation, metaflammation and immunometabolic disorders. In *Nature* (Vol. 542, Issue 7640, pp. 177–185). Nature Publishing Group. https://doi.org/10.1038/nature21363

Hu, W., Jiang, C., Kim, M., Xiao, Y., Richter, H. J., Guan, D., Zhu, K., Krusen, B. M., Roberts, A. N., Miller, J., Steger, D. J., & Lazar, M. A. (2022). Isoform-specific functions of PPARγ in gene regulation and metabolism. *Genes & Development*. https://doi.org/10.1101/gad.349232.121

Jacques, V., Bolze, S., Hallakou-Bozec, S., Czarnik, A. W., Divakaruni, A. S., Fouqueray, P., Murphy, A. N., van der Ploeg, L. H. T., & Dewitt, S. (2021). Deuterium-Stabilized (R)-Pioglitazone (PXL065) Is Responsible for Pioglitazone Efficacy in NASH yet

Exhibits Little to No PPARγ Activity. *Hepatology CommuniCations*, *0*(0), 2021. https://doi.org/10.1002/hep4.1723/suppinfo

Jha, A. K., Huang, S. C. C., Sergushichev, A., Lampropoulou, V., Ivanova, Y., Loginicheva, E., Chmielewski, K., Stewart, K. M., Ashall, J., Everts, B., Pearce, E. J., Driggers, E. M., & Artyomov, M. N. (2015). Network integration of parallel metabolic and transcriptional data reveals metabolic modules that regulate macrophage polarization. *Immunity*, *42*(3), 419–430. https://doi.org/10.1016/j.immuni.2015.02.005

Kerr, J., Anderson, C., & Lippman, S. M. (2017). Physical activity, sedentary behaviour, diet, and cancer: an update and emerging new evidence. *The Lancet Oncology*, *18*(8), e457–e471. https://doi.org/10.1016/S1470-2045(17)30411-4

Kohlroser, J., Mathai, J., Reichheld, J., Banner, B. F., & Bonkovsky, H. L. (2000). *Hepatotoxicity Due to Troglitazone: Report of Two Cases and Review of Adverse Events Reported to the United States Food and Drug Administration*.

Lampropoulou, V., Sergushichev, A., Bambouskova, M., Nair, S., Vincent, E. E., Loginicheva, E., Cervantes-Barragan, L., Ma, X., Huang, S. C. C., Griss, T., Weinheimer, C. J., Khader, S., Randolph, G. J., Pearce, E. J., Jones, R. G., Diwan, A., Diamond, M. S., & Artyomov, M. N. (2016). Itaconate Links Inhibition of Succinate Dehydrogenase with Macrophage Metabolic Remodeling and Regulation of Inflammation. *Cell Metabolism*, *24*(1), 158–166. https://doi.org/10.1016/j.cmet.2016.06.004

Lauterbach, M. A., Hanke, J. E., Serefidou, M., Mangan, M. S. J., Kolbe, C. C., Hess, T., Rothe, M., Kaiser, R., Hoss, F., Gehlen, J., Engels, G., Kreutzenbeck, M., Schmidt, S. v., Christ, A., Imhof, A., Hiller, K., & Latz, E. (2019). Toll-like Receptor Signaling Rewires Macrophage Metabolism and Promotes Histone Acetylation via ATP-Citrate Lyase. *Immunity*, *51*(6), 997-1011.e7. https://doi.org/10.1016/j.immuni.2019.11.009

Lee, J., Jin, Z., Lee, D., Yun, J. H., & Lee, W. (2020). Characteristic analysis of homo- and heterodimeric complexes of human mitochondrial pyruvate carrier related to metabolic diseases. *International Journal of Molecular Sciences*, *21*(9). https://doi.org/10.3390/ijms21093403

Lee, Y. S., & Olefsky, J. (2021). *Chronic tissue inflammation and metabolic disease*. https://doi.org/10.1101/gad.346312

Lehmann, J. M., Moore, L. B., Smith-Oliver, T. A., Wilkison, W. O., Willson, T. M., & Kliewer, S. A. (1995). An Antidiabetic Thiazolidinedione Is a High Affinity Ligand for

Peroxisome Proliferator-activated Receptor ɣ; (PPARɣ). *Journal of Biological Chemistry*, *270*(22), 12953–12956. https://doi.org/10.1074/jbc.270.22.12953

Liang, L., Li, Q., Huang, L., Li, D., & Li, X. (2015). Sirt3 binds to and deacetylates mitochondrial pyruvate carrier 1 to enhance its activity. *Biochemical and Biophysical Research Communications*, *468*(4), 807–812. https://doi.org/10.1016/j.bbrc.2015.11.036

Liu, X., Flores, A. A., Situ, L., Gu, W., Ding, H., Christofk, H. R., Lowry, W. E., & Jung, M. E. (2021). Development of Novel Mitochondrial Pyruvate Carrier Inhibitors to Treat Hair Loss. *Journal of Medicinal Chemistry*, *64*(4), 2046–2063. https://doi.org/10.1021/acs.jmedchem.0c01570

Lopez-Garcia, E., Schulze, M. B., Fung, T. T., Meigs, J. B., Rifai, N., Manson, J. E., & Hu, F. B. (2004). Major dietary patterns are related to plasma concentrations of markers of inflammation and endothelial dysfunction. *The American Journal of Clinical Nutrition*, *80*(4), 1029–1035. https://doi.org/10.1093/ajcn/80.4.1029

Lumeng, C. N., Bodzin, J. L., & Saltiel, A. R. (2007). Obesity induces a phenotypic switch in adipose tissue macrophage polarization. *The Journal of Clinical Investigation*, *117*(1), 175–184. https://doi.org/10.1172/JCI29881

Lumeng, C. N., DelProposto, J. B., Westcott, D. J., & Saltiel, A. R. (2008). Phenotypic Switching of Adipose Tissue Macrophages With Obesity Is Generated by Spatiotemporal Differences in Macrophage Subtypes. *Diabetes*, *57*(12), 3239–3246. https://doi.org/10.2337/db08-0872

Lumeng, C. N., Deyoung, S. M., & Saltiel, A. R. (2007). Macrophages block insulin action in adipocytes by altering expression of signaling and glucose transport proteins. *American Journal of Physiology-Endocrinology and Metabolism*, *292*(1), E166–E174. https://doi.org/10.1152/ajpendo.00284.2006

Mahaffey, K. W., Hafley, G., Dickerson, S., Burns, S., Tourt-Uhlig, S., White, J., Newby, L. K., Komajda, M., McMurray, J., Bigelow, R., Home, P. D., & Lopes, R. D. (2013). Results of a reevaluation of cardiovascular outcomes in the RECORD trial. *American Heart Journal*, *166*(2), 240-249.e1. https://doi.org/https://doi.org/10.1016/j.ahj.2013.05.004

Mallet, D., Goutaudier, R., Barbier, E. L., Carnicella, S., Colca, J. R., Fauvelle, F., & Boulet, S. (2022). Re-routing Metabolism by the Mitochondrial Pyruvate Carrier Inhibitor

MSDC-0160 Attenuates Neurodegeneration in a Rat Model of Parkinson's Disease. *Molecular Neurobiology*. https://doi.org/10.1007/s12035-022-02962-9

Mccommis, K. S., Hodges, W. T., Brunt, E. M., Nalbantoglu, I., Mcdonald, W. G., Holley, C., Fujiwara, H., Schaffer, J. E., Colca, J. R., & Finck, B. N. (2016). Targeting the Mitochondrial Pyruvate Carrier Attenuates Fibrosis in a Mouse Model of Nonalcoholic Steatohepatitis. *Hepatology*, *65*(5). https://doi.org/10.1002/hep.29025/suppinfo

McGettrick, A. F., & O'Neill, L. A. J. (2020). The Role of HIF in Immunity and Inflammation. In *Cell Metabolism* (Vol. 32, Issue 4, pp. 524–536). Cell Press. https://doi.org/10.1016/j.cmet.2020.08.002

Medzhitov, R. (2008). Origin and physiological roles of inflammation. In *Nature* (Vol. 454, Issue 7203, pp. 428–435). Nature Publishing Group. https://doi.org/10.1038/nature07201

Meiser, J., Krämer, L., Sapcariu, S. C., Battello, N., Ghelfi, J., D'Herouel, A. F., Skupin, A., & Hiller, K. (2016). Pro-inflammatory macrophages sustain pyruvate oxidation through pyruvate dehydrogenase for the synthesis of itaconate and to enable cytokine expression. *Journal of Biological Chemistry*, *291*(8), 3932–3946. https://doi.org/10.1074/jbc.M115.676817

Michailidou, Z., Gomez-Salazar, M., & Alexaki, V. I. (2022). Innate Immune Cells in the Adipose Tissue in Health and Metabolic Disease. In *Journal of Innate Immunity* (Vol. 14, Issue 1, pp. 4–30). S. Karger AG. https://doi.org/10.1159/000515117

Michelucci, A., Cordes, T., Ghelfi, J., Pailot, A., Reiling, N., Goldmann, O., Binz, T., Wegner, A., Tallam, A., Rausell, A., Buttini, M., Linster, C. L., Medina, E., Balling, R., & Hiller, K. (2013). Immune-responsive gene 1 protein links metabolism to immunity by catalyzing itaconic acid production. *Proceedings of the National Academy of Sciences of the United States of America*, *110*(19), 7820–7825. https://doi.org/10.1073/pnas.1218599110

Mozaffarian, D. (2016). Dietary and Policy Priorities for Cardiovascular Disease, Diabetes, and Obesity. In *Circulation* (Vol. 133, Issue 2, pp. 187–225). Lippincott Williams and Wilkins. https://doi.org/10.1161/CIRCULATIONAHA.115.018585

Murphy K. P., Janeway's Immunobiology 8th edition. London and New York: Garland Science, Taylor and Francis Group, LLC, 2012

Netea, M. G., Domínguez-Andrés, J., Barreiro, L. B., Chavakis, T., Divangahi, M., Fuchs, E., Joosten, L. A. B., van der Meer, J. W. M., Mhlanga, M. M., Mulder, W. J. M., Riksen, N. P., Schlitzer, A., Schultze, J. L., Stabell Benn, C., Sun, J. C., Xavier, R. J., & Latz, E. (2020). Defining trained immunity and its role in health and disease. In *Nature Reviews Immunology* (Vol. 20, Issue 6, pp. 375–388). Nature Research. https://doi.org/10.1038/s41577-020-0285-6

Newton, K., & Dixit, V. M. (2012). Signaling in innate immunity and inflammation. *Cold Spring Harbor Perspectives in Biology*, *4*(3). https://doi.org/10.1101/cshperspect.a006049

Nissen, S. E., & Wolski, K. (2010). Rosiglitazone Revisited: An Updated Meta-analysis of Risk for Myocardial Infarction and Cardiovascular Mortality. *Archives of Internal Medicine*, *170*(14), 1191–1201. https://doi.org/10.1001/archinternmed.2010.207

Nonnenmacher, Y., & Hiller, K. (2018). Biochemistry of proinflammatory macrophage activation. In *Cellular and Molecular Life Sciences* (Vol. 75, Issue 12, pp. 2093–2109). Birkhauser Verlag AG. https://doi.org/10.1007/s00018-018-2784-1

Papa, S., Francavilla, A., Paradies, G., & Meduri, B. (1971). *THE TRANSPORT OF PYRUVATE IN RAT LIVER MITOCHONDRIA* (Vol. 12).

Perkins, J. R., Dawes, J. M., Mcmahon, S. B., Lh Bennett, D., Orengo, C., & Kohl, M. (2012). SOFTWARE Open Access. In *BMC Genomics* (Vol. 13). http://www.biomedcentral.com/http://www.bioconductor.org/packages/release/bioc/html/ReadqPCR.htmlandhttp://www.bioconductor.org/packages/release/bioc/html/NormqPCR.html

Quansah, E., Peelaerts, W., Langston, J. W., Simon, D. K., Colca, J., & Brundin, P. (2018). Targeting energy metabolism via the mitochondrial pyruvate carrier as a novel approach to attenuate neurodegeneration. In *Molecular Neurodegeneration* (Vol. 13, Issue 1). BioMed Central Ltd. https://doi.org/10.1186/s13024-018-0260-x

Quintin, J., Saeed, S., Martens, J. H. A., Giamarellos-Bourboulis, E. J., Ifrim, D. C., Logie, C., Jacobs, L., Jansen, T., Kullberg, B. J., Wijmenga, C., Joosten, L. A. B., Xavier, R. J., van der Meer, J. W. M., Stunnenberg, H. G., & Netea, M. G. (2012). Candida albicans infection affords protection against reinfection via functional reprogramming of monocytes. *Cell Host and Microbe*, *12*(2), 223–232. https://doi.org/10.1016/j.chom.2012.06.006

Ramirez-Carrozzi, V. R., Braas, D., Bhatt, D. M., Cheng, C. S., Hong, C., Doty, K. R., Black, J. C., Hoffmann, A., Carey, M., & Smale, S. T. (2009). A Unifying Model for the Selective Regulation of Inducible Transcription by CpG Islands and Nucleosome Remodeling. *Cell*, *138*(1), 114–128. https://doi.org/https://doi.org/10.1016/j.cell.2009.04.020

Ran, L., Zhang, S., Zhao, P., Zhou, J., Gan, H., Jeon, R., Clinic, M., Li, Q., Herrmann, J., & Wang, F. (n.d.). *UK5099 inhibits macrophage activation independent of mitochondrial pyruvate carrier mediated metabolism*. https://doi.org/10.21203/rs.3.rs-888198/v1

Rauckhorst, A. J., Gray, L. R., Sheldon, R. D., Fu, X., Pewa, A. D., Feddersen, C. R., Dupuy, A. J., Gibson-Corley, K. N., Cox, J. E., Burgess, S. C., & Taylor, E. B. (2017). The mitochondrial pyruvate carrier mediates high fat diet-induced increases in hepatic TCA cycle capacity. *Molecular Metabolism*, *6*(11), 1468–1479. https://doi.org/10.1016/j.molmet.2017.09.002

Ricote, M., Li, A. C., Willson, T. M., Kelly, C. J., & Glass, C. K. (1998). The peroxisome proliferator-activated receptor-γ is a negative regulator of macrophage activation. *Nature*, *391*(6662), 79–82. https://doi.org/10.1038/34178

Rodríguez-Prados, J.-C., Través, P. G., Cuenca, J., Rico, D., Aragonés, J., Martín-Sanz, P., Cascante, M., & Boscá, L. (2010). Substrate Fate in Activated Macrophages: A Comparison between Innate, Classic, and Alternative Activation. *The Journal of Immunology*, *185*(1), 605–614. https://doi.org/10.4049/jimmunol.0901698

Schmidt, S., Moric, E., Schmidt, M., Sastre, M., Feinstein, D. L., & Heneka, M. T. (2004). Anti-inflammatory and antiproliferative actions of PPAR-γ agonists on T lymphocytes derived from MS patients. *Journal of Leukocyte Biology*, *75*(3), 478–485. https://doi.org/10.1189/jlb.0803402

Shah, R. C., Matthews, D. C., Andrews, R. D., Capuano, A. W., Fleischman, D. A., Vanderlugt, J. T., & Colca, J. R. (2014). An Evaluation of MSDC-0160, A Prototype mTOT Modulating Insulin Sensitizer, in Patients with Mild Alzheimer's Disease. In *Current Alzheimer Research* (Vol. 11). http://www.clinicaltrials.gov

Singh, S., Loke, Y. K., & Furberg, C. D. (2007). Long-term Risk of Cardiovascular Events With RosiglitazoneA Meta-analysis. *JAMA*, *298*(10), 1189–1195. https://doi.org/10.1001/jama.298.10.1189

Soccio, R. E., Chen, E. R., & Lazar, M. A. (2014). Thiazolidinediones and the promise of insulin sensitization in type 2 diabetes. In *Cell Metabolism* (Vol. 20, Issue 4, pp. 573–591). Cell Press. https://doi.org/10.1016/j.cmet.2014.08.005

Tan, Y., & Kagan, J. C. (2019). Innate Immune Signaling Organelles Display Natural and Programmable Signaling Flexibility. *Cell*, *177*(2), 384-398.e11. https://doi.org/10.1016/j.cell.2019.01.039

Tannahill, G. M., Curtis, A. M., Adamik, J., Palsson-Mcdermott, E. M., McGettrick, A. F., Goel, G., Frezza, C., Bernard, N. J., Kelly, B., Foley, N. H., Zheng, L., Gardet, A., Tong, Z., Jany, S. S., Corr, S. C., Haneklaus, M., Caffrey, B. E., Pierce, K., Walmsley, S., … O'Neill, L. A. J. (2013). Succinate is an inflammatory signal that induces IL-1β through HIF-1α. *Nature*, *496*(7444), 238–242. https://doi.org/10.1038/nature11986

Tavoulari, S., Schirris, T. J. J., Mavridou, V., Thangaratnarajah, C., King, M. S., Jones, D. T. D., Ding, S., Fearnley, I. M., & Kunji, E. R. S. (2022). Key features of inhibitor binding to the human mitochondrial pyruvate carrier hetero-dimer. *Molecular Metabolism*, *60*, 101469. https://doi.org/https://doi.org/10.1016/j.molmet.2022.101469

Touaibia, M., St-Coeur, P. D., Duff, P., Faye, D. C., & Pichaud, N. (2021). 5-Benzylidene, 5-benzyl, and 3-benzylthiazolidine-2,4-diones as potential inhibitors of the mitochondrial pyruvate carrier: Effects on mitochondrial functions and survival in Drosophila melanogaster. *European Journal of Pharmacology*, *913*. https://doi.org/10.1016/j.ejphar.2021.174627

Vacanti, N. M., Divakaruni, A. S., Green, C. R., Parker, S. J., Henry, R. R., Ciaraldi, T. P., Murphy, A. N., & Metallo, C. M. (2014). Regulation of substrate utilization by the mitochondrial pyruvate carrier. *Molecular Cell*, *56*(3), 425–435. https://doi.org/10.1016/j.molcel.2014.09.024

Vadvalkar, S. S., Matsuzaki, S., Eyster, C. A., Giorgione, J. R., Bockus, L. B., Kinter, C. S., Kinter, M., & Humphries, K. M. (2017). Decreased mitochondrial pyruvate transport activity in the diabetic heart: Role of Mitochondrial Pyruvate Carrier 2 (MPC2) acetylation. *Journal of Biological Chemistry*, *292*(11), 4423–4433. https://doi.org/10.1074/jbc.M116.753509

Vanderperre, B., Bender, T., Kunji, E. R. S., & Martinou, J. C. (2015). Mitochondrial pyruvate import and its effects on homeostasis. In *Current Opinion in Cell Biology* (Vol. 33, pp. 35–41). Elsevier Ltd. https://doi.org/10.1016/j.ceb.2014.10.008

Vanderperre, B., Herzig, S., Krznar, P., Hörl, M., Ammar, Z., Montessuit, S., Pierredon, S., Zamboni, N., & Martinou, J. C. (2016). Embryonic Lethality of Mitochondrial Pyruvate Carrier 1 Deficient Mouse Can Be Rescued by a Ketogenic Diet. *PLoS Genetics*, *12*(5). https://doi.org/10.1371/journal.pgen.1006056

Vigueira, P. A., McCommis, K. S., Schweitzer, G. G., Remedi, M. S., Chambers, K. T., Fu, X., McDonald, W. G., Cole, S. L., Colca, J. R., Kletzien, R. F., Burgess, S. C., & Finck, B. N. (2014). Mitochondrial Pyruvate Carrier 2 Hypomorphism in Mice Leads to Defects in Glucose-Stimulated Insulin Secretion. *Cell Reports*, *7*(6), 2042–2053. https://doi.org/10.1016/j.celrep.2014.05.017

Wang, T., Liu, H., Lian, G., Zhang, S. Y., Wang, X., & Jiang, C. (2017). HIF1 α -Induced Glycolysis Metabolism Is Essential to the Activation of Inflammatory Macrophages. *Mediators of Inflammation*, *2017*. https://doi.org/10.1155/2017/9029327

Warburg, O. (1924). Über den Stoffwechsel der Carcinomzelle. *Naturwissenschaften*, *12*(50), 1131–1137. https://doi.org/10.1007/BF01504608

Weisberg, S. P., McCann, D., Desai, M., Rosenbaum, M., Leibel, R. L., & Ferrante Jr., A. W. (2003). Obesity is associated with macrophage accumulation in adipose tissue. *The Journal of Clinical Investigation*, *112*(12), 1796–1808. https://doi.org/10.1172/JCI19246

Welch, J. S., Ricote, M., Akiyama, T. E., Gonzalez, F. J., Glass, C. K., & Steinberg, D. (2003). *PPAR and PPAR negatively regulate specific subsets of lipopolysaccharide and IFN-target genes in macrophages*. www.pnas.orgcgidoi10.1073pnas.1031789100

Wenes, M., Jaccard, A., Wyss, T., Maldonado-Pérez, N., Teoh, S. T., Lepez, A., Renaud, F., Franco, F., Waridel, P., Yacoub Maroun, C., Tschumi, B., Dumauthioz, N., Zhang, L., Donda, A., Martín, F., Migliorini, D., Lunt, S. Y., Ho, P.-C., & Romero, P. (2022). The mitochondrial pyruvate carrier regulates memory T cell differentiation and antitumor function. *Cell Metabolism*. https://doi.org/10.1016/j.cmet.2022.03.013

Wentworth, J. M., Naselli, G., Brown, W. A., Doyle, L., Phipson, B., Smyth, G. K., Wabitsch, M., O'Brien, P. E., & Harrison, L. C. (2010). Pro-Inflammatory CD11c+CD206+ Adipose Tissue Macrophages Are Associated With Insulin Resistance in Human Obesity. *Diabetes*, *59*(7), 1648–1656. https://doi.org/10.2337/db09-0287

Wilcox, R., Bousser, M.-G., Betteridge, D. J., Schernthaner, G., Pirags, V., Kupfer, S., & Dormandy, J. (2007). Effects of Pioglitazone in Patients With Type 2 Diabetes With or Without Previous Stroke. *Stroke*, *38*(3), 865–873. https://doi.org/10.1161/01.STR.0000257974.06317.49

Xu, H., Barnes, G. T., Yang, Q., Tan, G., Yang, D., Chou, C. J., Sole, J., Nichols, A., Ross, J. S., Tartaglia, L. A., & Chen, H. (2003). Chronic inflammation in fat plays a crucial role in the development of obesity-related insulin resistance. *Journal of Clinical Investigation*, *112*(12), 1821–1830. https://doi.org/10.1172/JCI200319451

Xu, L., Phelix, C. F., & Chen, L. Y. (2021). Structural Insights into the Human Mitochondrial Pyruvate Carrier Complexes. *Journal of Chemical Information and Modeling*, *61*(11), 5614–5625. https://doi.org/10.1021/acs.jcim.1c00879

Yiew, N. K. H., & Finck, B. N. (2022). The mitochondrial pyruvate carrier at the crossroads of intermediary metabolism. *American Journal of Physiology-Endocrinology and Metabolism*, *323*(1), E33–E52. https://doi.org/10.1152/ajpendo.00074.2022

Younossi, Z. M., Golabi, P., de Avila, L., Paik, J. M., Srishord, M., Fukui, N., Qiu, Y., Burns, L., Afendy, A., & Nader, F. (2019). The global epidemiology of NAFLD and NASH in patients with type 2 diabetes: A systematic review and meta-analysis. *Journal of Hepatology*, *71*(4), 793–801. https://doi.org/10.1016/j.jhep.2019.06.021

Zhou, M., Wu, R., Dong, W., Jacob, A., & Wang, P. (2008). Endotoxin downregulates peroxisome proliferator-activated receptor-γ via the increase in TNF-α release. *American Journal of Physiology-Regulatory, Integrative and Comparative Physiology*, *294*(1), R84–R92. https://doi.org/10.1152/ajpregu.00340.2007

8 Acknowledgments

I would like to express my deepest gratitude for my supervisor, Prof. Dr. Eicke Latz, for his generous support and the freedom granted throughout this journey. Additionally, I am extremely grateful to my defense committee, Prof. Dr. Mihai Netea, Prof. Dr. Dagmar Wachten and Prof. Dr. Anna-Christin Konermann, who graciously provided expertise and guidance.

I could not have undertaken this journey without the inspiration and brilliant advice provided by Mario Lauterbach. He provided the spark to the project that was ultimately presented in this thesis.

I am deeply indebted to my colleagues for all the on- and off-topic discussions, the willingness to share their knowledge and benevolent help. Taking on this journey together with you was a lot of fun and taught me heaps.

Last, but definitely not least, I would like to thank my friends and my family for their support, patience and critical feedback.